TRANSPORTATION RESEARCH RECORD 796

Highway Safety Appurtenances

TRANSPORTATION RESEARCH BOARD

COMMISSION ON SOCIOTECHNICAL SYSTEMS
NATIONAL RESEARCH COUNCIL

NATIONAL ACADEMY OF SCIENCES
WASHINGTON, D.C. 1981

Transportation Research Record 796
Price $5.60
Edited for TRB by Naomi Kassabian

mode
1 highway transportation

subject areas
21 facilities design
51 transportation safety

Library of Congress Cataloging in Publication Data
National Research Council. Transportation Research Board.
Highway safety appurtenances.

(Transportation research record; 796)
Reports presented at the 60th annual meeting of the Transportation Research Board.
1. Roads–Safety measures–Congresses. 2. Roads–Accessories–Congresses. I. National Research Council (U.S.). Transportation Research Board. II. Series.
TE7.H5 no. 796 [TE228] 380.5s 81-11222
ISBN 0-309-03210-5 ISSN 0361-1981 [625.7'042] AACR2

Sponsorship of the Papers in This Transportation Research Record

GROUP 2–DESIGN AND CONSTRUCTION OF TRANSPORTATION FACILITIES
R. V. LeClerc, Washington State Department of Transportation, chairman

General Design Section
Lester A. Herr, T. Y. Lin and Associates, chairman

Committee on Safety Appurtenances
Jarvis D. Michie, Southwest Research Institute, chairman
Gordon A. Alison, William E. Behm, Jeffrey Alan Bloom, James E. Bryden, Arthur M. Dinitz, Malcolm D. Graham, C. William Gray, James R. Hackney, James H. Hatton, Jr., Roger W. Hove, William W. Hunter, Max N. Jensen, Frank N. Lisle, Edwin C. Lokken, Roy J. Mohler, John F. Nixon, Eric F. Nordlin, Edward Robert Post, William L. Raymond, Jr., Hayes E. Ross, Jr., F. G. Schlosser, Flory J. Tamanini, Harry W. Taylor, John G. Viner

Committee on Utilities
Ronald L. Williams, West Virginia Department of Highways, chairman
James H. Anderson, James E. Attebery, James A. Bauer, William J. Boegly, Jr., Orbie M. Campbell, James A. Carney, Lloyd A. Dove, Albert R. Heidecke, David L. Houchin, Don H. Jones, James E. Kirk, John J. Labra, Albert F. Laube, Leroy P. McKenna, Roger C. McPherson, Paul F. Mundy, Joe G. Osendorf, Edward Robert Post, Harold E. Smith, Barry M. Sweedler, Kenneth W. Walker, Alvin M. Zager

Lawrence F. Spaine, Transportation Research Board staff

Sponsorship is indicated by a footnote at the end of each report. The organizational units, officers, and members are as of December 31, 1980.

Contents

Authors of the Papers in This Record

Arnold, A., Texas Transportation Institute, Highway Safety Research Center, Texas A&M University System, College Station, TX 77843

Bronstad, M.E., Southwest Research Institute, P.O. Drawer 28510, San Antonio, TX 78284

Bryden, James E., Engineering Research and Development Bureau, New York State Department of Transportation, 1220 Washington Avenue, Albany, NY 12232

Buth, C.E., Texas Transportation Institute, Highway Safety Research Center, Texas A&M University System, College Station, TX 77843

Hahn, Kenneth C., Engineering Research and Development Bureau, New York State Department of Transportation, 1220 Washington Avenue, Albany, NY 12232

Hirsch, T.J., Texas Transportation Institute, Highway Safety Research Center, Texas A&M University System, College Station, TX 77843

Hsueh, Richard T., Civil Engineering Department, University of Nebraska--Lincoln, Bancroft Hall 226, Lincoln, NE 68588

Ivey, Don L., Texas Transportation Institute, Texas A&M University System, College Station, TX 77843

Kimball, C.E., Jr., Southwest Research Institute, P.O. Drawer 28510, San Antonio, TX 78284

McCoy, Patrick T., Civil Engineering Department, University of Nebraska--Lincoln, Bancroft Hall 226, Lincoln, NE 68588

McDevitt, C.F., Office of Research, HRS/12, Federal Highway Administration, Washington, DC 20590

Michie, Jarvis D., Southwest Research Institute, P.O. Drawer 28510, San Antonio, TX 78284

Noel, James S., Texas Transportation Institute, Highway Safety Research Center, Texas A&M University System, College Station, TX 77843

Post, Edward R., Civil Engineering Department, University of Nebraska--Lincoln, Bancroft Hall 226, Lincoln, NE 68588

Robertson, Richard, Texas Transportation Institute, Texas A&M University System, College Station, TX 77843

Collision Risk Assessment Based on Occupant Flail-Space Model

JARVIS D. MICHIE

A method is presented to evaluate results of vehicle crash tests of highway safety appurtenances in terms of injury risk to the vehicle occupant. The occupant is assumed to be propelled through the vehicle compartment (flail space); to strike the instrument panel, windshield, or side door; and to subsequently ride down the remaining part of the collision event in contact with the vehicle. Injury is assessed in terms of (a) the impact velocity of the occupant and the instrument panel and (b) accelerations of occupant and vehicle that occur during the subsequent ride down. Evolution of present appurtenance safety criteria is reviewed. Dynamic conditions that produce human injury are briefly discussed along with recommended threshold values that will minimize the degree of the injuries. Finally, a typical application of the flail-space model to crash test results is presented.

Highway appurtenances are evaluated for their potential safety performance by full-scale vehicle crash tests and sometimes by pendulum or bogie tests. Since complete safety is an unattainable ideal, safety performance is measured in terms of degree of risk experienced by occupants when the vehicle collides with a roadside appurtenance.

The degree of risk is determined for two phases of a collision as illustrated in Figure 1. In stage 1, the occupant is flung through the compartment (flail space) and strikes the instrument panel, the windshield, or the door with an injury-dependent velocity and, in stage 2, the occupant rides down with the vehicle during the remaining portion of its velocity change (Figure 1b) and is subjected to injury-dependent accelerations.

The concept of this relatively simplified approach is not new; it has been suggested by several researchers. The purpose of this paper is to present the concept, discuss possible limitations, and then describe practical applications.

BACKGROUND

The first attempt to establish a human injury threshold based on vehicle dynamics during guardrail and median-barrier redirections is attributed to Shoemaker (1). He presented threshold vehicle lateral, longitudinal, and total accelerations along with three assumed occupant restraint conditions--no belt, lap belt only, and lap belt and shoulder belt. In addition, Shoemaker presented maximum duration and acceleration onset rates. Even though Shoemaker made a special effort to emphasize that his proposed criteria were tentative and based on very limited experience, his resultant table of values became "etched in stone" because of its uniqueness in the field. The table has subsequently been reproduced and referenced by numerous researchers (2-5). Since 1961, Shoemaker's criteria have been modified (6) by eliminating the 500 g/s acceleration onset rate limit and by using a maximum average vehicle acceleration of 50 ms and by applying the criteria only to tests with vehicle-barrier impact angles of 15° or less. In addition, data acquisition and processing parameters have been better defined (6). Even with these modifications, researchers have not been satisfied with the criteria because they do not adequately reflect the severity of a redirection and are believed to be overly conservative in some cases. Few longitudinal traffic barriers now satisfy the criteria; yet many are known to perform well in service.

In 1969, Edwards used vehicle velocity change as a measure of collision severity in evaluating breakaway luminaire supports (7). He concluded that, when velocity change exceeds 6 mph (10 km/h), there is a possibility of minor passenger injury; also, he stated that velocity change in excess of 12 mph (19 km/h) should be avoided. Edward's criteria were based on the work of Patrick (8) and Blamey (9), which indicated that head and chest injuries occur when the impact velocity of these body components on the compartment interior exceeds 11 mph (18 km/h). He concluded that the occupant and compartment interior impact velocity was approximately the same as the vehicle velocity change during a luminaire impact. By limiting the vehicle velocity change, he would also be limiting the occupant and compartment interior impact velocity and thus the occupant risk. [This relationship was intended for cases in which the vehicle undergoes full velocity change prior to the occupant impact; for other conditions, the 11-mph (18-km/h) criterion can become overly conservative.] In Federal Highway Administration (FHWA) Notice TO-20 (10) the criterion was converted from velocity change to a 1100-lbf/s (4892-N/s) momentum change. This 1100-lbf/s impulse is equivalent to a car that weighs 2000-4000 lb (907-1814 kg) undergoing a change in velocity from 12.1 to 6.0 mph (from 19.7 to 9.7 km/h). In 1975, the American Association of State Highway and Transportation Officials (AASHTO) (11) indicated that the preferred maximum momentum change should be 750 lbf/s (3336 N/s). In addition to luminaire supports, this criterion has been applied to other breakaway devices such as sign supports and devices that bend over on impact (12). Because of the protracted duration of collisions with yielding supports, Edward's criterion was modified in Transportation Research Circular (TRC) 191 (12) to apply only to that portion of the test vehicle or pendulum momentum change that occurred prior to the hypothetical impact of the occupant on the dashboard (stage 1).

A third set of vehicle-dynamics criteria was developed by Tamanini and Viner in 1970 for crash cushions (13). Essentially, vehicles in a weight range of 2000-4500 lb (907-2041 kg) that hit a crash cushion at speeds of up to 60 mph (97 km/h) were to be stopped at an acceleration that averaged less than 12 g. The vehicle average acceleration was computed, when the initial velocity and the total stopping distance were known, by using the equation

$$\bar{a} = V^2/29.9S \quad (1)$$

where $\bar{a}$ is average vehicle acceleration in g, V is vehicle impact speed in miles per hour, and S is the stopping distance in feet. A maximum acceleration onset rate of 500 g/s was also stipulated. FHWA collected more than 400 crash-cushion accident records, and the findings convincingly showed that devices that meet these criteria perform well in actual service (14).

A summary of existing occupant risk criteria is shown in Figure 2 [from TRC 191 (12)].

NEED FOR NEW MODEL

The question may be asked whether there is need for

Figure 1. Occupant flail-space kinematics.

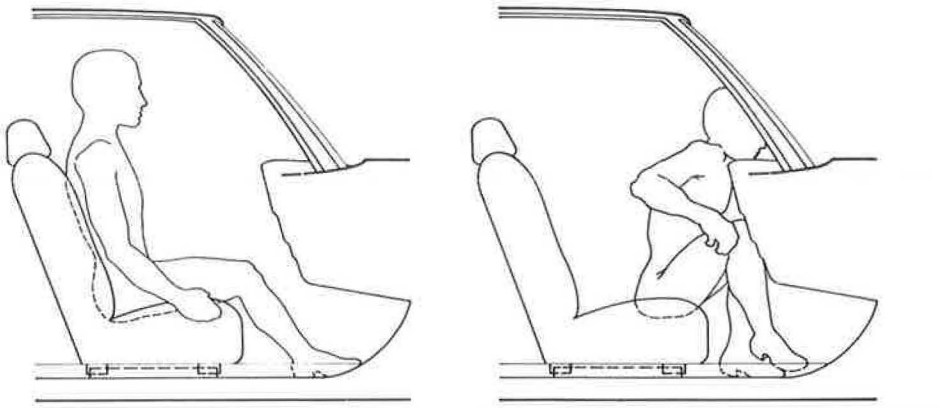

(a) Occupant Position at Instant of Vehicle/Barrier Impact

(b) Occupant Poisition at Instant of Impact with Instrument Panel/ Windshield and During Subsequent Vehicle Ridedown

Figure 2. Summary of TRC 191 evaluation criteria.

Evaluation Criteria	Applicable Criteria for Appurtenance			
	Longitudinal Barriers			
	Length-of-Need and Transitions	Terminals	Crash Cushions	Breakaway or Yielding Supports
A. Where test article functions by redirecting vehicle, maximum vehicle acceleration (50 ms avg) measured near the center of mass should be less than the following values:	●	●	●	
Maximum Vehicle Accelerations (g's): Lateral 3, Longitudinal 5, Total 6, Remarks Preferred; Lateral 5, Longitudinal 10, Total 12, Remarks Acceptable				
These rigid body accelerations apply to impact tests at 15 deg or less.				
B. For direct-on impacts of test article, vehicle is decelerated to a stop and where lateral accelerations are minimum, the preferred maximum vehicle acceleration average is 6 to 8 g's. The maximum average permissible vehicle deceleration is 12 g, as calculated from vehicle impact speed and passenger compartment stopping distance.		●	●	
C. Maximum momentum change of the vehicle during impact shall be 1100 lb-s (4892 Ns) and preferably less than 750 lb-s (3336 Ns).				●

a new model for occupant risk assessment. The response would be that the three criteria or models now in use are inconsistent, are inadequate measures of occupant risk, and may be overly conservative in some areas.

Even though the ultimate goal of safety performance in the three categories of highway appurtenances (i.e., longitudinal barriers, crash cushions, and breakaway or yielding supports) is to protect the vehicle occupants, the devices are evaluated by different vehicle responses. This inconsistency has caused confusion among researchers, hardware developers, and highway agencies and has unnecessarily added complexity to an existing area of technology.

All present criteria indicate (at least in an overall manner) the degree of occupant risk: The lower the vehicle accelerations and the momentum change are, the less risk is involved in the collision. The momentum-change criterion is probably the best indicator, since it reflects stage 1 occupant impact velocity. The criterion of average accelerations for crash cushions, based on stopping distance, is generally adequate, but there are devices such as lumpy systems that could subject occupants to a more severe ride down than that indicated by the average acceleration value. The criterion of a maximum average vehicle acceleration of 50 ms is probably the least adequate, since this speed may occur prior to the impact between occupant and instrument panel (stage 1) and thus can be irrelevant (except for the velocity change associated with the pulse).

The criterion for longitudinal barriers may be overly conservative to the point at which soon few systems will satisfy the preferred values. The systems that do are characterized as flexible (e.g., cable or weak post devices). These systems are being used by a decreasing number of states. In contrast, the rigid concrete safety shape is one of the more widely used barriers even though the typical crash test severity indicator (e.g., maximum average vehicle acceleration of 50 ms) exceeds the preferred range. In essence, researchers and highway agencies are, to a large degree, ignoring the recommended values and evaluating the crash test performance of a device on a more-subjective basis.

For these reasons, a general and more-indicative model of occupant risk assessment is needed. Such a model, based on the flail-space concept, has been developed and is presented in this paper.

VEHICLE COLLISION ENVIRONMENT

Performance Requirements

Although the main concern of this paper is collision severity as it refers to occupant hazard, appurtenances are evaluated during a series of vehicle crash tests for two other safety performance factors--structural adequacy and vehicle trajectory

hazard (12). For structural adequacy, the appurtenance must exhibit certain design strength properties. Based on its design function, the appurtenance must either smoothly redirect or gently stop the impacting test vehicle or must readily break away from it. In other words, the appurtenance must not snag, abruptly decelerate, or upset the test vehicle. Moreover, neither the appurtenance nor any of its components must penetrate or significantly deform the occupant compartment. Until an appurtenance has met these requirements for structural adequacy, it is generally not considered for occupant-risk evaluation. Vehicle trajectory hazard refers to the path the vehicle takes from the collision to the final stopping location. Ideally, the vehicle will be redirected or stopped near the appurtenance without subjecting adjacent traffic to undue hazard.

Collision Parameters

Occupant hazard during the collision of a vehicle with a roadside appurtenance is dependent on an extremely complex event that has a large number of variables. The more important of these includes (a) geometry, stiffness, mass, and fracture properties of the appurtenance; (b) mass, crush properties, dynamic stability, inertial properties, and impact speed and attitude of the vehicle; (c) occupant seating position and attitude, size, and physical condition; and (d) vehicle compartment space and stiffness, or energy absorption capacity of interior surfaces.

It may be noted that highway engineers have an influence only on the items in (a) and must attempt to accommodate variation in all other parameters. This has required the highway engineer to be extremely conservative and to design for combinations of worst conditions. Even so, the unforeseen rapid sizing down of the passenger vehicle fleet and the increased safety expectancy of the public have made many appurtenances obsolete well before their anticipated life of 20-30 years.

FLAIL-SPACE MODEL

Injury Mechanisms

It is well known that injury depends on dynamic factors such as duration and magnitude of acceleration, velocity, or momentum change as well as on the constitution of the body or part of the body under consideration. Moreover, these dynamic factors are identified by their duration and intensity: impact, dynamic force, and hydraulic force (15). Impact is characterized by such brisk force application as when the head strikes the windshield and the bone structure is fractured. The load history is much shorter than the natural period of the body element. Before the element response has developed, the impulse has elapsed. As far as the element is concerned, there is only a change of momentum, and neither the deceleration intensity nor the pulse duration is independently important. This injury potential is measured by (16)

$$\int_0^t a\,dt = \Delta V \leq (\Delta V)_{limit} \tag{2}$$

where a is acceleration (in feet per second squared) on the body element, t is the pulse duration (in seconds), and ΔV is the change in velocity of the body element (in feet per second). Equation 2 indicates the injury potential at the conclusion of stage 1.

Dynamic force had sufficient duration for the body response to be fully developed; the injury potential depends essentially on the amount of force that acts on the body rather than on the momentum. The sustained dynamic force results in deformation and crushing of the body elements and is measured by (16)

$$a \leq (a)_{limit} \tag{3}$$

where a is acceleration on the body element (in g). Depending on the direction of force application and the body region under consideration, the minimum duration for body response to develop fully varies from 7 to more than 40 ms (17). As the duration of force application decreases from the range of 7-40 ms, the intensity of force required to produce body damage increases (SAE 700398, revised August 1970). Thus, by setting $(a)_{limit}$ in Equation 3 on the lower bound and using a fully developed response of the body and a duration of interest of, say, 10 ms or more, the dynamic-force injury criterion is defined.

The third injury mechanism is a hydraulic phenomenon in which the dynamic forces act for extremely long periods, e.g., several minutes or more. An example of moderate acceleration for long duration is when body fluids have time to drain away from the brain and cause a blackout. In extreme cases, blood vessels will rupture and vital organs will hemorrhage (15). Because vehicle collisions generally have durations of less than 1 s, the hydraulic-force injury mechanism is not a factor in highway safety.

Flail-Space Hypothesis

The hypothesis divides the collision into two stages. In stage 1, the unrestrained occupant is propelled forward and/or sideways in the compartment space due to vehicle collision acceleration and then hits one or more surfaces and/or the steering wheel with a velocity V. Actually, the vehicle accelerates toward the unrestrained occupant. Thus the occupant experiences no injury-producing forces prior to contact with the compartment surface. In stage 2, the occupant is assumed to remain in contact with the compartment surface and experiences the same accelerations as the vehicle throughout the remainder of the collision. The occupant may sustain injury at the end of stage 1 as measured by Equation 2 and/or during stage 2 as measured by Equation 3.

Simplifications

In order to simplify application of the flail-space hypothesis to full-scale crash testing of highway appurtenances, some assumptions are made:

1. The impact time and velocity of the occupant at initial contact with the compartment surface can be calculated from the vehicle acceleration, compartment geometry, and the consideration that the occupant moves as a free body. (The use of anthropomorphic dummies in a crash test is not required.) Results from sled and vehicle crash tests (18) show that simulated occupants respond as a free body within experimental accuracy. If we consider the wide variation in compartment geometry and flail space in the passenger car fleet, the assumption is judged consistent with the precision of occupant hazard assessment. In the event that an unusually high vehicle acceleration peak occurs just prior to the calculated time of occupant impact, one may wish to include the peak as a part of the stage 2 evalua-

tion to allow for imprecision in calculation of impact time.

2. The occupant does not rebound; therefore, the occupant impact velocity is also the occupant relative velocity change. Moreover, the occupant is assumed to remain in contact with the surface and is directly subject to vehicle accelerations. Movies of dummy kinematics during typical vehicle-appurtenance tests confirm that the dummy remains in contact with the surface at least through the period of high vehicle accelerations (18).

3. The occupant is unrestrained by either a lap or shoulder belt. Less than 20 percent of vehicle occupants use the manual restraint systems at the present time. Although the introduction of compulsory automatic restraints is scheduled for the early 1980s, it will be 7-10 years before a majority of the passenger car fleet is so equipped. Thus this assumption is fairly realistic now but will probably become conservative in time.

4. The occupant is a 50th-percentile male and is considered to be in a normal upright and back-sitting position. This establishes the distances that the occupant can traverse prior to hitting an interior surface. It is noted that a smaller flail space, due either to a small passenger compartment or to the occupant's sitting forward or closer to the impact side, will generally lessen the impact velocity of the occupant on the interior surface.

5. The compartment remains intact; there are no inward penetrations or partial collapse that would affect the occupant trajectory. Also, the windows and doors remain closed during the impact.

6. For redirection or side impacts, only the near-side occupant is considered critical. This coincides with accident statistics to be discussed in the next section.

7. Vehicle accelerations are measured at vehicle center of mass. Only forward and lateral accelerations are considered; since the vehicle remains upright, vertical accelerations are limited to subcritical values.

8. Pitching and rolling motions of the vehicle are not explicitly considered. Front-seat occupant positions are near and just aft of the center of mass for both compact and subcompact sedans; thus these motions do not significantly affect the occupant impact velocities.

HUMAN TOLERANCES

Degree of Injury

Occupant risk is ultimately referenced to the degree of injury sustained by the vehicle occupant during collision. Ideally, the roadside appurtenance should perform so that the degree of injury is zero; however, this is technically unattainable, regardless of cost (19).

In recent years, a number of injury scales have been used by highway accident investigators to quantify the degree of injury and collision severity. The Abbreviated Injury Scale (AIS) (20), developed and endorsed by the American Association for Automotive Medicine, has emerged as a national and international standard. The scale is presented below. AIS-80 is used in this report and links laboratory and experimental research with actual highway experience.

Code	Category
0	No injury
1	Minor
2	Moderate
3	Severe (not life threatening)
4	Serious (life threatening, survival probable)
5	Critical (survival uncertain)
6	Maximum (currently untreatable)
9	Unknown
-	Death (recorded or separate element)

In line with current Federal Motor Vehicle Safety Standard (FMVSS) 208, an upper design limit for occupant protection falls between codes 3 and 4. That is, severe injury is accepted as long as it is not life threatening. This seems to be a reasonable upper bound for appurtenance safety performance. Depending on the class of appurtenance, the mechanics involved, and the state of the possible, the developer and the highway agency would, of course, be encouraged to set the acceptable injury level at a lower code. As discussed in the subsequent section, this can be accomplished by dividing the vehicle dynamic response factor that corresponds to the code 3 or 4 limit by the appropriate design margin.

Threshold Values

Human tolerances and injury responses are presented in Table 1 as a function of the abrupt velocity change that occurs when the occupant, dummy, test animal, or cadaver hits a rigid or yielding surface or restraint system. Results have been assembled from sled tests with both human and animal subjects and from automobile and other types of accident data. It is noted that some accident statistics were gathered prior to 1965 and represent the more-hostile environment of the automobile compartment space before the emphasis on safety, e.g., cluttered instrument panel, unyielding windshields, and noncollapsible steering columns.

Longitudinal Velocity Change

Based principally on head impacts into windshields at velocities that range from 44 to 51 fps (13-16 m/s) and a FMVSS 208 head injury criterion less than 1000, a nominal 40 fps (12 m/s) appears to be a reasonable upper impact velocity threshold [$(\Delta V)_{limit}$] for unrestrained occupants that strike the instrument panel or windshield. It is believed that the 40-fps (12-m/s) value is consistent with the compartment design and padding of most of the current vehicle population. As a frame of reference, it is noted that a crash cushion designed to the current TRC 191 12-g criterion could subject the occupants to a 39-fps (12-m/s) impact velocity with the dashboard or windshield. Obviously, an appurtenance developer should strive to achieve a lower occupant impact velocity and thus further reduce the risk to the occupants. The design ΔV can be established by the equation

$$(\Delta V)_{design} = (\Delta V)_{limit}/F \quad (4)$$

where F is an appropriate factor of safety, governed to a large extent by the state of the possible with the consideration that there are sometimes conflicting requirements of vehicle sizes within the traffic population.

For test purposes, the longitudinal impact velocity of the unrestrained occupant can be experimentally acquired from instrumented dummies, from analysis of high-speed movies of dummy kinematics, or from calculations, if we assume that the occupant moves as a free missile toward the compartment surface, propelled by vehicle accelerations. In the calculations, a 2-ft (0.6-m) travel space may be

Table 1. Summary of expected effects of abrupt velocity change on injury severity.

Body Element	Impact Surface	Impact Velocity (ft/s)	Severity	Acquisition Method	Ref.
Longitudinal Direction					
Whole	Contoured couch	80	Survival limit	Accident cases; human in supine position	16, p. 335
	Couch/head pad	53.6	Gross injury limit	Empirical and general testing	17, p. 211
	Aviator restraint	48	AIS 3	Sled test of human (Capt. Beeding)	16, p. 341
	Unspecified	34	AIS ≥ 5	Automobile statistics prior to 1960	16, p. 342
	Three-point restraint	47	OAIS ≤ 3	Accident data from Germany	21, p. 217
Head	Windshield (several types)	44	HIC < 1000	Wham III sled tests with dummy	22, p. 560
	Windshield (type 10-20)	51	HIC < 700	Wham III sled tests with dummy	23, p. 155
Whole	Lap and/or shoulder belt	39	Fatality threshold	Literature review	15, p. 34
	Unspecified	39[a]	Acceptable (crash cushion)	Occupant/vehicle impact based on constant 12 *g* and 2-ft distance	12, p. 10
	Unspecified	32[a]	Preferred (crash cushion)	Occupant/vehicle impact based on constant 8 *g* and 2-ft distance	12, p. 10
	Unspecified	36[a]	Acceptable (redirectional barrier)	Occupant/vehicle impact based on constant 10 *g* and 2-ft distance	12, p. 10
	Unspecified	25[a]	Preferred (redirectional barrier)	Occupant/vehicle impact based on constant 5 *g* and 2-ft distance	12, p. 10
	Unspecified	11[a]	Preferred (breakaway support)	Occupant/vehicle impact based on 2250-lb car and 750 lbf/s	12, p. 10
	Unspecified	16	Acceptable (breakaway support)	Occupant/vehicle impact based on 2250-lb car and 1100 lbf/s	12, p. 10
Lateral Direction					
Whole	Vehicle interior	30-37	10 percent AIS ≥ 4	MDAI accident files	24, p. 8
	Vehicle interior	58	100 percent AIS ≥ 4	MDAI accident files	25, p. 8
Chest	Vehicle interior	30	AIS ≤ 3	FMVSS 214 Advance Notice	25
Whole	Vehicle interior	32	0 percent AIS ≥ 3	Car-to-car accident statistics (France) (near-side occupant, no intrusion)	26, p. 202
	Vehicle interior	23	22 percent AIS ≥ 3	Car-to-car accident statistics (France) (near-side occupant, with intrusion)	26, p. 202
	Vehicle interior	31	50 percent ≥ 3	Car-to-fixed-object statistics (France)[b]	26, p. 209
	Vehicle interior	19	10 percent ≥ 3	Car-to-fixed-object statistics (France)[b]	26, p. 209
	Lap and shoulder belt	39	Fatality threshold	Literature review	15, p. 34
	Lap belt or unrestrained	20	Fatality threshold	Literature review	15, p. 34
	Unspecified	18[a]	Acceptable (redirectional barrier)	Occupant/vehicle impact based on constant 5 *g* and 1-ft distance	12, p. 10
	Unspecified	14[a]	Preferred (redirectional barrier)	Occupant/vehicle impact based on constant 3 *g* and 1-ft distance	12, p. 10

Notes: Force = ΔV. 1 ft/s = 0.3 m/s; 1 lb = 0.45 kg. OAIS = Occupant Abbreviated Injury Scale. HIC = head injury criteria. MDAI = Multidisciplinary Accident Investigation.
[a]Calculated from TRC 191 criterion. [b]Generally with compartment intrusion.

assumed when actual values are unknown.

Lateral Velocity Change

Most human tolerance data for lateral impact have been acquired from automobile accident data files. The following factors complicate analysis of accident statistics:

1. The occupant next to the affected side sustains a higher level of injury than does the far-side occupant (26,27),
2. The injury to the near-side occupant is greater when there is intrusion to the compartment space (26),
3. Collisions between the side of a car and a fixed object are generally more severe than car-to-car impacts (26,27), and
4. Restraint systems provide little benefit other than ejection prevention for the near-side occupant (26).

The human being may exhibit similar longitudinal and lateral velocity change tolerances; however, this fact cannot be concluded from automobile accident data. This is probably due to compartment-space intrusion, which is typical of car-to-car and car-to-fixed-object collisions. When the compartment space is not intruded, an upper lateral occupant impact velocity of 30 fps (9 m/s) appears to be a reasonable limit that is consistent with the FMVSS 214 Advance Notice proposal and with accident statistics from France (Table 1). It is noted that compartment-space intrusion rarely, if ever, occurs during vehicle redirectional crash tests. On the other hand, accident records show that side intrusion frequently occurs when the vehicle skids sideways into a rigid narrow fixed object or even into a breakaway support. Breakaway performance for side-impact conditions is not specified or evaluated by crash testing at present. If such a requirement is deemed necessary in the future, performance of a breakaway device should first be assessed for the lack of compartment intrusion and then for occupant collision risk.

To be noted in Table 2 are the lateral velocity changes that can be inferred by TRC 191 (12) severity criteria. As with the threshold level of the longitudinal velocity change, this value is divided by an appropriate factor F to establish a less-severe design limit.

Accelerations

For the unrestrained conditions, the occupant experiences essentially no absolute accelerations prior to hitting some part of the compartment surface; that is, the vehicle is accelerating relative to the occupant. At impact, the degree of injury sustained by the occupant is indicated by the occupant and compartment impact velocity. Subsequent to this impact, the occupant is assumed to remain in contact with the surface hit and then to directly experience the vehicle accelerations. The occupant may or may not sustain further injuries, depending on the magnitude of these accelerations.

Typical long-term acceleration values are presented in Table 2 for both longitudinal and lateral directions. For both directions it appears that an upper limiting value of 20 g is survivable, even for pulses of long duration. Even discounting the lower threshold record for smoothed 50-ms accelerations, current values from TRC 191 are probably unnecessarily conservative in order to minimize the unconsidered stage 1 occupant and compartment impact. As with the velocity change, it is suggested that the

Table 2. Summary of expected effects of average acceleration on injury severity.

Body Element	Impact Surface	Acceleration (g)	Severity	Acquistion Method	Ref.
Longitudinal Direction, Acceleration Force					
Whole	Contoured couch	20	Survival limit	Sled tests; human in supine position	16, p. 335
	Contoured couch	40	Critical long term	Empirical	17, p. 211
	Aviator restraint	40	Survival limit	Sled tests; human in sitting position	27, p. 739
	Lap and shoulder belts	25[a]	Reasonable limit	Literature review	15, p. 34
	Lap belt only or no belt	20[a]	Reasonable limit	Literature review	15, p. 34
	Unspecified	12	Maximum acceptable (crash cushion)	Average test vehicle acceleration calculated from stopping distance	12, p. 10
	Unspecified	8	Preferred (crash cushion)	Average test vehicle acceleration calculated from stopping distance	12, p. 10
	Unspecified	10	Maximum acceptable (redirectional barrier)	Maximum vehicle acceleration (50-ms avg)	12, p. 10
	Unspecified	5	Preferred (redirectional barrier)	Maximum vehicle acceleration (50-ms avg)	12, p. 10
Lateral Direction, Acceleration Force					
Whole	Aviator restraint	33.6	Fainting shock	Sled tests; human in sitting position	SAE 700 398, p. 740
	Aviator restraint	25	Reversible injury	Sled tests; human seated facing forward	SAE 700 398, p. 742
Chest	Unspecified	60	Survival limit	FMVSS 214 performance criteria (proposed)	24, p. 24
Whole	Lap and shoulder belts	25[a]	Reasonable limit	Literature review	15, p. 34
	Lap only or no belt	20[a]	Reasonable limit	Literature review	15, p. 34
	Unspecified	5	Maximum acceptable (redirectional barrier)	Maximum vehicle acceleration (50-ms avg)	12, p. 10
	Unspecified	3	Preferred (redirectional barrier)	Maximum vehicle acceleration (50-ms avg)	12, p. 10

[a]Average over duration of event.

20-g upper limit be divided by an appropriate factor to obtain an appropriate design acceleration level.

The vehicle acceleration values to be compared with the design levels are the highest 10-ms averages that occur during the pulse duration that begins at, or just prior to, the calculated time of occupant impact. It is noted that, when compared to the highest 50-ms averages, test data processed to the 10-ms average requirement will generally result in higher acceleration indices.

Recommended threshold and design values for both occupant impact velocity and accelerations are presented in Table 3.

APPLICATION

Test Conditions

Highway appurtenances are evaluated by occupant risk under selected test conditions (12). Generally excluded are tests to evaluate the structural adequacy of a system or device. Because of its low mass, the small-car tests of length of need and terminals of longitudinal barriers, crash cushions, and breakaway or yielding supports are critical, since velocity changes and acceleration levels are greater than they are for heavier vehicles. The larger passenger sedan end-on impact into the guardrail terminal and crash cushion is also evaluated for occupant risk.

Data Acquisition and Processing

Vehicle accleration data are acquired according to SAE J211b, Channel Class 180, for processing and integration for free-missile velocity and displacements (28). Typical test data results are shown as a function of time in Table 4.

To determine the occupant impact velocity, the longitudinal and lateral accelerations of the vehicle are integrated to acquire occupant relative velocity and relative displacement as a function of time after initial vehicle impact. At the instant the occupant has traveled, say, 2 ft (0.6 m) in the longitudinal direction and/or, say, 1 ft (0.3 m) in the lateral direction, the occupant relative velocity is calculated or read, which yields the hypothetical occupant impact velocity.

The vehicle 10-ms average accelerations are scanned (Table 4) from the instant of occupant impact to the end of the pulse or impact event. The highest value is identified. Since the time of occupant impact is an approximation, one may wish to expand the time of interest from 20 to 40 ms before impact on through the pulse duration. It is noted in Table 4, for example, that very little occupant movement occurs in the first half of the 155-ms flail duration.

Critical values from Table 4 are as follows (1 fps = 0.3 m/s):

	Occupant Impact	
Impact Direction	Velocity (fps)	Acceleration (g)
Longitudinal	Not critical	Not critical
Lateral	17.0	9.7

These values are then compared with those in Table 3.

For redirectional barrier impacts, the occupant impact velocity is sensitive to the actual vehicle impact conditions; that is, occupant lateral impact velocity will be higher when either the actual vehicle impact velocity or the approach speed (or both) exceeds the target test conditions. Accordingly, when the actual vehicle impact conditions vary from the target conditions, the occupant impact velocity should be normalized to the target conditions by the following equation:

$$(\Delta V)^* = [(V \sin\phi)_{target}/(V \sin\phi)_{actual}](\Delta V) \quad (5)$$

where $(\Delta V)^*$ is normalized occupant impact velocity (in feet per second), (ΔV) is occupant impact velocity for actual test conditions (in feet per second) and $[(V \sin\phi)_{target}/(V \sin\phi)_{actual}]$ is

Table 3. Occupant risk values.

Appurtenance Type	Occupant/Dashboard Impact Velocity[b] (fps)			Occupant Ride-Down Acceleration[e] (g)		
	Flail-Space Recommendation			Flail-Space Recommendation		
	$(\Delta V)_{limit}/F$[c]	$(\Delta V)_{design}$	TRC 191[d]	$(a)_{limit}/F$	$(a)_{design}$	TRC 191[f]
Longitudinal (X) Direction[a]						
Breakaway/yielding support						
Sign and luminaire	40/2.67	15	11-16	20/1.33	15	
Timber utility pole	40/1.33	30		20/1.33	15	
Vehicle deceleration device						
Crash cushion and barrier terminal	40/1.33	30	32-39	20/1.33	15	
Redirectional barrier						
Longitudinal, transition, and crash cushion side impact	40/1.33	30	25-36	20/1.33	15	
Lateral (Y) Direction[a]						
Redirectional barrier						
Longitudinal, transition, and crash cushion side impact	30/1.50	20	14-18	20/1.33	15	

[a] With respect to vehicle axis.
[b] Occupant to windshield, dashboard, or door impact velocity; occupant propelled by vehicle deceleration pulse through 2-ft forward or 1-ft lateral flail space.
[c] F is design factor.
[d] Values calculated from Transportation Research Circular 191 criteria assuming most severe interpretation.
[e] Flail-space accelerations are highest 10-ms averages from occupant impact to completion of pulse.
[f] TRC 191 accelerations are less severe, highest 50-ms averages or those averaged over vehicle stopping distance and are not directly comparable.

Table 4. Evaluation of typical redirecting barrier for occupant risk.

SwRI Test—SRB-4 Vehicle Type—Mini-Auto Vehicle Wt.—2083 lbs
Test Date—10/24/1979 Nominal Impact Vel.—60.0 mph Nominal Impact Angle—15.0 degrees

Time-Sec.	Vehicle Acceleration-G's*		Occupant Velocity-ft/sec		Occupant Displacement-inches	
	AX	AY	VX	VY	DX	DY
.000	-1.7	.7	.0	.0	.0	.0
.005	.3	.6	.1	.1	.0	.0
.010	.6	-.2	-.0	.1	.0	.0
.015	.1	.1	-.1	.1	.0	.0
.020	.2	-.0	-.1	.1	-.0	.0
.025	-.5	.0	-.0	.1	-.0	.0
.030	-.3	.4	.1	.1	-.0	.0
.035	-1.9	5.1	.4	.9	.0	.1
.040	-.0	3.0	.3	1.4	.0	.1
.045	-2.1	3.5	.7	2.0	.1	.2
.050	-3.0	2.3	1.1	2.4	.1	.4
.055	-2.7	4.1	1.5	2.9	.2	.5
.060	2.2	3.2	1.3	3.6	.3	.7
.065	-1.9	5.2	1.6	4.4	.4	.9
.070	-1.2	1.5	1.8	4.6	.5	1.2
.075	-1.7	1.5	2.1	4.9	.6	1.5
.080	-2.7	3.2	2.5	5.3	.7	1.8
.085	-1.8	3.0	2.7	5.9	.9	2.2
.090	.2	3.2	2.7	6.3	1.0	2.5
.095	-2.2	3.3	3.0	6.9	1.2	2.9
.100	.5	4.4	3.0	7.6	1.4	3.3
.105	-1.0	4.5	3.2	8.3	1.6	3.8
.110	-.9	7.0	3.3	9.4	1.8	4.4
.115	-1.6	7.7	3.5	10.6	2.0	5.0
.120	-2.9	6.4	4.0	11.7	2.2	5.6
.125	-1.2	6.0	4.2	12.6	2.5	6.4
.130	-2.1	8.6	4.5	14.0	2.7	7.1
.135	1.0	.6	4.3	14.1	3.0	8.0
.140	-1.4	5.5	4.6	15.1	3.2	8.9
.145	-.1	4.7	4.6	15.8	3.5	9.8
.150	.4	3.8	4.6	16.4	3.8	10.8
.155	.1	4.4	4.6	17.0	4.1	11.8
.160	-1.1	5.7	4.8	18.0	4.4	12.8
.165	-1.8	9.7 ←	5.0	19.5	4.7	13.9
.170	-.4	7.8	5.1	20.7	5.0	15.1
.175	-1.5	8.4	5.3	22.2	5.3	16.4
.180	-.7	8.1	5.4	23.4	5.6	17.8
.185	-1.9	5.6	5.7	24.4	5.9	19.2
.190	.5	5.1	5.7	25.2	6.3	20.7
.195	.2	4.6	5.7	26.0	6.6	22.3
.200	.4	3.3	5.6	26.5	7.0	23.8
.205	-.3	1.4	5.7	26.8	7.3	25.4
.210	-.5	1.1	5.8	27.0	.7	27.1
.215	.2	.7	5.8	27.1	8.0	28.7
.220	.6	.7	5.7	27.2	8.3	30.3
.225	-1.2	.5	5.8	27.3	8.7	31.9
.230	.5	-.2	5.7	27.3	9.0	33.6
.235	.2	-1.8	5.8	27.0	9.4	35.2
.240	-.6	-1.1	5.8	26.9	9.7	36.8
.245	-.4	.6	5.9	26.9	10.1	38.4
.250	-.4	-.5	6.0	26.8	10.4	40.0

Summary
Vy = 17.0 fps
Ay = 9.7 g
V_x, A_x Non-critical as occupant moves less than 24 in.

*10 ms moving average; analog signal sampled at minimum rate of 1000 per second.

Note: 1 mph = 0.45 m/s; 1 lb = 0.45 kg; 1 fps = 0.3 m/s; 1 in = 25 mm.

Table 5. Typical longitudinal barrier severity tests.

Item	Southwest Research Institute Crash Test[a]				
	RF-22	CMB-7	CMB-9	CMB-13	SRB-4
	Barrier Type				
	Vertical Concrete Wall	GM Safety Shape	NJ Safety Shape	F Safety Shape	Self-Restoring Thrie Beam
Test condition					
Vehicle mass (lb)	2140	2250	2250	2250	2083
Impact speed (mph)	61.9	57.1	58.9	56.4	54.7
Approach angle (°)	18.3	16.5	15.5	14.3	17.1
TRC 191 evaluation					
Vehicle acceleration (highest 50-ms avg, *g*)					
Lateral/maximum limit	16.1/5	4.6/5	6.0/5	7.3/5	9.7/5
Longitudinal/maximum limit	8.2/10	3.4/10	0.9/10	3.8/10	3.0/10
TRC 191 appraisal	Poor (lateral acceleration)	Good	Marginal	Marginal	Poor
Flail-space evaluation					
Occupant lateral impact velocity (fps)					
Test	28.0	22.4	17.7	16.2	17.0
Normalized[a]	22.4	21.4	17.5	17.8	16.4
Design limit[b]	20.0	20.0	20.0	20.0	20.0
Occupant ride-down lateral acceleration (highest 10-ms avg, *g*)					
Test	8.6	4.8	4.9	4.6	9.7
Design limit[b]	15.0	15.0	15.0	15.0	15.0
Flail-space appraisal	Poor	Marginal	Good	Good	Good

[a]Occupant impact velocities normalized by the factor $[(V \sin\phi)_{target}/(V \sin\phi)_{actual}]$. [b]As suggested in Table 3.

the ratio of target to actual vehicle impact conditions.

Results from five occupant-risk tests of longitudinal barriers are shown in Table 5. Test RF-22 is on a vertical rigid concrete wall. Tests CMB-7, CMB-9, and CMB-13 are on concrete safety shapes. Test SRB-4 is on a semiflexible metal beam barrier.

SUMMARY

A new criterion of highway-appurtenance crash-test evaluation is presented. The criterion evaluates all appurtenances regardless of function to the same flail-space approach and thus presents a more-consistent evaluation yardstick. The new criteria should simplify data acquisition and processing. Finally, the criteria and the suggested threshold values are not believed to be significantly more stringent or liberal than current evaluation standards.

REFERENCES

1. N.E. Shoemaker. Summary Report of Highway Barrier Analysis and Test Program. Cornell Aeronautical Laboratory, Cornell Univ., Buffalo, NY, Rept. VJ-1472-V-3, 1961.
2. M.D. Graham, W.C. Burnett, J.L. Gibson, and R.H. Freer. New Highway Barriers: The Practical Application of Theoretical Design. HRB, Highway Research Record 174, 1969, pp. 88-183.
3. R.M. Olson, E.R. Post, and W.F. McFarland. Tentative Service Requirements for Bridge Rail Systems. NCHRP, Rept. 86, 1970.
4. E.F. Nordlin, J.H. Woodstrom, R.P. Hackett, and J.J. Folsom. Dynamic Tests of the California Type 20 Bridge Barrier Rail. HRB, Highway Research Record 343, 1971, pp. 57-74.
5. J.D. Michie and M.E. Bronstad. Location, Selection, and Maintenance of Highway Traffic Barriers. NCHRP, Rept. 118, 1971.
6. M.E. Bronstad and J.D. Michie. Recommended Procedures for Vehicle Crash Testing of Highway Appurtenances. NCHRP, Rept. 153, 1974.
7. T.C. Edwards, J.E. Martinez, W.F. McFarland, and H.E. Ross. Development of Design Criteria for Safer Luminaire Supports. NCHRP, Rept. 77, 1969.
8. L.M. Patrick, H.J. Mertz, and C.K. Kroll. Knee, Chest, and Head Impact Loads. Proc., 11th Stapp Car Crash Conference, Anaheim, CA, SAE, New York, 1967, p. 116.
9. C. Blamey. Results from Impact Tests on Telegraph Poles. Highways and Bridges, Vol. 32, 1964, pp. 7, 8, 13.
10. Application of Highway Safety Measures--Breakaway Luminaire Supports. Federal Highway Administration, U.S. Deparment of Transportation, FHWA Notice TO-20, Nov. 1970.
11. Subcommittee on Bridges and Structures. Standard Specifications for Structural Supports for Highway Signs, Luminaires and Traffic Signals. AASHTO, Washington, DC, 1975.
12. Recommended Procedures for Vehicle Crash Testing of Highway Appurtenances. TRB, Transportation Research Circular 191, 1978.
13. F.J. Tamanini and J.G. Viner. Energy-Absorbing Roadside Crash Barriers. Civil Engineering, Jan. 1970, pp. 63-67.
14. J.G. Viner and C.M. Boyer. Accident Experience with Impact Attenuation Devices. Federal Highway Administration, U.S. Department of Transportation, Rept. FHWA-RD-73-71, 1973.
15. M. Chi. Assessment of Injury Criteria in Roadside Barrier Tests. Federal Highway Administration, U.S. Department of Transportation, Rept. FHWA-RD-75-74, Feb. 1976.
16. M. Kornhauser and A. Gold. Application of Impact Sensitivity Method to Animate Structures. In Impact Acceleration Stress, NAS-NRC Publ. 977, 1961, pp. 333-344.
17. P.R. Payne. The Dynamics of Human Restraint Systems. In Impact Acceleration Stress, NAS-NRC Publ. 977, 1961, pp. 195-258.
18. J.D. Michie. Development of Improved Criteria for Evaluating Safety Performance of Highway Appurtenances. Southwest Research Institute, San Antonio, TX, Final Rept., Project 03-9254, June 1980.
19. W.W. Lowrance. Of Acceptable Risk. In Science

and the Determination of Safety, William Kaufmann, Inc., Los Altos, CA, 1976.
20. The Abbreviated Injury Scale (AIS-80). American Association for Automotive Medicine, Morton Grove, IL, 1980.
21. K. Langwielder, M. Danner, and W. Schmelzing. Comparison of Passenger Injuries in Frontal Car Collisions with Dummy Loadings in Equivalent Simulations. SAE Paper 791009, 1979.
22. P.C. Begeman, A.I. King, P. Weigt, and W. Patrick. Safety Performance of Asymmetric Windshields. SAE Paper 780900, 1978.
23. S.E. Kay, J. Pickard, and W. Patrick. Improved Laminated Windshield with Reduced Laceration Properties. Proc., 17th Stapp Car Crash Conference, SAE, New York, 1973.
24. A. Burget and J. Hackney. Status of the National Highway Traffic Safety Administration's Research and Rulemaking Activities for Upgrading Side Impact Protection. Presented at the Seventh International Technical Conference on Experimental Vehicles, Paris, 1979.
25. Side Impact Protection (Upgrade). Federal Motor Vehicle Safety Standard 214, Advance Notice of Proposed Rulemaking. 44 Federal Register 70204, Dec. 1979.
26. F. Hartemann, C. Thomas, J. Foret-Bruno, C. Henry, A. Fayon, and C. Tarriere. Occupant Protection in Lateral Impacts. Proc., 20th Stapp Car Crash Conference, SAE, New York, 1976.
27. J.M. Danner. Accident and Injury Characteristics in Side Collisions and Protection Criteria in Respect of Belted Occupants. Proc., 21st Stapp Car Crash Conference, SAE, New York, 1977.
28. Instrumentation for Barrier Collision Tests: SAE Standard J211b. In Handbook, Society of Automotive Engineers, New York, Dec. 1974 (revised).

Publication of this paper sponsored by Committee on Safety Appurtenances.

Heavy-Vehicle Tests of Tubular Thrie-Beam Retrofit Bridge Railing

C.E. KIMBALL, JR., M.E. BRONSTAD, AND J.D. MICHIE

A retrofit modification has been developed for a current concrete parapet design that has a narrow walkway configuration to improve its safety performance with impacting vehicles. The retrofit was originally developed for and tested with subcompact and standard-sized automobiles; the successful results indicated that the design might also perform with heavier vehicles that weigh up to 40 000 lb (18 144 kg). An earlier paper covered the automobile tests performed with the original retrofit system. Reported here are findings from six vehicle crash tests performed with the retrofit system—four tests with the original design and two tests with a modified design necessitated when vehicle rollovers occurred during the test series. The modified retrofit system successfully redirected a 40 000-lb intercity bus that impacted at 56.3 mph (90.6 km/h) and a 14.5° angle. In addition, it redirected a minicompact automobile that impacted at 58.1 mph (93.5 km/h) and an 18.8° angle; the vehicle exhibited no tendency to wedge under the higher rail design. Tests were documented by using both vehicle accelerometers and high-speed photography.

In a 1976 Federal Highway Administration report (1), existing bridge-rail designs used along the nation's highways are reviewed in terms of current safety performance criteria. Since the majority of these designs were found to be deficient in performance and their replacement to be cost-prohibitive, a methodology for upgrading their performance by retrofitting was developed. One existing design common to many states was a concrete parapet that has a curb and a narrow walkway. Although aluminum and concrete retrofits were developed for this particular bridge rail, the most promising retrofit system appeared to be a steel system that used a back-to-back triple-corrugated beam rail or tubular Thrie beam. Impact tests that used subcompact and standard-sized automobiles were successful, and it appeared that this system might be capable of performance with a heavier vehicle such as a school bus or an intercity bus. This paper presents the results of the continuation program that used heavy vehicles.

ORIGINAL DESIGN

As shown in Figure 1, the original concrete parapet was 25 in (635 mm) high and was located behind a walkway 18 in (457 mm) wide that had a curb 10 in (254 mm) high. This configuration was retrofitted with a tubular Thrie beam 20 in (508 mm) wide attached to the concrete by means of TS6x6x0.1875 box-beam posts spaced at 8.33-ft (2.54-m) intervals and with intermediate collapsing-tube elements 6 in (152 mm) in diameter. The front of the tubular Thrie beam was located in line with the curb face. Rail height was 32 in (813 mm).

The original test installation design was 125 ft (38 m) long and each end was transitioned off the simulated bridge deck into a single Thrie beam 25 ft (7.6 m) long on soil-mounted W6x8.5 steel posts. Each end of the rail was anchored by using a standard 0.75-in (19-mm) cable attached to a concrete footing 24 in (610 mm) in diameter.

MODIFIED DESIGN

Modification to the original retrofit design was deemed desirable when the large vehicle rolled on its side after redirection in the third and fourth tests of the series. These rollovers were attributed to two factors--insufficient rail height and the yield of the collapsing tubes that allowed rail deflection and corresponding vehicle body roll while the nonyielding curb face kept the vehicle wheels along a fixed trajectory. As shown in Figure 2, significant changes to the barrier system were that the beam rail height was increased to 38 in (965 mm) and the 6-in (152-mm) diameter collapsing tube on each post was replaced by a 3-in (76-mm) diameter tube and a TS6x6x0.1875 box-beam spacer. This latter modification projected the beam rail 3 in in

Figure 1. Test installation—initial retrofit of concrete parapet that has narrow walkway.

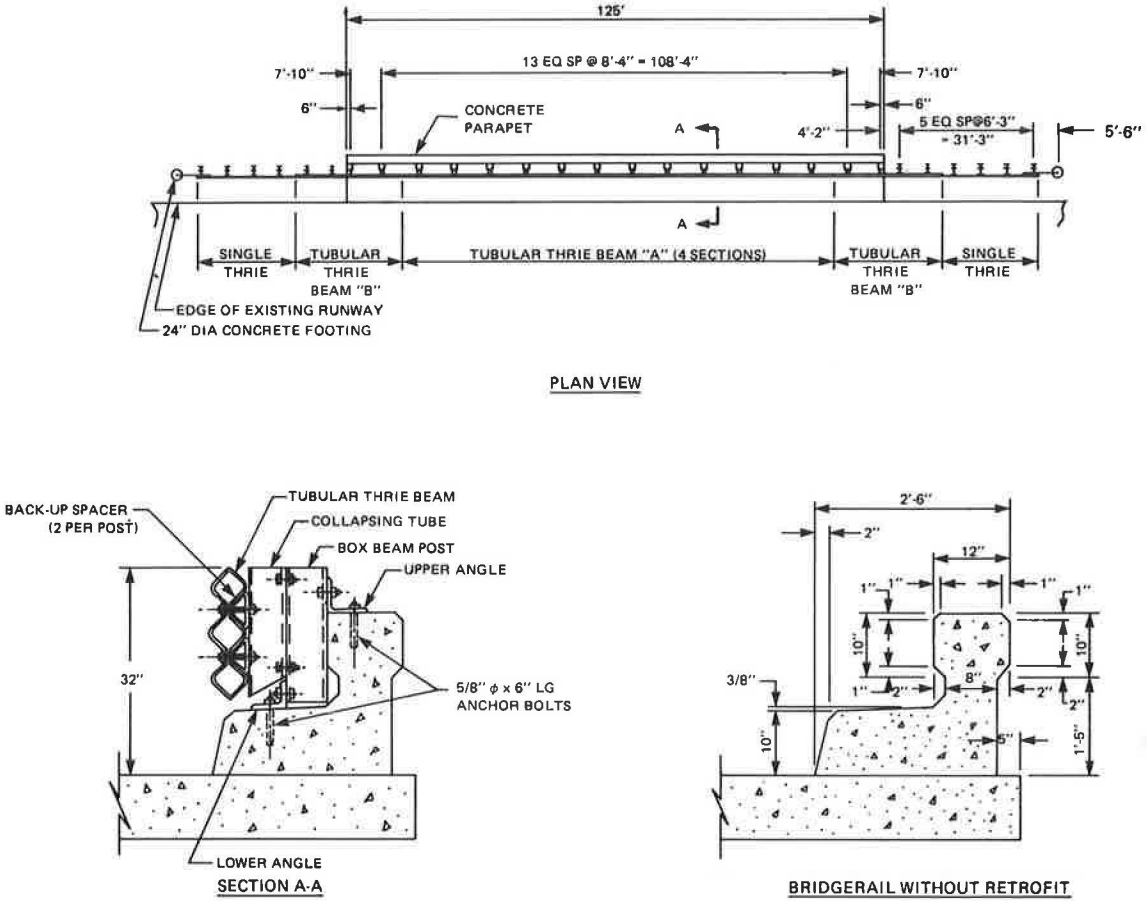

Note: All bolts have 5/8-in diameter.
1 ft = 0.3 m; 1 in = 25 mm.

Figure 2. Modified retrofit design.

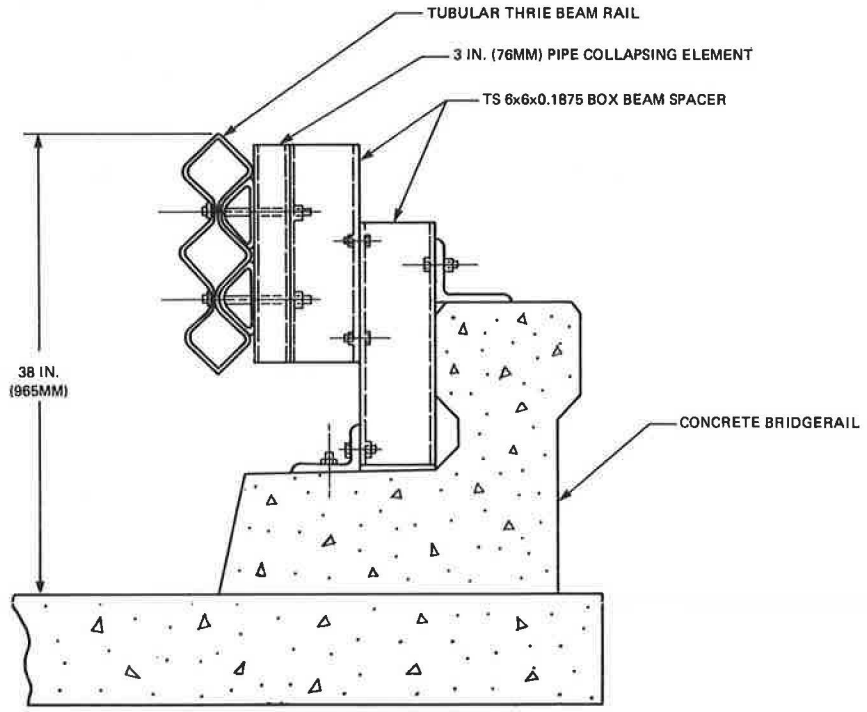

Table 1. Summary of test results.

Test	Barrier Design	Vehicle	Ballast Added (lb)	Vehicle Weight Including Ballast (lb)	Impact Speed (mph)	Impact Angle (°)	Vehicle Acceleration[a] (g)		Maximum Roll Angle (°)	Maximum Permanent Barrier Deflection (in)
							Lateral	Longitudinal		
RF-24	Original	1963 International chassis with Wayne school bus body	7 200	23 000	58.3	6.8	1.4/2.7	-4.6/-0.3	17	5.4
RF-25	Original	1954 GMC Scenicruiser	10 200	40 000	57.2	7.6	1.9/1.7	-0.7/-0.7	10	5.5
RF-26	Original	Same as in RF-24	7 200	23 000	57.1	14.7	2.9/3.9	-6.6/-2.1	90	6.8
RF-27	Original	Same as in RF-25	10 200	40 000	59.7	17.6	0.8/ND[b]	-1.5/ND[b]	90	8.8
RF-28	Modified	1953 GMC Scenicruiser	10 200	40 000	56.3	14.5	1.8/4.1	-4.6/-4.6	14	10.0
RF-29	Modified	1976 Honda Civic	0	1 840	58.1	18.8	6.5/9.6	-4.0/-1.8	0	0

Note: 1 lb = 0.45 kg; 1 mph = 1.6 km/h; 1 in = 25 mm.

[a]Measured by movies/electronics (50-ms average). [b]ND = no data.

Figure 3. Impact sequence for tests RF-24 through RF-29 (top to bottom).

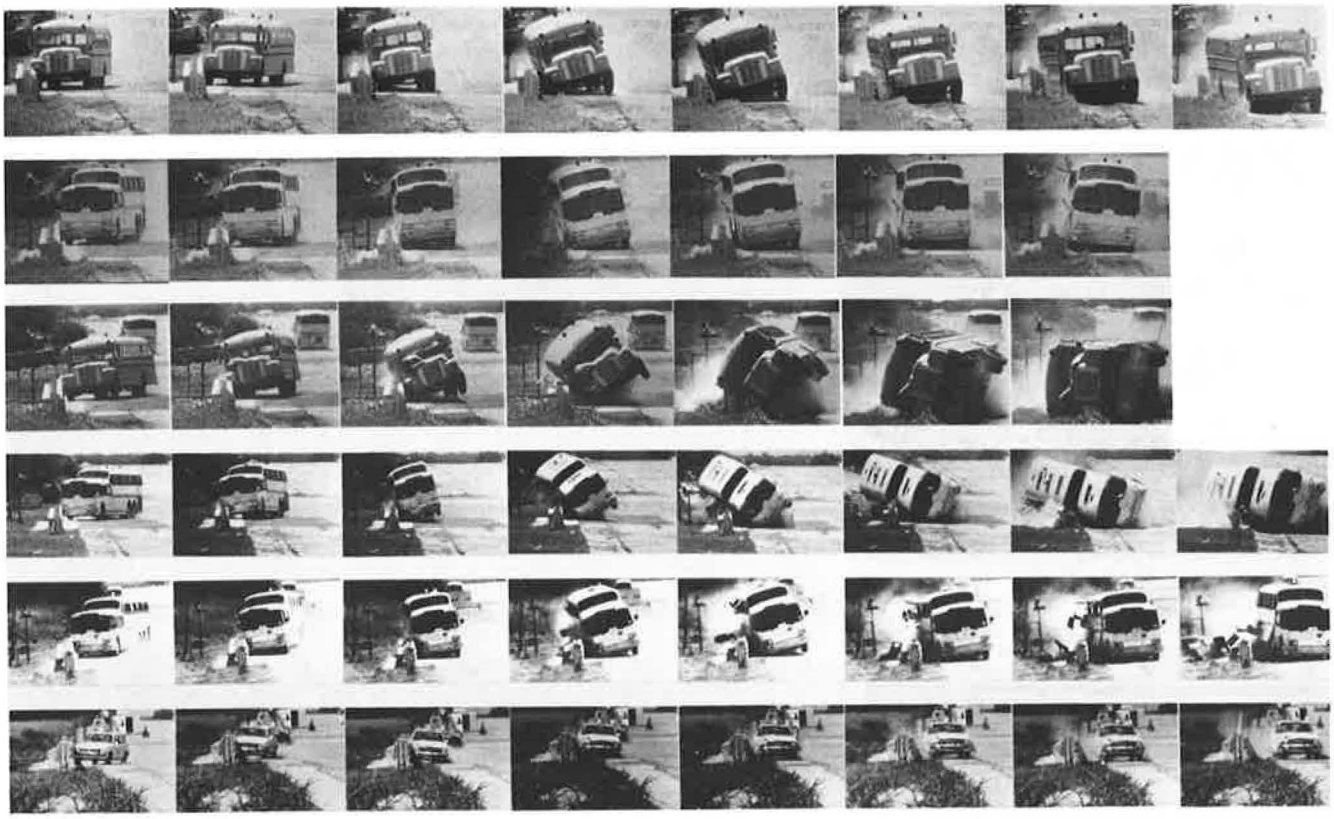

front of the curb face. In addition, intermediate posts (with spacers but without collapsing tubes) were placed midway between the existing posts. These intermediate posts were for severe impacts only, in which front-rail deflections were 3 in or greater, and then presented an effective post spacing of 4.17 ft (1.27 m).

TEST PROGRAM

A series of six vehicle tests was performed; the first four used the original barrier design, whereas the last two used the modified design. A summary of test results is contained in Table 1 and a brief description of each test follows.

Test RF-24

In the initial test of the program, a 23 000-lb (10 433-kg) school bus that impacted the installation at 58.3 mph (93.8 km/h) and a 6.8° angle was readily redirected although it reached a 17° roll angle as shown in Figure 3 (first row). Maximum barrier deflection was 5.37 in (136 mm); seven tube elements required replacement after the test. As shown in Figure 4, the bus received only minor damage and was reusable for test RF-26 after the front fender and bumper had been repaired.

Test RF-25

In this test a 40 000-lb (18 144-kg) intercity bus impacted the barrier at 57.2 mph (92.0 km/h) and a 7.6° angle. As shown in Figure 3 (second row), the barrier was deflected 5.50 in (140 mm), and the bus rolled to a maximum of 10° (toward the barrier) as it was being redirected. Six tube elements required replacement prior to further testing and, as shown in Figure 5, damage to the bus was minimal (mostly sheet-metal damage and a bent wheel); it was reus-

Figure 4. Vehicle and barrier damage, test RF-24.

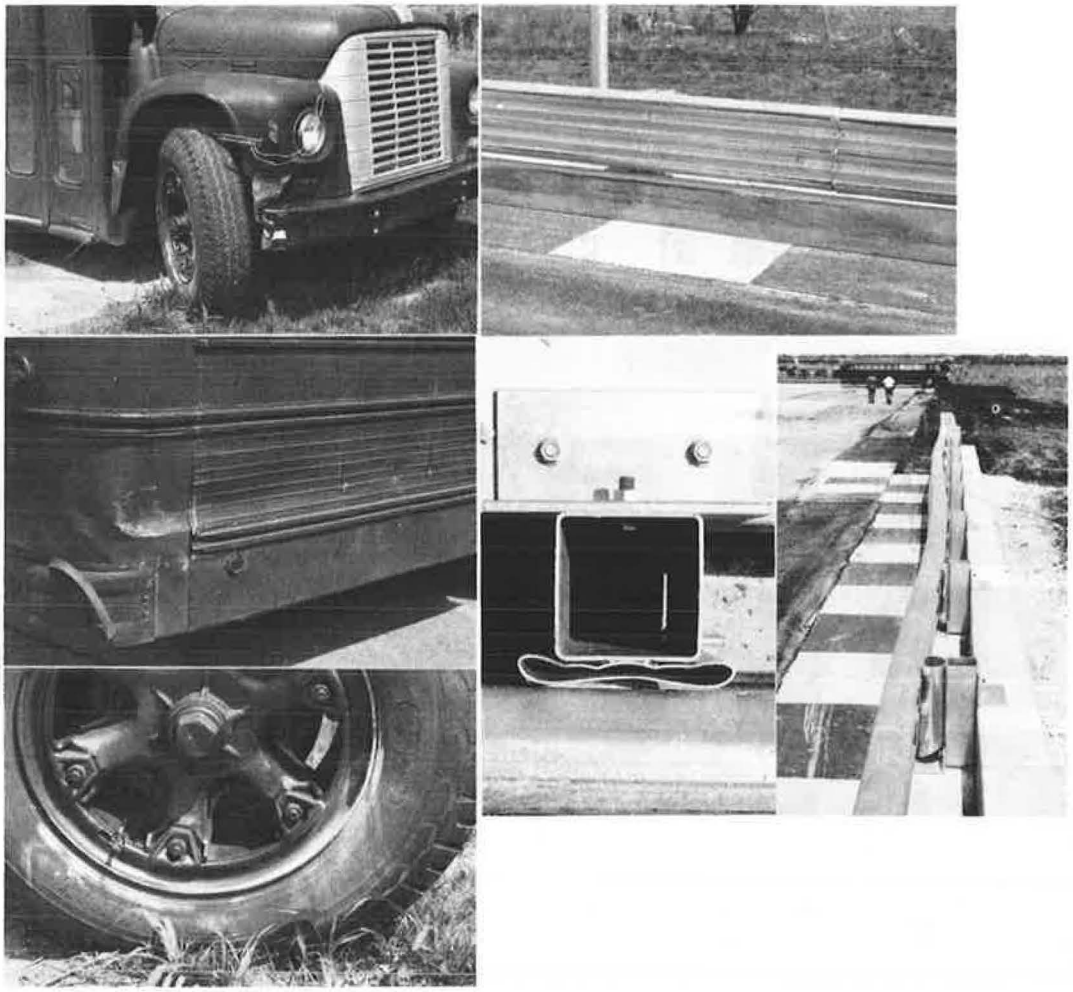

Figure 5. Vehicle and barrier damage, test RF-25.

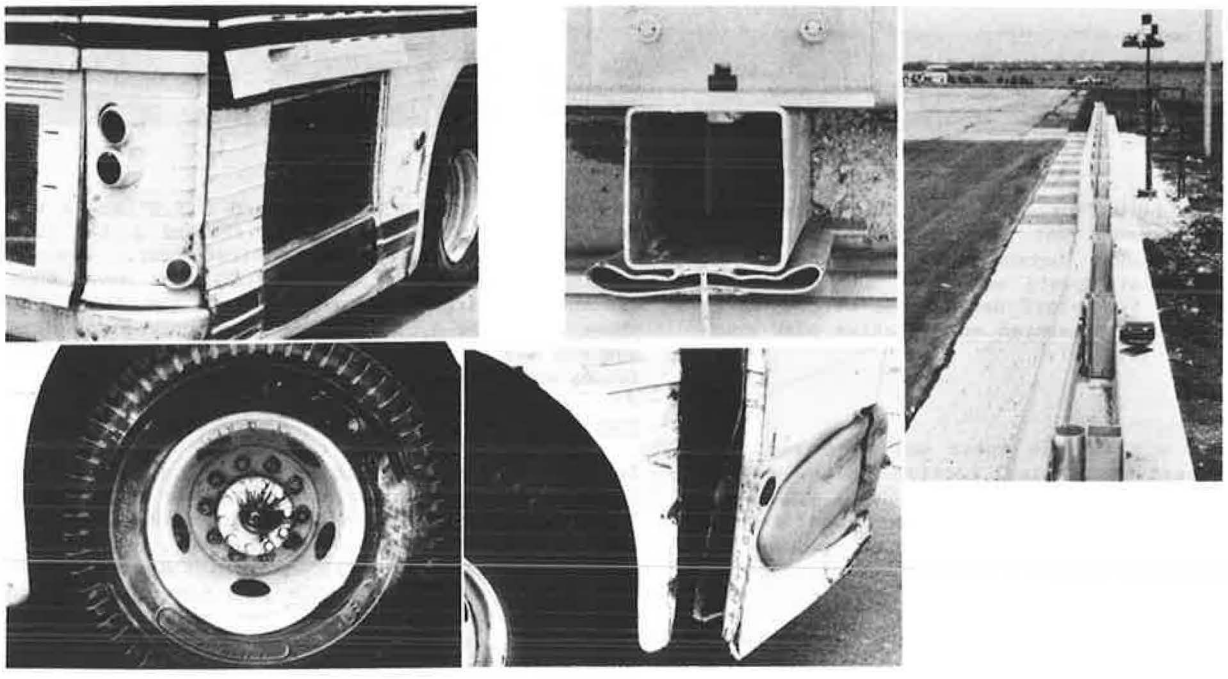

Figure 6. Vehicle and barrier damage, test RF-26.

Figure 7. Vehicle damage, test RF-27.

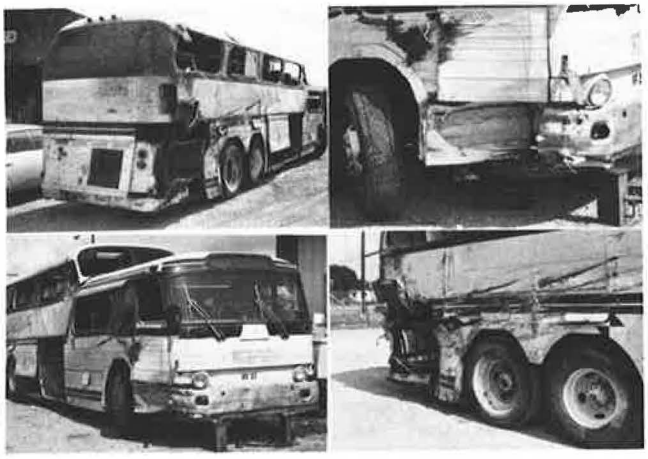

Figure 8. Installation damage, test RF-27.

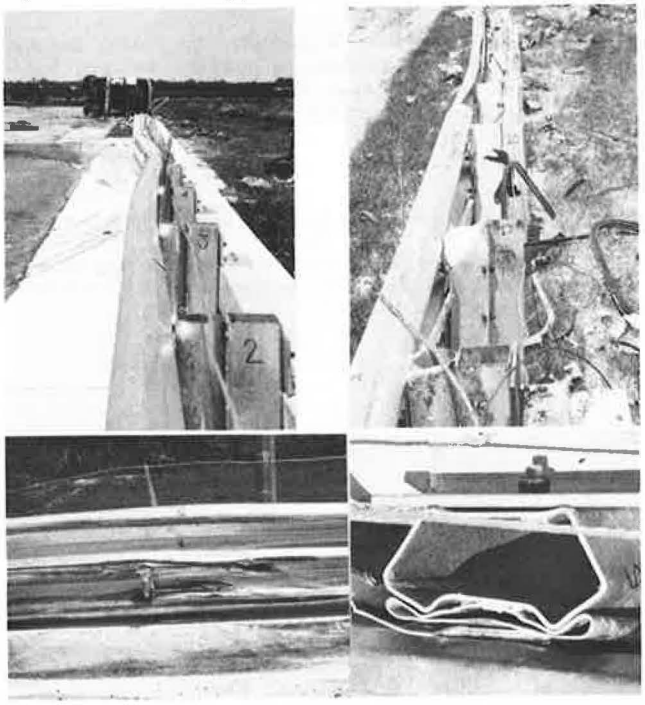

Figure 9. Vehicle damage, test RF-28.

Figure 10. Barrier damage, test RF-28.

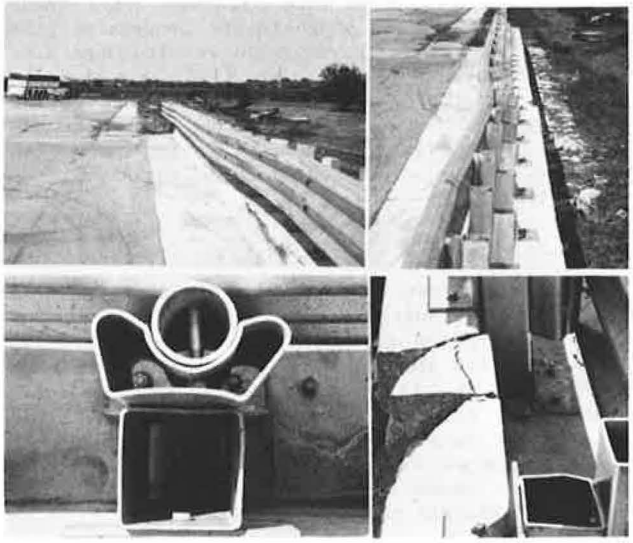

Figure 11. Vehicle and barrier damage, test RF-29.

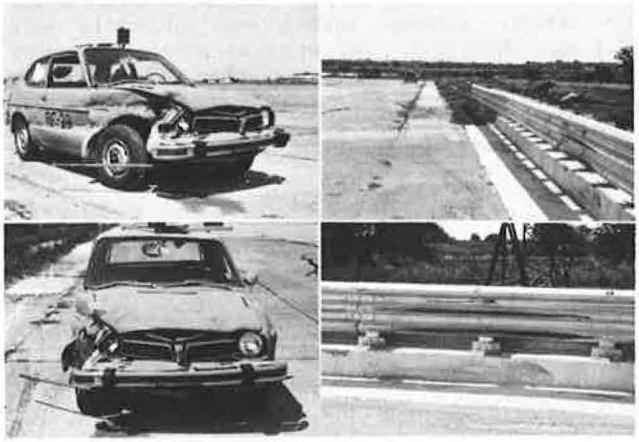

able for test RF-27 after the damaged wheel had been replaced.

Test RF-26

This was a test at a steeper angle (15°) then that of the original design by using the vehicle from RF-24. Impact conditions were 57.1 mph (91.9 km/h) and a 14.7° angle. As shown in Figure 3 (third row) the school bus initially rolled toward the barrier as the front end was being redirected and continued that roll as the rear section impacted. The result was that the bus rolled on top of the barrier and slid on it until the downstream end was reached. At that point the bus dropped to grade and continued sliding an additional 95 ft (29 m). Figure 6 shows the extensive body damage sustained by the bus in the rollover. It also shows the barrier damage, which included deformation to six collapsing-tube elements, two tubular Thrie-beam rail sections, and one post.

Test RF-27

The intercity bus used for RF-25 was reused for this test. Impact conditions were 59.7 mph (96.1 km/h) and a 17.6° angle. As shown in the sequential photographs of Figure 3 (fourth row), results were similar to those of test RF-26; i.e., the vehicle rolled on top of the barrier, slid along it to the end, dropped to grade, and continued sliding an additional 102 ft (33 m). Figures 7 and 8 show the extensive vehicle and barrier damage sustained during the test.

Test RF-28

This was the first test of the modified retrofit design. Test conditions were similar to those of RF-27 in which the rollover occurred. As shown in Figure 3 (fifth row) the bus impacted at 56.3 mph (90.6 km/h) and a 14.5° angle and was smoothly redirected after reaching a maximum roll angle of 14°. The bus was only moderately damaged, as shown in Figure 9, and was driven from the test site. Figure 10 shows the damage sustained by the retrofit system and by the concrete parapet.

Test RF-29

Since the rail height had been increased to 38 in (965 mm), this test was necessary to ensure that smaller automobiles would not become wedged under the front rail of the system. Impact conditions for the 1840-lb (835-kg) minicompact automobile were 58.1 mph (93.5 km/h) and an 18.8° angle. As shown in Figure 3 (bottom row), the vehicle was smoothly redirected and there was no apparent snagging. Figure 11 shows the sheet-metal damage of the vehicle (confined mostly to the right front fender) and the rail and curb scuffing sustained by the barrier. The vehicle suspension and drive train were undamaged, and the vehicle was driven from the test site.

CONCLUSIONS

From the six tests performed, it appears that the tubular Thrie-beam retrofit is quite capable of redirecting the school-bus and intercity-bus classes of test vehicles but that some modifications are required in the original design to prevent the vehicle from rolling on top of the barrier. The following observations were made concerning the retrofit barrier:

1. The original design 32 in (813 mm) high is capable of redirecting heavy vehicles and, at shallow angles, vehicle roll is slight. However, at sharper angles (approximately 15°) vehicle rollover occurs during redirection.
2. Retrofits that use the modified design 38 in (965 mm) high not only will redirect a heavy vehicle but will also greatly reduce its roll angle.
3. The modified design performs well with a minicompact automobile; i.e., redirection occurs and there is no tendency to underride or snag the barrier.
4. Higher bending stresses are placed on the concrete parapet by the modified design, as shown by the concrete failure during test RF-28.
5. The reduced post spacing (by use of interim posts) in the modified design was successful in achieving a stiffer barrier for heavy vehicles. This is shown by the smaller rail deflection of test RF-28 [6.88 in (175 mm)] compared with the 8.75-in (222-mm) deflection measured following test RF-27. It was observed after test RF-28 that three interim posts had been contacted by the tubular Thrie-beam rail and that they provided backup support.
6. Some tuning of the 3-in (76-mm) tube element in the modified design might offer better collapse and energy absorption properties (for automobiles) than the tube that has a 0.216-in (5.5-mm) thick wall that brinells into the box-beam spacer instead of deforming.

REFERENCE

1. J.D. Michie and M.E. Bronstad. Upgrading Safety Performance in Retrofitting Traffic Railing Systems. Federal Highway Administration, U.S. Department of Transportation, Rept. FHWA-RD-77-40, Sept. 1976.

Publication of this paper sponsored by Committee on Safety Appurtenances.

Barrel/W-Section Barriers for Construction Zones

DON L. IVEY AND RICHARD ROBERTSON

The history of barrel/W-section construction barriers is traced. Three crash tests conducted by Southwest Research Institute are analyzed to indicate a probable performance zone for the current barrel/W-section design. This design is the 12-gauge W-section mounted on barrels spaced at intervals of 6 ft 3 in (1.91 m) and filled with sand. Three new designs of barrel/W-section barriers are presented. By using a formal comparative structural analysis, the conventional design and the three new designs are analyzed and predictions are made of comparative performance. Stabilized barrel/W-section 3 is shown to perform at much more critical levels of impact than the current barrel/W-section barrier does. However, its use is applicable where large deflections can be accommodated.

Of the many barrier designs that have found use in construction and maintenance zones, the one that seems to have followed a reasonably well-defined evolutionary path is the barrel/W-section barrier. Over the past 10 years, steel barrels [55-gal (170-L) oil drums] have been put to a wide variety of uses by highway engineers. The range of uses that affect traffic is from simple delineation through barrel crash cushions. When barrels are effectively painted to achieve high visibility and arranged in lines to delineate the appropriate path of vehicles, they form a barricade, depending on their spacing and ballast, to discourage vehicle entry into an inappropriate zone. The physical effectiveness of this barricade is almost negligible except when barrels are spaced closely and filled with heavy ballast. In this case an intruding vehicle will not be redirected by the lines of weighted barrels unless the impact angle is extremely low, but significant deceleration of the vehicle will result.

The next evolutionary step was the addition of a W-section (flex-beam) guardrail. It is not known when this step was taken, but it was probably in the early 1970s. Since there were quantities of used guardrail available, this step probably seemed natural to an engineer, and suddenly the barrel-delineation system was converted from a barrier that had only inertia properties to a barrier that was capable of some significant positive structural redirection. It resulted in stabilization of barrier spacing in multiples of 25 ft (7.62 m), which is the standard guardrail length.

The barrier of this type that has the most positive automobile redirection potential is the standard barrel/W-section barrier shown in Figure 1. It consists of steel barrels spaced 6 ft 3 in (1.91 m) apart that have a section of standard steel flex beam (12 gauge) attached directly to their sides. The top edge of the flex beam is 27 in (68.6 cm) above the ground. The ballast normally used in the barrels is sand, which produces a total barrel weight of approximately 800 lb (363 kg). Although barriers that have larger spacing and lower amounts of ballast are commonly used, either of these changes results in severely decreased barrier performance.

TEST RESULTS

Three tests of the standard barrel/W-section barrier were conducted and reported by Southwest Research Institute (SwRI) early in 1977. These tests were described by Bronstad and Kimball (1) in December 1977. Principal results and descriptions of these three tests are given in Table 1, which shows that tests TB-3 and TB-4 were reasonably acceptable but that test TB-5 was unacceptable. Since experience with this barrier in the field had shown that vehicles occasionally penetrate it, the performance range prior to testing was speculative. SwRI began with the relatively modest impact conditions of a 4500-lb (2040-kg) vehicle that was moving 35.0 mph (57 km/h) at an impact angle of 15°. The actual test conditions in test TB-3 were 4303 lb (1952 kg), 35.5 mph (57.1 km/h), and 14.3°. In terms of the performance with respect to the impacting vehicle, the test was quite successful. The vehicle was smoothly redirected and there was minor damage; the deflection of the barrier was initially 1.9 ft (0.58 m) in the major impact zone. However, the entire 100-ft (30.48-m) test installation overturned subsequent to impact. Structural damage to the barrier was minor. Bronstad and Kimball reported that the barrier was easily restored to an upright position and reused for test TB-4.

In test TB-4 the speed was increased to a nominal value of 45 mph (73.0 km/h). Actual test conditions were 4303 lb, 45.4 mph (73.1 km/h), and 14.6°. Again, vehicle redirection performance was excellent. The maximum deflection in the main impact area was 3.4 ft (1.04 m) and smooth redirection was produced on the vehicle. As in the 35-mph test, the entire length of the barrier overturned. In this case, due to impact damage, a few barrels needed to be replaced after the barrier had been set upright.

In the final test (TB-5) the speed was raised to a level of 60 mph (95 km/h). Actual test conditions were 4424 lb (2007 kg), 57.6 mph (92.7 km/h), and 15.8°. This test proved unacceptable from the standpoint of vehicle reaction. The vehicle moved into the barrier approximately 5 ft (1.52 m) while overturning the first four barrels encountered. It deformed and snagged the W-section, which severed it at a connection point, and proceeded to ramp on the last 40 ft (12.19 m) of the barrier. The vehicle penetrated a maximum of 16 ft (4.88 m) into the protected zone and a section of the detached rail was thrown approximately 30 ft (9.14 m) inside the protected zone. All but 3 of the 17 barrels were overturned. The test must be considered inadequate in that several criteria of Transportation Research Circular (TRC) 191 (2) were not satisfied, specifically those in the Safety Evaluations Guidelines. Criterion I.A states, "The test article shall redirect the vehicle; hence the vehicle shall not penetrate or vault over the installation." Criterion I.B was violated because fragments of the barrier were displaced that could have penetrated the passenger compartment. Criterion III was also violated because the final testing position of the vehicle was inside the protected area.

In an effort to extrapolate the maximum information from these three tests, Figure 2 was developed in which the impact angle is the ordinate and the automobile speed is the abscissa. The results of each of the three tests are shown by solid circles. From this plot, the boundary zone between acceptable and unacceptable performance levels for the standard barrier was developed (3). It is based on a 4500-lb vehicle that strikes the barrier under various combinations of impact angle and speed. The performance boundary zone (the area between the two curves) must be viewed with some reservation since only the middle segment is reasonably justified by full-scale tests. The outer end of the boundary zone [50-70 mph (80.45-112.63 km/h)] is probably accurate, due to the fact that the basic interaction between vehicle and barrier is reasonably well de-

Figure 1. Standard barrel/W-section barrier.

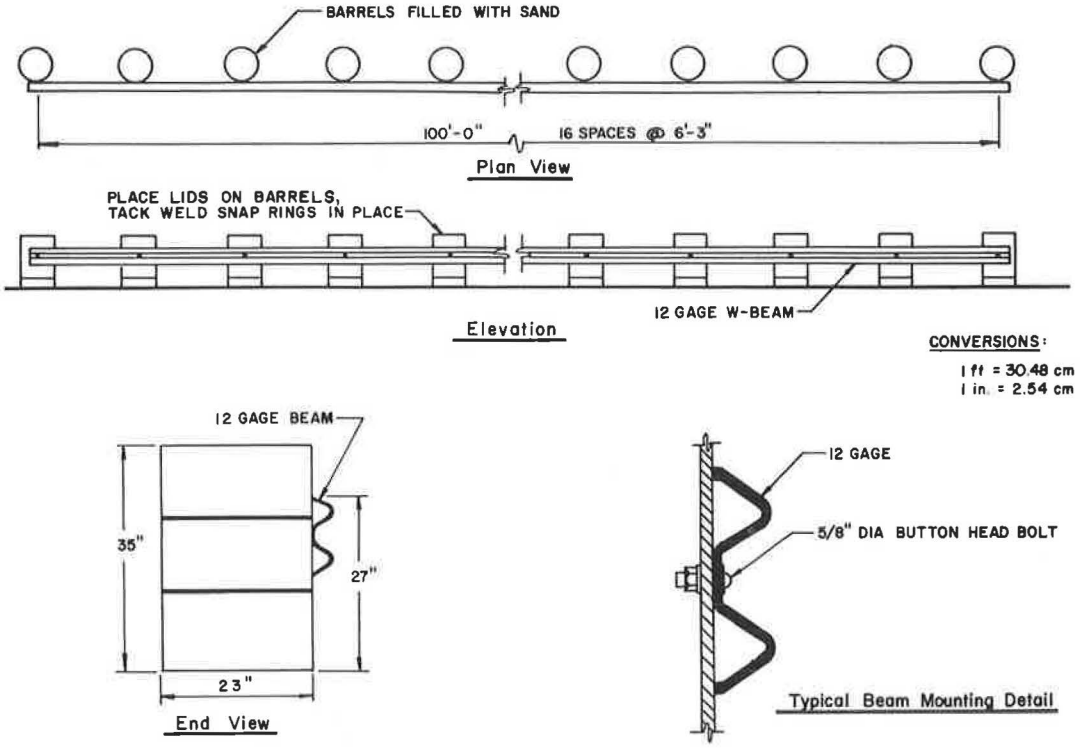

Table 1. Summary of SwRI test results.

Test Parameter	Test Number TB-3	TB-4	TB-5
Vehicle	1969 Chevy Impala	1969 Chevy Impala	1975 Plymouth Grand Fury
Vehicle weight (lb)	4303	4303	4424
Test speed (mph)	35.5	45.4	57.6
Test angle (°)	14.3	14.6	15.8
Exit angle (°)	-8.0	-10.8	-60
Vehicle accelerations (maximum 50-ms avg) (g)			
Lateral	-1.9	-2.7	-2.2
Longitudinal	-0.6	-1.2	-3.5
Vehicle rebound distance (ft)	21	23	3
Maximum deflection (ft)			
Dynamic	1.9	3.4	5[a]
Permanent	1.9	3.4	30[b]

Note: 1 lb = 0.45 kg; 1 mph = 1.609 km/h; 1 ft = 30.48 cm.

[a]Approximate dynamic deflection of barrier while in contact with vehicle.
[b]Position of one rail section that was dislodged from the barrier and knocked 30 ft inside the original barrier line.

fined by the crash tests conducted at an angle of 15°. The inner end, between 25 and 35 mph (40.23 and 56.32 km/h), is somewhat more questionable, since the high impact angle between 20° and 30° could allow an interaction due to pocketing that has not been adequately defined by the previous tests. For this reason, the zones of questionable barrier performance are shown to be between 10 and 40 mph (16.09 and 64.36 km/h) and between 20° and 30°.

It is obvious that this barrier will not perform adequately at the level of the test parameters that is considered a strength test for permanent barriers. Those parameters, defined in TRC 191 (2) as 4500 lb (2041 kg), 60 mph (96.56 km/h), and 25°, are shown in Figure 2 to be well into the unacceptable performance zone.

The reasons for the performance limitations of the barrel/W-section barrier can be summarized as inadequacies in structure, stability, connection, and geometrics. If those reasons are considered in the order listed, test TB-5 illustrates the inadequacy of the W-section bending stiffness, represented primarily by the moment of inertia of the cross section in the plane of primary bending. The vehicle severely deforms the W-section, which results in direct contact of the vehicle with the barrels.

This contact with the barrels is further aggravated by the rotation of the barrels in front of the vehicle; this allows a ramping condition that brings elements of the vehicle's undercarriage in contact with the upper end of the barrels. This is a problem of stability and geometrics that results in forces so large on individual barrels that they are torn free of the W-section and scattered about the assumed construction zone. During this interaction, connections between W-section elements are also severed. If it is assumed that the W-section is strong enough to remain intact during a collision, the main problem is reducing the contact between the vehicle and the barrels. Obvious solutions seem to be (a) blocking out the W-section and (b) preventing the barrels from overturning.

DESIGN OF UPGRADED BARREL/W-SECTION BARRIERS

The major elements to be considered in the design of a barrel/W-section barrier for increased performance are the same as those items listed as reasons for the limited capacity of the standard barrier. Designs were developed that would increase the beam stiffness, increase the overall barrier stability, strengthen all connections, and correct geometric problems.

Although numerous new designs were proposed, all but two were discarded for reasons that ranged from low probability of performance to excess complexity. The two designs that were finally accepted for

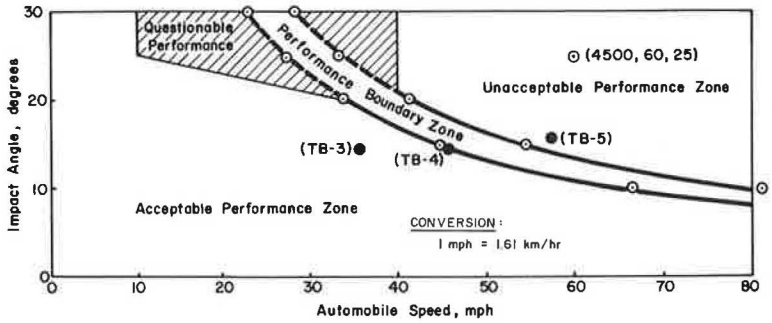

Figure 2. Estimate of performance boundary for standard barrel/W-section barrier.

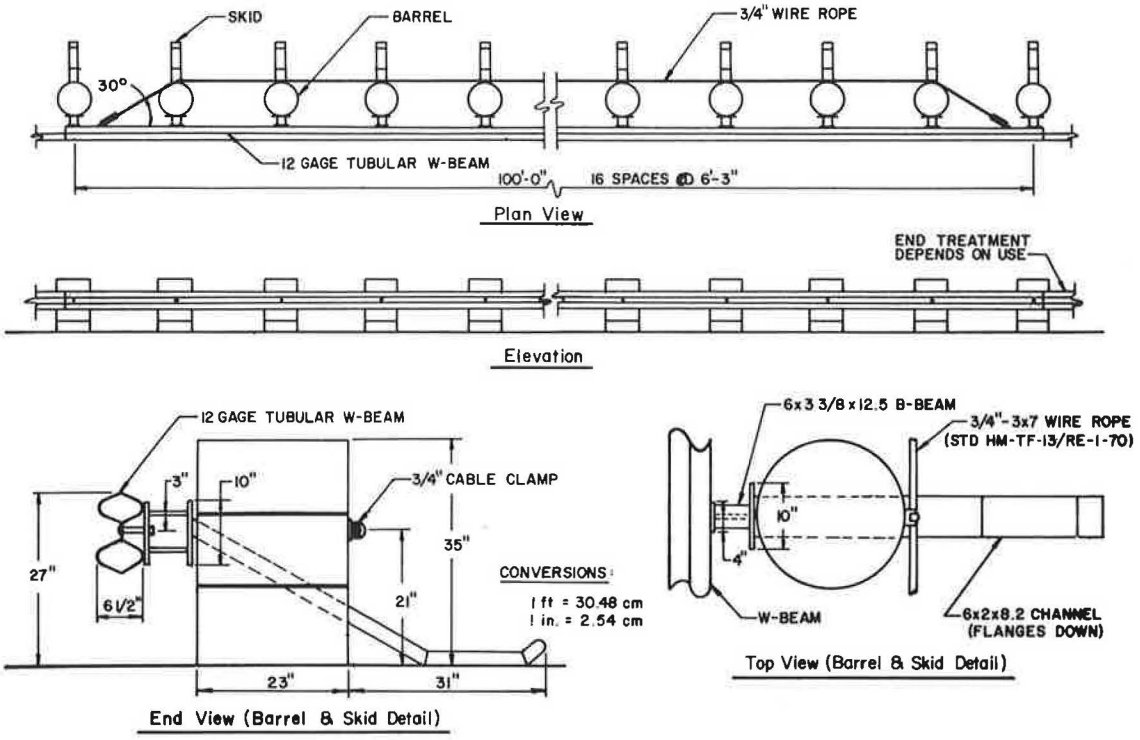

Figure 3. Stabilized barrel/W-section 1 (SBW1).

further analysis and possible testing are shown in Figures 3 and 4. They are designated stabilized barrel/W-sections 1 and 2 (SBW1 and SBW2).

SBW1 is the barrier that demonstrated the highest performance potential. It is shown by Figure 3 to have four major changes from the standard system:

1. Use of the double, or closed, W-section beam;
2. Addition of a 0.75-in (2-cm) wire rope on the side of the barrel away from the impact plane,
3. Use of a B-beam to form a 6-in (15-cm) block out from the supporting barrels, and
4. Use of a skid channel that extends from the tubular W-beam through the barrel to a point of support 40 in (101 cm) behind the impact plane.

SBW2 is shown in Figure 4. There are three major design changes from the standard barrier:

1. Use of the double, or closed, W-section beam [this also affects a 3.25-in (8-cm) block out compared with the standard barrier];
2. Grouping the barrels in sets of three; and
3. Changing the distance between the centroids of the groups of barrels to 12 ft 6 in (3.8 m).

Each of the design changes for SBW1 and SBW2 is responsive to a specific limitation of the standard system, except the final item under SBW2, which was required for practical reasons.

The two designs were submitted to Federal Highway Administration contract managers and to certain other interested engineers, including Dexter Jones of the Texas State Department of Highways and Urban Transportation. Jones reviewed these designs critically and stated that SBW1 was too complicated to construct; he suggested several changes. These suggestions were used to develop design SBW3 (Figure 5).

Design SBW3 is very similar to SBW1 and incorporates three major changes from the standard system:

1. Use of the double, or closed, W-section;
2. Use of a 6-in block out from the supporting barrels, and
3. Use of a skid plate welded to the base of the barrel.

This design was developed to keep the structural characteristics of the SBW1 barrier but to eliminate its complexity. The following analysis of the

Figure 4. Stabilized barrel/W-section 2 (SBW2).

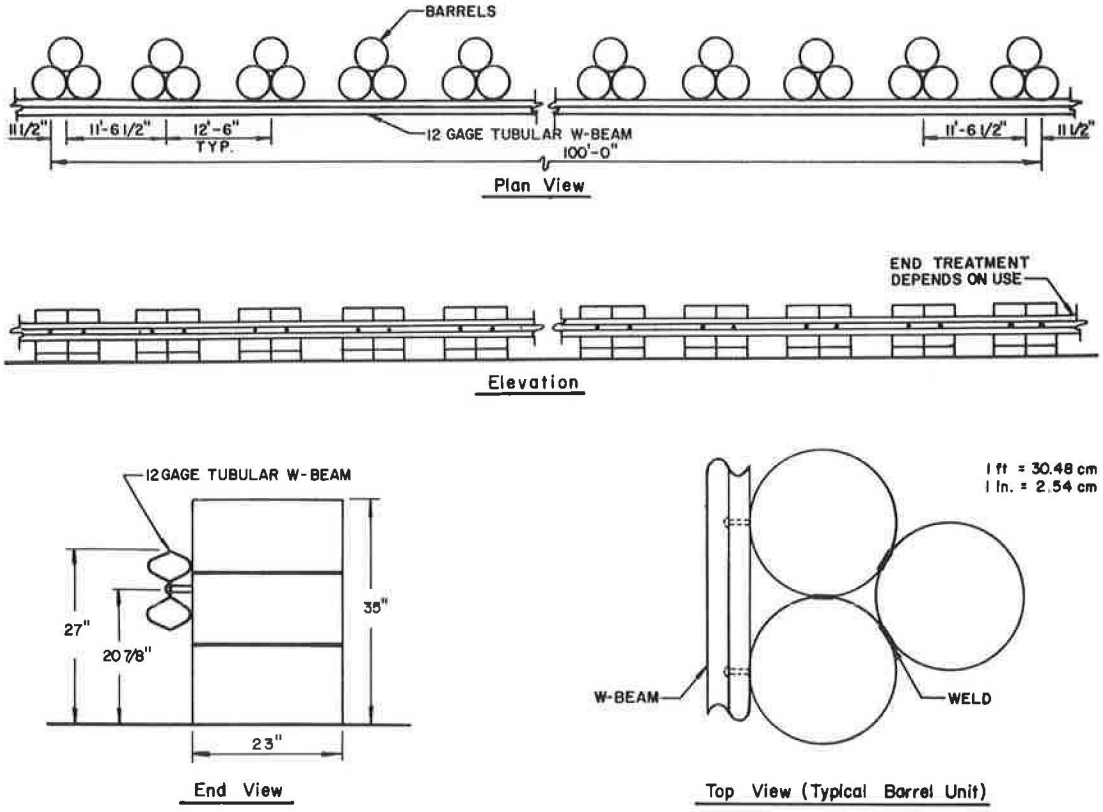

Figure 5. Stabilized barrel/W-section 3 (SBW3).

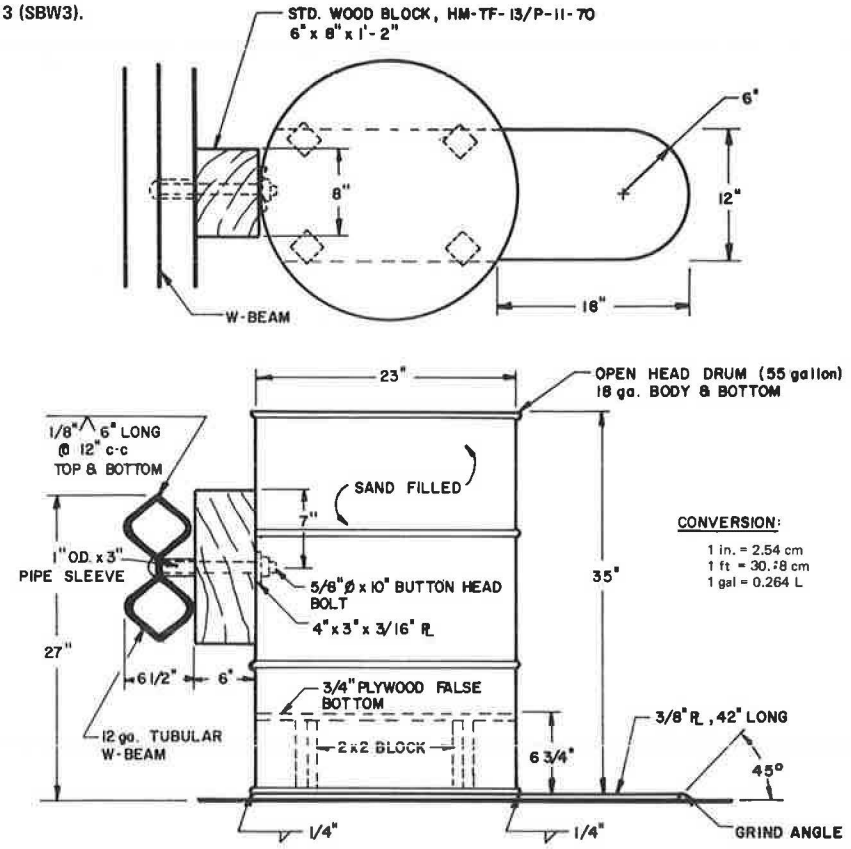

structural characteristics of all the designs will show their similarities.

ANALYSIS OF PROPOSED SYSTEMS

An approach that may be termed "comparative structural analysis" was used to analyze the barrier systems. Comparative structural analysis requires the listing and/or development of a number of performance factors by which the relative performances of new designs and known designs can be compared. For example, if it is known that the standard barrier performs reasonably up to a certain level by using a beam stiffness of BS_1 and if beam stiffness is one of the factors that limits the performance level of the standard barrier, it may be assumed that raising beam stiffness to level BS_2 will have a positive effect on the performance of a new barrier. Comparative structural analysis is not new. It is continually practiced in the field of collision dynamics engineering in a less formal format and has resulted in some major design improvements.

The comparative factors developed here can be shown by theory and by analysis of test results to affect barrier performance significantly (3). The factors developed are defined as follows.

Mass Mobilization Factor

Mass mobilization (MM) is the average weight of the barrier in pounds per 10 ft (3 m) of length.

Beam Stiffness Factor

Beam stiffness (BS) is defined as the moment of inertia of the beam cross section about the axis of major bending (in inches) divided by the cube of the unsupported beam length between major attachment points: $BS = I_y/L^3$.

Table 2. Structural properties of individual barrier designs.

Design Property	Barrier Design: Standard Barrel/W-Section	SBW1	SBW2	SBW3
Beam				
Area[a] (in^2)	1.99	3.98 (4.18)	3.98	3.98
I_y[a] (in^4)	2.31	16.42 (245)	16.42	16.42
I_x (in^4)	30.00	60.00	60.00	60.00
J_{eq} (in^4)	7.33×10^{-3}	34.38	34.38	34.38
L[b] (ft)	6.25	6.25	10.58	6.25
Barrel spacing (ft)	1 at 6.25	1 at 6.25	3 at 12.5	1 at 6.25
Full barrel weight (lb)	800	800	800	800

Note: 1 in^2 = 6.45 cm^2; 1 in^4 = 41.62 cm^4; 1 ft = 30.48 cm; 1 lb = 0.45 kg.
[a]The larger values are appropriate wherever the barrier is operating in the positive moment condition (i.e., the cable is in tension).
[b]Unsupported beam length.

Torsional Stiffness Factor

The torsional stiffness (TS) factor is the equivalent polar moment of inertia (as defined for the determination of torsional rotation in response to an applied torque) divided by the unsupported beam length between attachment points (in cubic inches): $TS = J_{eq}/L$.

Unit Stability Factor

Unit stability (US) is the maximum force that can be applied at the automobile impact level to a 10-ft length of barrier without creating a rotational barrier acceleration (in pounds per 10 ft). It is to be used only on systems not rigidly attached at the base.

Unit Attachment Factor

The maximum force that the attachment of the barrier to the pavement or ground surface generates (in pounds per 10 ft of barrier) is the unit attachment (UA) factor. This includes friction forces and the lateral forces generated by adjacent pavement layers as well as the strength of such positive attachments as dowels, bolts, footings, and the like.

Each of these five factors has been calculated for the three new barrel/W-section designs (SBW1, SBW2, and SBW3) and, for comparison, the standard barrel/W-section barrier. Properties of the barrier systems are listed in Table 2, and the values of the factors for each barrier system are given in Table 3.

Comparison of the factors given in Table 3 shows, in general, relatively high values for the three new designs. MM increases to 1530 lb/10 ft (695 kg/3 m) for SBW1 and SBW3 and to 2080 lb/10 ft (945 kg/3 m) for SBW2. These increases in barrier mass should result in lower barrier deflections.

BS increases radically for SBW1 and SBW3. BS is calculated as I_y/L^3, where I_y was increased from 2.31 in^4 to 16.42 in^4 (96.15-683.45 cm^4) due to the use of the double W-section beam. L remains constant at 6 ft 3 in. BS increases only moderately for SBW2. Although the value of I_y is increased to 16.42 in^4 as in SBW3, the clear span of the beam in SBW2 is increased to 10.58 ft (3.22 m). The adverse effect of L^3 in BS is almost equivalent to the positive effect of increased I_y.

TS is most important to barrier stability. It is the lack of torsional stiffness that allows the first few barrels to be overturned while other barrels remain upright and the connecting single W-section is relatively unstressed. Although TS is calculated by dividing the equivalent section polar moment of inertia (J_{eq}) by the clear span between barrel supports, the major contribution is from the equivalent polar moment of inertia. The value of J_{eq} for the closed double W-section is 4790 times as large as that for the open single section. Cal-

Table 3. Factors that indicate barrier performance.

Design Factors	Barrier Design: Standard Barrel/W-Section	SBW1	SBW2	SBW3
MM (lb/10 ft)	1360	1530	2080	1530
BS[a] (in)	5.47×10^{-6}	39.9×10^{-6} (580×10^{-6})	8.04×10^{-6}	39.9×10^{-6} (580×10^{-6})
TS (in^3)	0.098×10^{-3}	0.46 (NC)[a]	0.27	0.46 (NC)[a]
US[b] (lb/10 ft)	1070 (1150)	13 570 (39 170)	9590 (35 190)	8850 (34 450)
UA (lb/10 ft)	680	770	1040	770

Note: 1 lb = 0.45 kg; 1 ft = 30.48 cm; 1 in = 2.54 cm; 1 in^3 = 16.38 cm^3.
[a]The larger values are appropriate wherever the barrier is operating in the positive moment condition (i.e., the cable is in tension). NC = not computed.
[b]Including the torque generated by adjacent beam sections.

culations indicate that the torque necessary to produce a yielding shear stress on the closed section is 22.4 lbf•ft (29 232 N•m) at a rotation in 6 ft 3 in of 2.8° compared with a torque on the open section of 0.13 lbf•ft (169.7 N•m) at a rotation in 6 ft 3 in of 132°. This greater stiffness increase in the torsion mode mobilizes much more of the barrier to resist overturning.

Probably the single most important factor that indicates relative barrier performance is unit stability. This factor, based on the analysis of the structure shown in Figure 6, is a value of force F that can be applied to a 10-ft section of barrier without producing an angular acceleration (i.e., movement that leads to overturning). It can be shown that this force is defined by the barrier weight and barrier dimensions as follows:

$$F = W[(r - \mu\bar{y})/(a - \bar{y})] \quad (\bar{y} < a) \tag{1}$$

or

$$F = -W[(r + \mu\bar{y})/(a - \bar{y})] \quad (\bar{y} > a) \tag{2}$$

where

F = lateral force applied by an impacting vehicle,
W = barrier weight,
r = horizontal distance from the barrier center of gravity (c.g.) to the required rotation point for overturning,
μ = coefficient of friction,
a = height of force F, and
$\bar{y}$ = vertical distance from the ground surface to the barrier c.g.

Figure 6. Free-body diagram that represents 10 ft of barrier.

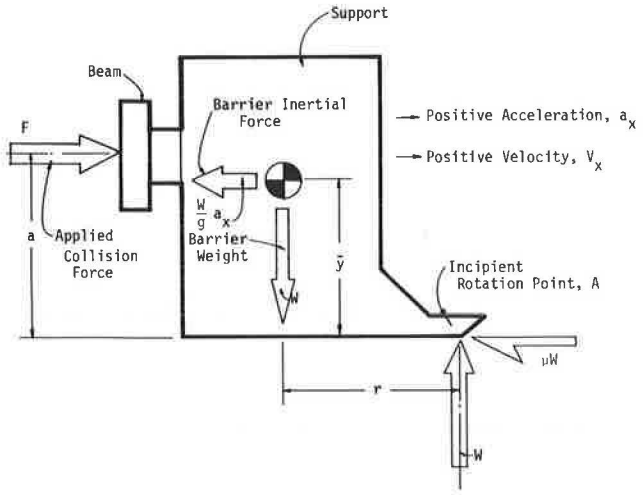

Figure 7. Influence of c.g. height on the unit stability factor.

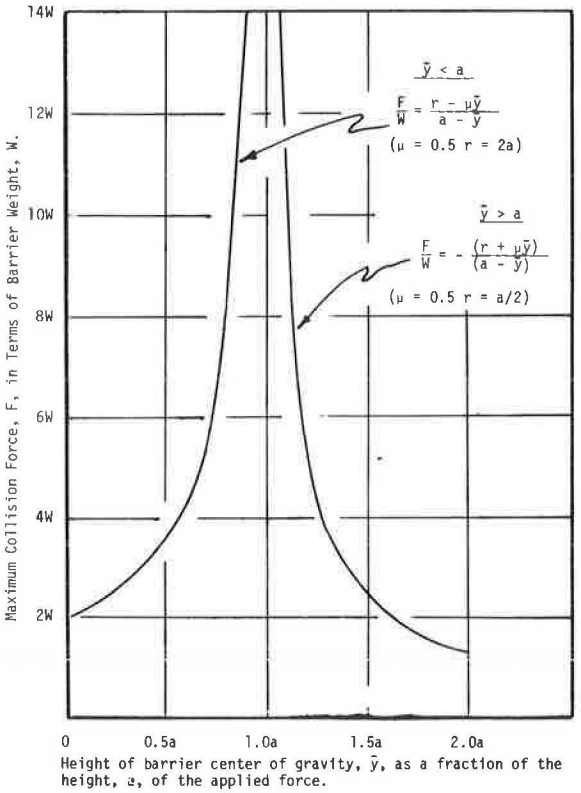

Equations 1 and 2 are the result of eliminating a_x in the equations developed from a summation of moments about the point of incipient rotation A and a summation of forces in the X-direction (where g is acceleration of gravity):

$$\Sigma M_A = 0$$
$$Fa = (W/g)a_x\bar{y} + Wr \tag{3}$$

$$\Sigma F_H = 0$$
$$F = (W/g)a_x + \mu W \tag{4}$$

The force so derived is directly proportional to the weight of the barrier and a nonlinear function of the dimensions a, r, and $\bar{y}$ and the coefficient of friction μ. Equations 1 and 2 must not be taken literally for all imaginable values of a_x. For example, the equations imply that as a approaches $\bar{y}$, F approaches ∞. Consideration of Equations 5 and 6 indicates that this is theoretically true as long as μ is less than the static overturning ratio r/a.

$$\Sigma M_A = 0$$
$$Fa = Wr \tag{5}$$

$$\Sigma F_H = 0$$
$$F = \mu W \tag{6}$$

This is practically impossible, however, since consideration of Equation 3 indicates that a_x must approach ∞ in order for F to approach ∞. It is emphasized that the optimum position of the c.g. of an inertially responding and sliding barrier of this type is on the same vertical level as the applied-force position. Figure 7 illustrates this fact but limits the applied-force level to those practically achievable.

The applicability of Equations 3 and 4 for any value of a_x does depend on whether μ is less than the ratio r/a. If μ is greater than r/a (see Equations 5 and 6), the barrier will tip over before it starts to move laterally (i.e., lateral velocity conditions less than zero). This is why it is of fundamental importance to performance that the barrels skid on the surface rather than dig in.

The values in parentheses for US in Table 3 include the basic US value plus a value of force (2F). This force is the value necessary to place adjacent segments of rail into a yield stress condition of torsion. As an example, adjacent beam segments of SBW1 and SBW3 are double closed W-beam sections 6 ft 3 in long. This beam can accept a torque of 22.4 lbf•ft before the material yields in shear, when a total rotation of one end with respect to the other is 2.8°. By dividing this moment by

dimension a (the height of applied collision load), the necessary force F' to produce this torque is calculated. The result is a hybrid stability factor, which to some degree accounts for the tremendous increase in torsional stiffness of all the barriers.

UA will be of great significance to barriers that are mechanically attached to support media, but it is only a reflection of MM in the case of a barrier subject only to friction that acts at the base. In this case, the factors calculated are simply the MM-value multiplied by the coefficient of friction, which is assumed to be 0.5.

TESTS OF SBW3

Based on the analyses of SBW1 and SBW2 and the comparable characteristics of SBW3, a decision was made to test the relatively simple SBW3. These tests were designated 3825-1 through 3825-4 and conducted on the installation shown in Figures 5 and 8. The test installation was placed on unpaved level soil similar to that found in construction zones. The installation was 250 ft (76.2 m) long, which included a 25-ft (7.63-m) end treatment (Figure 8). The details of each test and the subsequent results are summarized in Table 4. The vehicle damage is given in terms of the Traffic Accident Scale Damage Index (TAD), determined from National Safety Council Bulletin 1 (4), and the Society of Automotive Engineers (SAE) damage classification (5).

Test 3825-1

A 1975 Plymouth Grand Fury that weighed 4500 lb including instrumentation was used in this test. Initial impact occurred 1.5 ft (0.46 m) downstream from barrel 6. The rear of the car contacted the rail near the point of initial impact. Contact with the barrier was maintained through barrel 14. The car was exceptionally stable during redirection and left the rail at a 3.5° exit angle. The maximum dynamic rail deflection was 2.1 ft (0.54 m). The rail rebounded 0.3 ft (0.09 m), leaving a 1.8-ft (0.64-m) deflection after collision.

Figure 9 gives sequential photographs of this test. The maximum 50-ms average transverse acceleration was 4 g, which is within the acceptable 5-g limit given in TRC 191. The lateral acceleration when the vehicle motion became parallel to the barrier was only 1.3 g. The longitudinal 50-ms average was a modest -1.4 g. Damage to both vehicle and barrier was negligible. The same vehicle was used to conduct test 3825-2.

Figure 8. Test installation and layout for SBW3 tests.

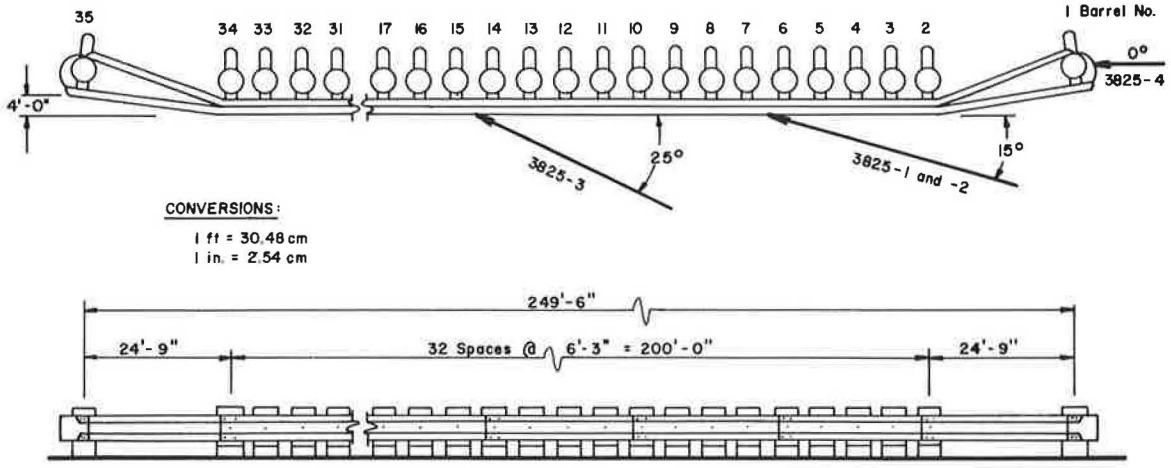

Table 4. Summary of SBW3 test results.

Item	Test Number			
	3825-1	3825-2	3825-3	3825-4
Parameter				
Vehicle	1975 Plymouth Grand Fury	1975 Plymouth Grand Fury	1974 Plymouth Fury III	1975 Plymouth Grand Fury
Vehicle weight (lb)	4500	4500	4500	4500
Test speed (mph)	44.3	61.7	62.4	61.4
Test angle (°)	15	15.5	22.5	0[a]
Exit speed (mph)	33.3	51.9	45.4	NA
Exit angle (°)	3.5	12.3	18	NA
Vehicle accelerations (maximum 50-ms avg) (g)				
Transverse	4.0	4.6	5.43	-3.07
Longitudinal	-1.4	-2.0	-1.36	-15.78
Maximum deflection (m)				
Dynamic	2.1	5.4	11	NA
Permanent	1.8	5.0	10.7	NA
Vehicle damage[b]				
TAD	1-RFQ-1	1-RFQ-2	1-RFQ-3	12-FD-3
SAE	01RFEW1	01RFEW1	01RFEW2	12-FDEW1

Note: 1 lb = 0.45 kg; 1 mph = 1.6 km/h; 1 ft = 0.3 m.
[a]Impact parallel to the barrier at the end terminal.
[b]See Traffic Accident Data Project Bulletin 1 (4) and SAE damage classification document (5).

Figure 9. Test 3825-1.

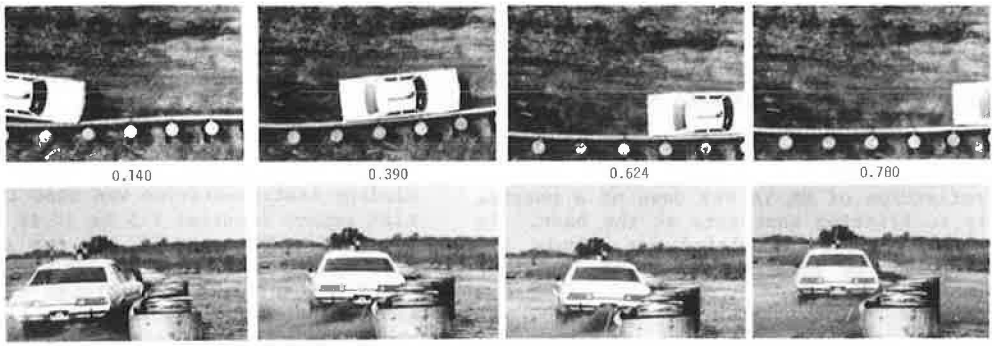

Figure 10. Test 3825-2.

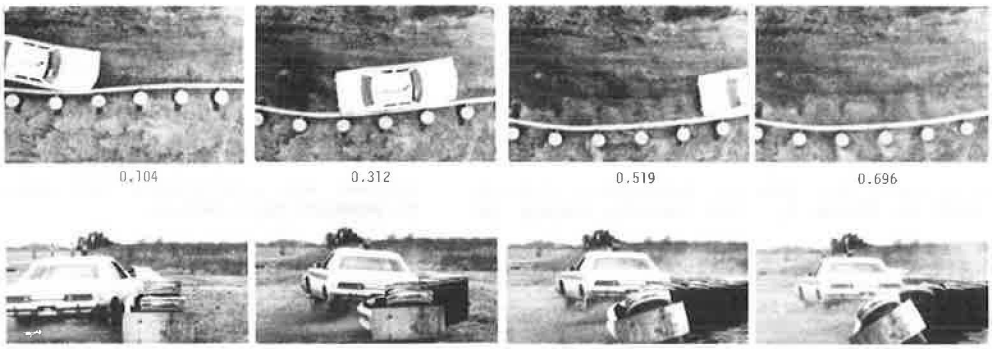

Figure 11. Vehicle before and after test 3825-2.

The barrier was pushed to its original position in 30 min by two men and a forklift. The extent of the permanent deformation was isolated to one 25-ft (7.63-m) rail segment between barrels 6 and 10 that had a 0.5-in (1.27-cm) permanent set. The damage to the rail segment was so slight that replacement was not considered necessary. Four barrels in the immediate area of impact were slightly deformed adjacent to the wooden block. The barrels were not replaced because the deformations were not sufficient to affect performance.

Test 3825-2

In the second test a 1975 Plymouth Grand Fury that weighed 4500 lb including telemetry equipment impacted the barrier at 15.5° and 61.7 mph (99.34 km/h). Figure 10 gives the sequential photographs of this test. The vehicle remained quite stable during redirection; it exhibited no tendency to mount the rail. The vehicle exited the barrier at an angle of 12.3° and a speed of 51.9 mph (83.56 km/h). The maximum 50-ms average transverse acceleration was 4.6 g. This compares favorably with the 5-g acceptable limit from TRC 191. The longitudinal acceleration was -2.0 g, well within the 5-g preferred limit. The maximum rail deflection was 5.4 ft (1.65 m), but the vehicle only penetrated into the protected zone 4.7 ft (1.43 m). The vehicle before and after test 3825-2 is shown in Figure 11.

Two men and a forklift were needed to push the barrier back to its original position. Restoration was completed within 60 min. Significant permanent deformation was confined to the 25-ft rail section between barrels 6 and 10. The maximum permanent set was 3.9 in (9.90 cm) located 2 ft (0.61 m) downstream from barrel 7. This rail section and barrels 6 through 8 were replaced before testing continued.

Test 3825-3

The test vehicle, a 1974 Plymouth Fury, impacted the barrier at 22.5° at a velocity of 62.4 mph (100.4 km/h). The vehicle weighed a total of 4500 lb, which included the telemetry equipment. The vehicle and the barrier before and after the test are shown in Figures 12 and 13.

Sequential photographs of test 3825-3 are presented in Figure 14. Point of impact occurred 3 ft

Figure 12. Vehicle before and after test 3825-3.

Figure 13. SBW3 installation before and after test 3825-3.

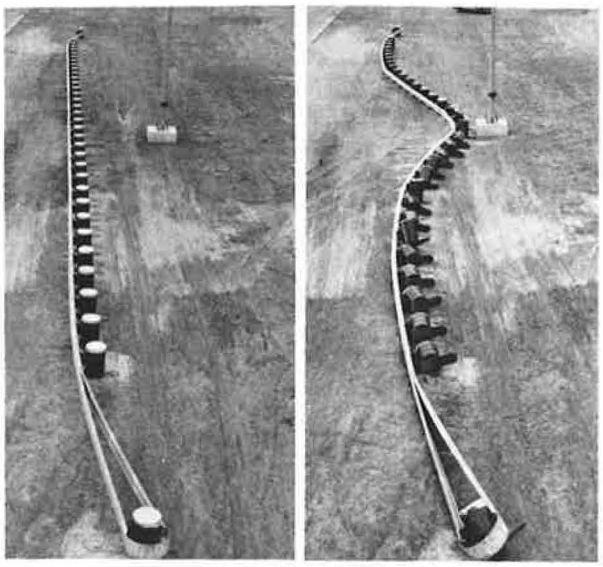

Figure 14. Test 3825-3.

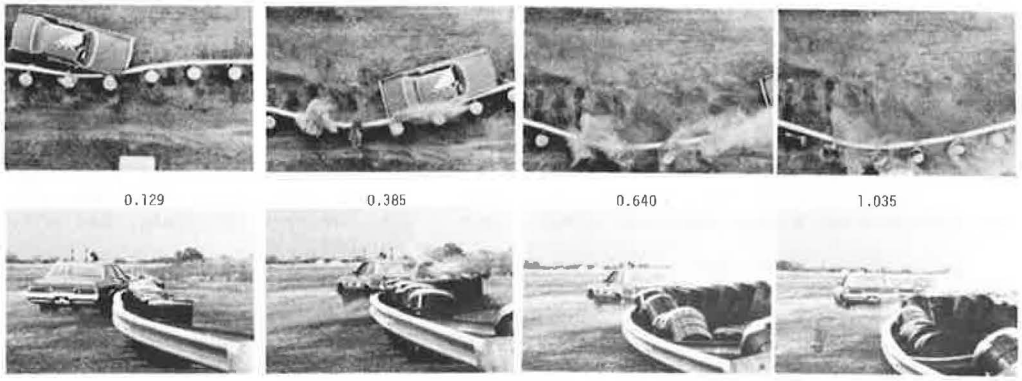

Figure 15. SBW3 installation restored after test 3825-3.

(0.9 m) downstream of barrel 14. At approximately 0.21 s, the vehicle swung into the rail 2.5 ft (0.76 m) downstream of barrel 15. By 0.236 s, the upstream barrels were beginning to rotate. By 0.641 s, the first of the upstream barrels had fallen over and succeeding downstream barrels began to fall. But in the vicinity of the vehicle, the barrels remained upright and resisting throughout the test. The vehicle exited the rail at an angle of 18° and a velocity of 45.4 mph (73.0 km/h). The maximum dynamic deflection of the barrier was 11 ft (3.35 m); this returned to 10.7 ft (3.26 m) after the test.

The barrier was returned to its original position by three men and two forklifts in 90 min. The extent of the permanent deformation after repositioning was between barrels 13-20. The maximum deformation, 5.7 in (0.15 m), occurred at barrel 16. The restored barrier is shown in Figure 15. The 25-ft rail section between barrels 13 and 17 was replaced. Barrels 14 through 18 were also replaced before testing continued.

Test 3825-4

In this test, a 1974 Plymouth Grand Fury impacted the terminal of the barrier at 0° and 61.4 mph (98.9 km/h). The vehicle weighed 4500 lb including telem-

Figure 16. Test 3825-4.

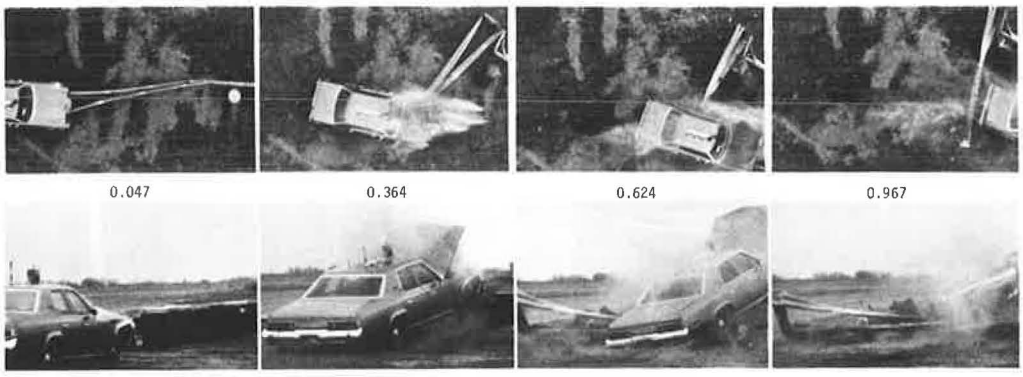

etry equipment. Sequential photographs are presented in Figure 16.

As shown in the sequentials, impact occurred at the end of the terminal. The W-beam began to buckle upstream of barrel 2 and folded inward toward the back of the barrier, which caused the vehicle to ride up and over it. Outward buckling occurred at barrels 2 and 3. The vehicle yawed to the left and came to rest behind the barrier. Damage to the front of the vehicle was extensive.

The peak longitudinal acceleration was high and would have been much too high for a small vehicle. We therefore propose to reduce the sand ballast in the end barrel to roughly 200 lb (90.7 kg) and to elevate the c.g. of this sand to prevent the vehicle from ramping on the end barrel.

Although the barrier was not repaired following test 3825-4, it was severely damaged upstream of barrel 3. Repairs that would have been required to restore the barrier included the replacement of the first two sections of W-beam and the first eight barrels.

CONCLUSION

The technique of comparative structural analysis indicated the high probability that barriers SBW1, SBW2, and SBW3 would perform at a level of impact much more critical than those accepted by the standard barrel/W-section barrier.

This statement has been verified by the first three tests of SBW3. The performance of this design is excellent; there is one major drawback--the relatively large barrier deflection. The barrier is not highly portable and should be considered for use only when it is expected that it will be needed at one point for a considerable period. Unless surplus barrels and the W-section are available, the cost is comparable with that of conventional portable concrete median barriers.

We recommend the use of this barrier design when cost factors warrant it and when deflections during anticipated vehicle collisions can be accommodated.

ACKNOWLEDGMENT

We wish to acknowledge the Federal Highway Administration and in particular Morton S. Oskard, contract manager for this project. In addition, valuable input was received from Dexter Jones of the Texas State Department of Highways and Urban Transportation.

The contents of this paper reflect our views and we are responsible for the facts and accuracy of the data. The contents do not necessarily reflect the official views or policy of the U.S. Department of Transportation.

This paper does not constitute a standard, specification, or regulation.

REFERENCES

1. M.E. Bronstad and C.E. Kimball, Jr. Temporary Barriers Used in Construction Zones. Southwest Research Institute, San Antonio, TX, Task Rept., Dec. 1977.
2. Recommended Procedures for Vehicle Crash Testing of Highway Appurtenances. TRB, Transportation Research Circular 191, Feb. 1978.
3. D.L. Ivey and E.L. Marquis. Portable Barriers for Construction Zones: Analysis and Redesign of Current Systems. Texas Transportation Institute, Texas A&M Univ. System, College Station, Unpublished Interim Rept., Tasks 1 and 2, DOT-FH-11-9458, April 1979.
4. Vehicle Damage Scale for Traffic Accident Investigators. National Safety Council, Chicago, IL, Traffic Accident Data Project Bull. 1, 1968.
5. Collision Deformation Classification, Recommended Practice J224a. SAE, New York, 1972.

Publication of this paper sponsored by Committee on Safety Appurtenances.

Notice: The Transportation Research Board does not endorse products or manufacturers. Trade and manufacturers' names appear in this paper because they are considered essential to its object.

Methodology for Evaluation of Safety Improvement Alternatives for Utility Poles

PATRICK T. McCOY, RICHARD T. HSUEH, AND EDWARD R. POST

The object of this paper is to present the formulation and demonstration of a methodology for evaluation of safety improvement alternatives for utility poles. It is a total-annual-cost method of economic analysis, which features the calculation of expected annual accident and collision maintenance costs on the probabilities and severities of single-vehicle collisions with utility poles and other fixed objects on the roadside. The probabilities and severities of these collisions are in turn computed from a definition of the speed and volume of traffic, distribution of vehicle sizes, and the numbers, types, and locations of utility poles and other fixed objects on the roadside. The methodology can be used to evaluate several types of improvement alternatives, including multiple use of poles, relocation of poles, breakaway poles, impact-attenuation systems, and underground placement of utility lines. It can also be used to evaluate alternatives for a specific situation or for various combinations of traffic and roadside conditions in order to identify the circumstances for which each is most economical. The methodology is demonstrated for various traffic and roadside conditions on two hypothetical street sections typical of many arterial street sections in Lincoln, Nebraska. The results of this demonstration show the applicability of the methodology and serve to illustrate the sensitivity of the selection of the best alternative to traffic and roadside conditions.

The serious accident problem associated with the location of utility poles close to the edge of roadways, particularly in urban areas, has been the subject of considerable research in recent years. Some studies have been concerned with the nature and extent of the problem, whereas others have concentrated on developing various countermeasures. But few studies have been directed at determining the cost-effectiveness of alternative countermeasures (1).

During the past year, the Civil Engineering Department at the University of Nebraska--Lincoln has been conducting research on the design and testing of a breakaway-pole concept for wooden utility poles (2). As part of this research, a methodology was developed for evaluating various safety improvement alternatives for utility poles. It has been used during the conduct of the research to compare the concept being developed with other countermeasures in order to define the concept's cost limits of economic feasibility for various traffic and roadside conditions.

The methodology developed computes the total annual cost of an alternative, which includes its capital recovery and annual maintenance costs plus the expected annual cost of accidents between a single vehicle and a fixed object on the roadside. Based on a description of the speed and volume of traffic and the size, location, and type of fixed objects along the roadway, the probabilities and severities of single-vehicle collisions with the fixed objects are computed. The accident costs of these collisions are then computed and added to the capital recovery and annual maintenance costs of the improvement alternative. By comparing the total annual costs of the alternatives and the existing condition, the most economical course of action is identified. The methodology can be used to evaluate a specific case or it can be used to evaluate the total annual cost of various alternatives over a range of traffic and roadside conditions to identify the circumstances for which each would be most economical.

This paper presents a description of the formulation of the methodology. Also included are the results of a demonstration of its application, in which the total annual costs of a number of safety improvement alternatives were compared for various traffic and roadside conditions typical of some arterial streets in Lincoln, Nebraska. The alternatives evaluated were (a) relocating the utility poles to increase their lateral distance from the edge of the roadway, (b) retrofitting the utility poles to make them break away when hit, and (c) placing the utility lines underground.

FORMULATION

The methodology developed is basically the conventional annual-cost method of analyzing alternatives, in which the total annual costs of the existing condition and the alternatives are computed and compared to identify the one with the lowest annual cost. The total annual cost of an alternative or the existing condition is computed (in dollars per year) as follows:

$$\Sigma C = A + C + NMC + CMC \quad (1)$$

where

- ΣC = total annual cost of improvement alternative or existing condition,
- A = expected annual accident cost of improvement alternative or existing condition,
- C = capital recovery cost of improvement alternative or existing condition,
- NMC = annual normal maintenance cost of improvement alternative or existing condition, and
- CMC = annual collision maintenance cost of improvement alternative or existing condition.

The distinguishing feature of the methodology is the computation of expected accident costs and collision-maintenance costs based on probabilities and severities of potential single-vehicle collisions with fixed objects (including utility poles) on the roadside. A description of the calculation of these costs follows.

Accident Costs

The general equation used to compute the expected annual accident cost of an improvement alternative or existing condition is as follows:

$$A = E\Sigma_{\theta v}\Sigma\{P(E_{\theta,v}/E)\Sigma_w[P(w)\Sigma_F P(C^{w,F}_{\theta,v}/E_{\theta,v})(AC^{w,F}_{\theta,v})]\} \quad (2)$$

where

- A = expected annual accident cost (dollars per year);
- E = encroachment rate (number of roadside encroachments per mile per year);
- $P(E_{\theta,v}/E)$ = probability of an encroachment at angle θ and speed v given that an encroachment has occurred $[\Sigma_{\theta v}\Sigma P(E_{\theta,v}/E) = 1.0]$;
- $P(w)$ = decimal fraction of vehicles of size w in traffic stream $[\Sigma_w P(w) = 1.0]$;
- $P(C^{w,F}_{\theta,v}/E_{\theta,v})$ = probability of a collision at angle θ and speed v of a vehicle of

size w with a fixed object of type F given an encroachment at angle θ and speed v;

$AC^{w,F}_{\theta,v}$ = accident cost of a collision at angle θ and speed v of a vehicle of size w with a fixed object of type F;

θ = encroachment and collision angle (°);

v = encroachment and collision speed (mph);

w = vehicle size designation, which defines width and weight of vehicle; and

F = fixed-object type designation, which defines size and impact severities of fixed object.

In Equation 2, the effect of an improvement alternative or existing condition is determined by the probability and severity of collision terms [$P(C^{w,F}_{\theta,v}/E_{\theta,v})$ and $AC^{w,F}_{\theta,v}$]. These and the other variables in this equation are described below.

Encroachment Rate

Knowledge of the rate at which vehicles encroach on the roadside of various types of roadways is very limited. In fact, the only pure encroachment data available are those of Hutchinson and Kennedy (3), which were collected on freeway medians. More recently, Glennon and Wilton (4) have estimated encroachment rates for different classes of roadways as linear functions of average daily traffic (ADT). These relationships, which were derived from an analysis of roadside accident rates for various classes of roadways and a comparison of the freeway encroachment rate determined by Hutchinson and Kennedy with the roadside accident rate on freeways in Missouri, are presented below. (It should be noted that these encroachment rates are for the total number on both sides of the roadway; therefore, if only one side of a roadway is being considered, as is often the case with utility poles, the rate should be divided by 2.)

Class of Roadway	Encroachment Rate (no./mile/year)
Rural highway	
Interstate	0.000 9
Multilane divided	0.000 59
Wide two-lane (roadbed ≥36 ft)	0.000 742
Narrow two-lane (road <36 ft)	0.001 21
Urban highway	
Interstate	0.000 9
Multilane divided	0.000 9
Major arterial street	0.001 33

Probabilities of Combinations of Encroachment Angle and Speed

As in the case of encroachment rates, knowledge of the probabilities of combinations of encroachment angle and speed is also extremely limited. Therefore, for purposes of developing the methodology, these probabilities are computed by combining the distributions of encroachment angles and traffic speeds as follows:

$$P(E_{\theta,v}/E) = P(E_\theta/E)P(v) \quad (3)$$

where $P(E_\theta/E)$ is the probability of an encroachment at angle θ given that an encroachment has occurred [$\Sigma_\theta P(E_\theta/E) = 1.0$] and P(v) is the probability of a vehicle speed v in the traffic stream [$\Sigma_v P(v) = 1.0$]. Thus, encroachment speed is assumed to be equal to the traffic speed on the roadway and independent of encroachment angle. Of course, the point-mass model presented by Ross (5) indicates that some high-angle high-speed encroachments are not possible. However, because of the lack of encroachment data to support this theory and because of their low probabilities of occurrence, no adjustment is made to account for the apparent impossibility of high-angle high-speed encroachments.

In the methodology, the range of encroachment angles is divided into six intervals. The interval probabilities, which were derived from the encroachment-angle distribution reported by Hutchinson and Kennedy (3), are presented below. The encroachment angle is assumed to be independent of vehicle size and type of roadway.

Encroachment Angle (°)	Probability
<7.5	0.48
7.5-12.5	0.20
12.5-17.5	0.12
17.5-22.5	0.08
22.5-27.5	0.05
>27.5	0.07

Encroachment speeds are assumed to be normally distributed; the standard deviation is ±5.0 mph, which is representative of many roadways (6). The range of encroachment speeds is divided into five intervals based on the speed limit on the roadway. The probabilities of speeds within these intervals, based on the assumption that the speed limit (S) is equal to the 85th-percentile speed, are presented below. Encroachment speeds are also assumed to be independent of vehicle size.

Encroachment Speed (mph)	Probability
<(S - 12.5)	0.07
(S - 12.5) to (S - 7.5)	0.25
(S - 7.5) to (S - 2.5)	0.39
(S - 2.5) to (S + 2.5)	0.23
≥(S + 2.5)	0.06

Thus, in the methodology, 30 combinations of encroachment angle and speed are evaluated for each combination of vehicle size and fixed-object type.

Vehicle Size Probabilities

The probabilities and severities of single-vehicle collisions with fixed objects on the side of a roadway are dependent on the size of the encroaching vehicles. In general, the wider an encroaching vehicle is, the greater the probability is that it will collide with a fixed object on the roadside. Likewise, the smaller a vehicle is, the greater the severity of its collision will be with a fixed object. Therefore, the methodology developed in this research is designed to account for these effects of vehicle size.

The encroachment rates are assumed to be independent of vehicle size. Therefore, the probability that an encroaching vehicle will be of a particular size is assumed to be equal to the decimal fraction of vehicles of that size in the traffic stream.

Collision Probabilities

The probability that an encroaching vehicle will collide with a fixed object on the side of the roadway depends on (a) the number, size, and location of the fixed objects on the roadside and (b) the width

Figure 1. Idealization of roadside.

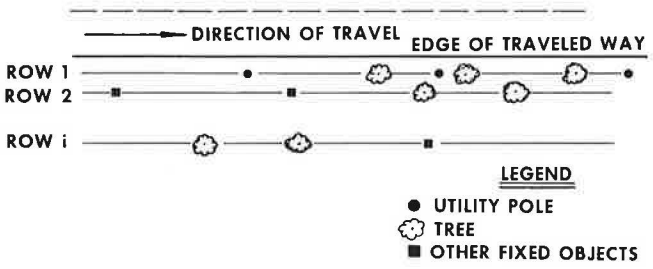

of the encroaching vehicle and the angle of its encroachment. In general, the more fixed objects there are along the roadside, the greater the probability of a collision will be.

To facilitate the formulation of this methodology, the description of the roadside is idealized in terms of rows and types of fixed objects as illustrated in Figure 1. The designation of each type of fixed object defines the size and severities of collision with a particular type of fixed object. For example, nonbreakaway utility poles 1 ft in diameter would be one type of fixed object that might be found on the roadside. Since the subject of this study is utility poles, they are the type of fixed objects that are of the greatest concern. However, other types of fixed objects cannot be ignored, because their sizes and locations could reduce the probability of a collision with a utility pole. In general, the greater the number of other fixed objects on the roadside is, the lower the probability of colliding with a utility pole is.

The equation derived for computing the collision probability is as follows:

$$P(C^{w,F}_{\theta,v}/E_{\theta,v}) = \sum_{i=1}^{n} P_i(C^{w,F}_{\theta,v}/E_{\theta,v}) \cdot P_{i-1}(NC^{w}_{\theta,v}/E_{\theta,v}) \cdot P_{i-2}(NC^{w}_{\theta,v}/E_{\theta,v}) \ldots P_o(NC^{w}_{\theta,v}/E_{\theta,v}) \quad (4)$$

where

$P_i(C^{w,F}_{\theta,v}/E_{\theta,v})$ = probability of a collision at angle θ and speed v of a vehicle of size w with a fixed object of type F in row i given an encroachment at angle θ and speed v,

$P_i(NC^{w}_{\theta,v}/E_{\theta,v})$ = probability of no collision at angle θ and speed v of a vehicle of size w with a fixed object of any type in row i given an encroachment at angle θ and speed v [$P_i(NC^{w}_{\theta,v}) = 1 - \Sigma_F P_i(C^{w,F}_{\theta,v}/E_{\theta,v})$],

$P_o(NC^{w}_{\theta,v}/E_{\theta,v})$ = 1.0, and

n = number of rows of fixed objects.

The probability of a collision with a fixed object in one row is dependent on the probability that an encroaching vehicle will not collide with a fixed object in a preceding row (i.e., a row closer to the roadway). However, given that an encroaching vehicle has not collided with a fixed object in a preceding row, the probability that it will collide with a particular type of fixed object in row i is the product of two other conditional probabilities:

$$P_i(C^{w,F}_{\theta,v}/E_{\theta,v}) = P_i(X^{w,F}_{\theta,v}/E_{\theta,v}) P_i(C^{w,F}_{\theta,v}/X^{w,F}_{\theta,v}) \quad (5)$$

where $P_i(X^{w,F}_{\theta,v}/E_{\theta,v})$ is the probability that the encroachment path of a vehicle of size w will intersect the location of a fixed object of type F in row i given an encroachment of angle θ and speed v, and $P_i(C^{w,F}_{\theta,v}/X^{w,F}_{\theta,v})$ is the probability that there will be a collision at angle θ and speed v of a vehicle of size w with a fixed object of type F in row i given that the vehicle is on an intersecting path at angle θ and speed v.

The conditional probability that an encroaching vehicle will be on a path that intersects the location of a fixed object of a particular type in row i is proportional to the length of the roadway within which this could occur. As illustrated in Figure 2, this length for a single fixed object is a function of the encroachment angle, the width of the vehicle, and the diameter of the fixed object. This relationship is defined by the following equation:

$$L^{w,F}_{\theta,v,i} = (d^F_i + y^w) \csc\theta \quad (6)$$

where

$L^{w,F}_{\theta,v,i}$ = length of roadway within which encroachment path at angle θ and speed v of a vehicle of size w would intersect the location of a single fixed object of type F in row i (ft),

d^F_i = diameter of fixed object of type F in row i (ft), and

y^w = width of encroaching vehicle of size w (ft).

However, if fixed objects in row i are close enough together, the presence of those upstream will screen those downstream, thus reducing the length of roadway within which the locations of those downstream could be intersected by encroaching vehicles. This reduction would be equal to the amount by which their roadway lengths overlap, as illustrated in Figure 3.

Due to a lack of data on the effects of roadway geometrics on the frequency and nature of encroachments, it is assumed that the distribution of encroachments along the length of a roadway is uniform. Therefore, the probability that a vehicle encroachment will be on a path that intersects the location of a fixed object in row i is as follows:

$$P_i(X^{w,F}_{\theta,v}/E_{\theta,v}) = (1/5280) \sum_{j=1}^{N_i} (L^{w,F}_{\theta,v,i,j} - O^{w,F}_{\theta,v,i,j}) \quad (7)$$

where

N_i = number of fixed objects of type F per mile in row i,

$L^{w,F}_{\theta,v,i,j}$ = length of roadway within which encroachment path at angle θ and speed v of a vehicle of size w would intersect the location of the jth fixed object of type F in row i (ft), and

$O^{w,F}_{\theta,v,i,j}$ = portion of $L^{w,F}_{\theta,v,i,j}$ that overlaps with that of other fixed objects in row i upstream of the jth fixed object of type F in row i (ft).

The conditional probability $[P_i(C^{w,F}_{\theta,v}/X^{w,F}_{\theta,v})]$ that an encroaching vehicle on an intersecting path with a fixed object in row i will collide with that fixed object given that it has not collided with one in a preceding row is a function of the lateral distance

Figure 2. Length of roadway within which encroachment at angle θ would intersect location of fixed object.

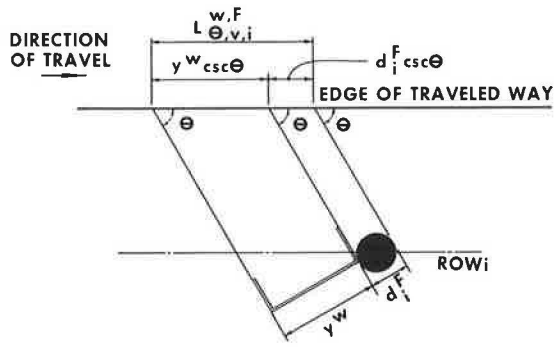

d_i^F = DIAMETER OF FIXED OBJECT

w = WIDTH OF VEHICLE

θ = ENCROACHMENT ANGLE

Figure 3. Illustration of screening effect.

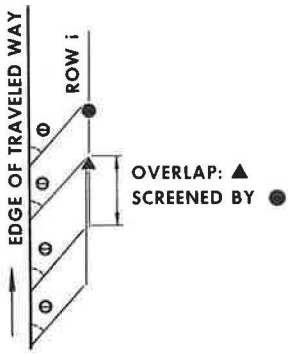

between the edge of the traveled way and row i. The greater this distance is, the farther the vehicle must travel along its encroachment path to reach the fixed object and the less likely it is that it will collide with it. This conditional probability is determined from the appropriate distribution of lateral extent of encroachments shown in Figure 4. These distribution curves were derived from an analysis of the encroachment data reported by Hutchinson and Kennedy (3). It is assumed that these distributions are independent of encroachment speed and vehicle and are only dependent on the encroachment angle.

Collision Costs

The accident costs of a collision with a fixed object are computed as a function of the severity of the collision in terms of the probability that an injury accident would result. The relationship between accident costs and probability of an injury accident shown in Table 1 is the one used in the methodology developed in this study.

This relationship, developed by Post (7) in previous research, equates various levels of injury-accident probability with a percentage distribution of accident severities [i.e., percent fatal, percent nonfatal-injury, and percent property-damage-only (PDO) accidents]. The mean accident costs shown in Table 1 are computed by applying the percentage distributions to the following figures for unit accident cost: $150 000 per fatal accident, $5800 per nonfatal-injury accident, and $850 per PDO accident.

Figure 4. Distributions of lateral extent of encroachments.

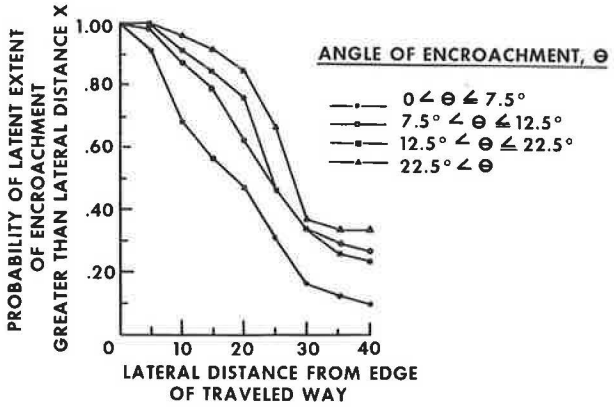

Table 1. Relationship between mean accident cost and injury-accident probability.

Injury-Accident Probability	PDO[a] Accidents (%)	Nonfatal-Injury Accidents (%)	Fatal Accidents (%)	Mean Accident Cost ($)
0.1	90	10	0	1 400
0.3	60	40	0	2 300
0.5	40	60	0	3 820
0.7	10	88	2	8 190
0.8	0	96	4	11 570
1.0	0	94	6	14 450

[a]PDO = Property damage only.

The probability that a collision with a fixed object will result in an injury accident is a function of the angle and speed of impact, the size of the vehicle involved, and the type and size of fixed object struck. By using mathematical modeling and computer simulation, the probabilities of an injury accident were computed for collisions with breakaway (B) and nonbreakaway (N) wooden utility poles in research conducted at the University of Nebraska (2). These values, presented below for a 4500-lb vehicle, were used in the demonstration of the methodology presented in this paper. Similar relationships can be developed for other types of fixed objects. However, for an in-depth discussion of the derivation of such relationships, the reader is referred to a study by Post and others (8).

Vehicle Impact Speed (mph)	Probability of Injury Accident	
	B	N
10	0.19	0.28
15	0.28	0.45
20	0.42	0.59
25	0.57	0.74
30	0.62	0.89
35	0.62	1.00

Other Costs

When the methodology presented in this paper is applied, the capital recovery and maintenance costs in Equation 1 should be based on local unit costs and interest rates. Also, the collision maintenance cost of an improvement alternative or existing condition is computed in the same way as the accident cost is computed except that, in using Equation 2, the term for collision accident cost

$(AC^{w,F}_{\theta,v})$ is replaced with a term for collision maintenance cost, as follows:

$$CMC = E\Sigma_\theta \Sigma\{P(E_{\theta,v}/E)\ \Sigma_w [P(w)\ \Sigma_F\ P(C^{w,F}_{\theta,v}/E_{\theta,v})(CM^{w,F}_{\theta,v})]\} \quad (8)$$

where CMC is the expected annual collision maintenance cost (in dollars per year) and $CM^{w,F}_{\theta,v}$ is the maintenance cost of a collision at angle θ and speed v of a vehicle of size w with a fixed object of type F. Depending on the amount of knowledge the user of the methodology has regarding the collision maintenance cost of the improvement alternative or existing condition, the term for collision maintenance cost in Equation 8 could be an average collision maintenance cost for all collisions or it could be related to the severity of the collision as is the term for collision accident cost.

DEMONSTRATION

To demonstrate the use of the methodology presented in this paper, it was used to evaluate utility-pole safety improvement alternatives on two hypothetical sections of arterial street typical of several in Lincoln, Nebraska. Also, to illustrate the effects of traffic volume and number of other fixed objects on the relative costs of the alternatives, they were evaluated over a range of traffic and roadside conditions. A computer program was written and used to calculate the terms for collision accident and collision maintenance costs of the total-annual-cost equation (Equation 1). A description of the cases evaluated and the results of the evaluations follow.

Streets

The two street sections used in this demonstration were 1000 ft long. Each had utility poles on one side, which were uniformly spaced at 80-ft intervals and set back 2 ft from the edge of the traveled way. The utility poles were standard 40-ft, class 4 poles made of southern yellow pine. The injury-accident probabilities of collisions with these poles were assumed to be the same as those presented in the section on collision costs for nonbreakaway poles.

On one of the sections (street A), the fixed objects other than utility poles were located in the same row as the utility poles (i.e., 2 ft from the edge of the traveled way) and, on the other (street B), they were located in a row 10 ft from the edge of the traveled way. The numbers of fixed objects in these rows were varied from none to 20 (i.e., 0, 6, 13, and 20 fixed objects). In each case, the fixed objects were distributed at random throughout the 1000-ft length of the section. All fixed objects were assumed to be 1 ft in diameter, and they were assigned the same injury-accident probabilities as those for the nonbreakaway utility poles.

In all cases, the speed limit on the street was 35 mph, and all vehicles in the traffic stream were standard-sized passenger cars that were 6.5 ft wide and weighed 4500 lb. The encroachment rate used for a major urban arterial street was 0.001 33 accident per mile per year. The encroachment angle and speed probabilities used were those shown previously. The evaluations were conducted for two traffic volumes: 15 000 and 30 000 ADT.

Thus, on each of the two streets, eight cases were evaluated (i.e., four numbers of fixed objects times two traffic volumes).

Improvement Alternatives

For each of the eight cases on each street, the following three improvement alternatives were evaluated:

1. Breakaway: The utility poles were made to break away by applying the breakaway concept developed at the University of Nebraska--Lincoln (2). The utility poles were assigned the injury-accident probabilities given in the section on collision costs for breakaway poles, thus reducing the probability that a collision with a utility pole would result in an injury accident.
2. Relocate: The utility poles were moved 2-10 ft from the edge of the traveled way, thus reducing the probability of a collision with a utility pole.
3. Underground: The utility poles were removed and the utility lines were placed underground, thus eliminating collisions with utility poles.

The capital and maintenance cost data for the existing conditions and the improvement alternatives were provided by D. Redding, supervisor of transmission and substation of the Lincoln Electric System. The capital cost data are presented in Table 2. All alternatives were assumed to have 30-year service lives and zero salvage values, and a 10 percent interest rate was used. Also, the normal maintenance costs of alternatives were assumed to be the same, and the collision maintenance costs of the existing conditions and of the breakaway and relocation alternatives were all computed by using an average collision maintenance cost of $250 per collision. The collision maintenance costs computed by using Equation 8 are presented in Table 3 for 15 000 ADT (multiply these costs by 2 to obtain costs for 30 000 ADT). As noted, the collision maintenance costs for 30 000 ADT were twice those for 15 000 ADT because the encroachment rate is a linear function of ADT; therefore, there were twice as many collisions for 30 000 ADT.

RESULTS

The annual accident costs for 15 000 and 30 000 ADT are shown in Figure 5 (top and bottom, respectively). These costs include the accident costs of collisions with other fixed objects in addition to those of collisions with utility poles.

The number and location of utility poles on street A are the same as those on street B. Therefore, at a given traffic volume, the annual accident costs are the same on both streets when there are no fixed objects other than utility poles along the streets. However, when there are other fixed objects, the annual accident costs are higher on street A because the fixed objects on street A are closer to the edge of the traveled way and thus more likely to be struck by an encroaching vehicle. Likewise, on either street, as the number of fixed objects is increased, the accident costs increase because of the greater probability of collisions with fixed objects. Of course, at some point as the number of fixed objects is increased, the probability that an encroaching vehicle will be on a path that intersects the location of a fixed object reaches 1. At this point, the annual accident cost for a particular alternative is maximized.

In all cases, the existing condition has the highest annual accident cost, and the underground alternative has the lowest. However, on street A, the order of the other two alternatives with respect to annual accident cost reverses as the number of fixed objects is increased. With fewer fixed objects or with none, the relocation alternative has the lower annual accident cost. But with more fixed

Table 2. Capital cost data.

Alternative	Unit Cost ($)	First Cost ($)	Capital Recovery[a] Cost ($)
Existing	0	0	0
Breakaway	20/pole	260	30
Relocate	30 000/mile	5 700	630
Underground	18/ft	18 000	1950

[a]Capital recovery factor for 10 percent interest rate, 30-year service life, and zero salvage value = 0.11.

Table 3. Collision maintenance costs for 15 000 ADT.

Alternative	No. of Fixed Objects 0	6	13	20
Costs for Street A ($)				
Existing[a]	210	140	117	45
Breakaway[a]	210	140	115	45
Relocate[b]	170	105	75	45
Underground[c]	0	0	0	0
Costs for Street B ($)				
Existing[a]	210	210	210	210
Breakaway[a]	210	210	210	210
Relocate[b]	170	115	95	40
Underground[c]	0	0	0	0

[a]Utility poles located 2 ft from edge of traveled way.
[b]Utility poles located 10 ft from edge of traveled way.
[c]No utility poles.

objects, the breakaway alternative has the lower annual accident cost. This is because, when there are fewer fixed objects, the effect of the increased offset of the utility poles as in the relocation alternative is greater than the reduced collision severity is of utility poles as in the breakaway alternative. However, where there are more fixed objects, the probability that an encroaching vehicle will be on a path that intersects the location of a fixed object increases, which causes the screening of fixed objects by the utility poles to become the dominant factor. This favors the breakaway alternative because collisions with breakaway utility poles are less severe than are those with fixed objects.

However, on street B, the screening effect of utility poles is less significant because the fixed objects are located farther back from the edge of the traveled way. Consequently, on street B, the relocation alternative has a lower annual accident cost than the breakaway alternative does over the entire range of the number of fixed objects evaluated.

Also, in all cases, the annual accident costs for 30 000 ADT are twice those for 15 000 ADT. This is because the encroachment rate used is simply a linear function of ADT.

The total annual costs for 15 000 and 30 000 ADT are shown in Figure 6 (top and bottom, respectively). A comparison of the curves for total annual cost shown in Figure 6 indicates that the best alternative when there are 13 or fewer fixed objects is underground placement of utility lines. But as the number of fixed objects is increased, the increase in accident costs of fixed-object collisions offsets the effect of removing the utility poles. Thus, on street A, underground placement is no longer the lowest cost alternative, and breakaway poles become the best alternative due to the screening of fixed objects by the utility poles described earlier. However, on street B, this screening ef-

Figure 5. Annual accident costs for 15 000 (top) and 30 000 (bottom) ADT.

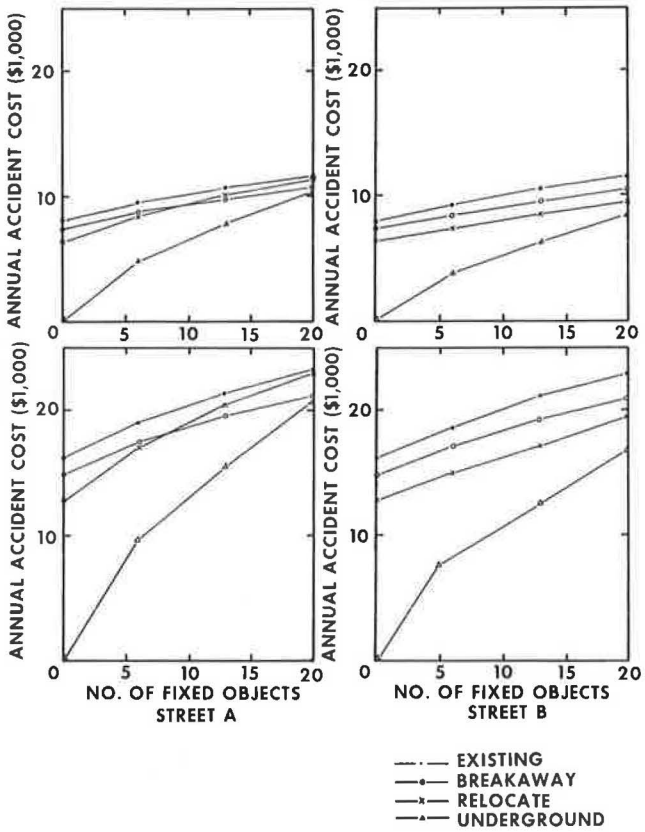

Figure 6. Total annual costs for 15 000 (top) and 30 000 (bottom) ADT.

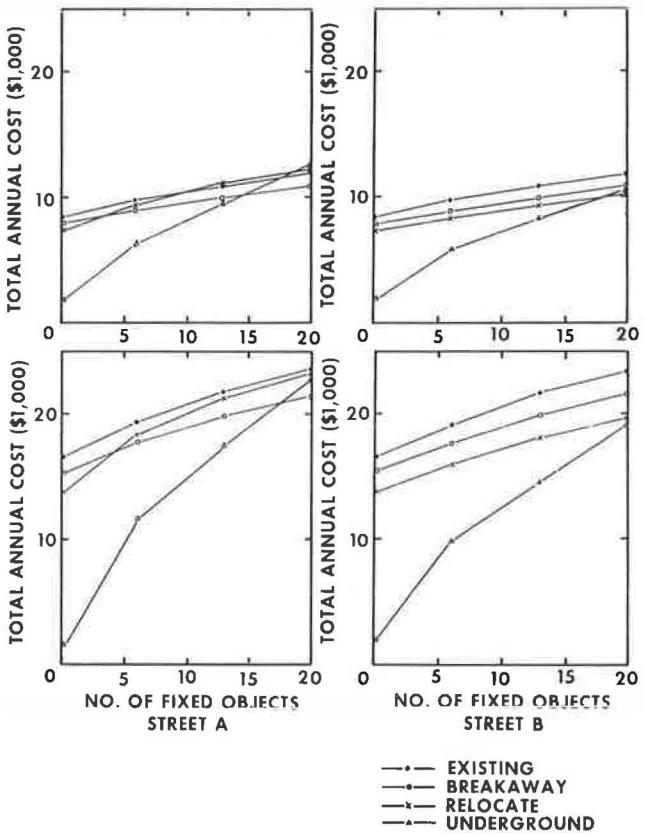

fect is less significant because the fixed objects are farther from the edge of the traveled way. Therefore, underground placement is the best alternative for a greater number of fixed objects on street B.

The results shown in Figure 6 for 30 000 ADT show a similar best-alternative pattern. However, on street B, because of the higher annual accident costs, the effects of zero utility-pole accident costs by using underground placement are not offset as quickly with increased numbers of fixed objects. Thus, underground placement is the best alternative in all cases for 30 000 ADT on street B.

CONCLUSIONS

The demonstration of the methodology presented above indicates its applicability to a variety of improvement alternatives and various traffic and roadside conditions. Also, it illustrates the sensitivity of the selection of the best improvement alternative to traffic and roadside conditions. However, generalization concerning the relative economies of the alternatives should not be made on the basis of these results. It must be remembered that these results were for only one vehicle size, one utility-pole spacing, and one other type of fixed object, which was assumed to have the same collision properties as the nonbreakaway utility poles. Again, the purpose of the demonstration was not to identify the best alternatives for all conditions but to show the applicability of the methodology and some effects of traffic and roadside conditions on the relative economies of the alternatives. Also, although not described in this paper, the demonstration was conducted with the aid of a computer program of the methodology, which obviously facilitated the computations.

Finally, it should be noted that meaningful results from the use of the methodology require that local unit cost data be used. The costs used in the demonstration will most likely not be appropriate for other times and other places. Also, in the presentation of the formulation of the methodology, the results of research on the nature and frequency of roadside encroachments and collision severities, which are used in the calculation of accident and collision maintenance costs, were included. Their inclusion was primarily for the purpose of showing the nature of these factors and how they are incorporated within the methodology. However, the integrity of the methodology would not be compromised if the values of these factors were modified in accordance with the results of more recent (or future) research. In fact, such modifications should be made as more knowledge is gained.

REFERENCES

1. Cost-Effectiveness of Countermeasures for Utility Poles. Federal Highway Administration, U.S. Department of Transportation, June 1980.
2. E.R. Post, P.T. McCoy, and others. Feasibility Study of Breakaway Stub Concept for Wooden Utility Poles. Civil Engineering Department, Univ. of Nebraska--Lincoln, Res. Rept. TRP-03-005-79, Dec. 1979.
3. J.W. Hutchinson and T.W. Kennedy. Median of Divided Highways--Frequency and Nature of Vehicle Encroachments. Univ. of Illinois, Urbana-Champaign, Engineering Experiment Station Bull. 487, 1966.
4. J.C. Glennon and C.J. Wilton. Methodology for Determining the Safety Effectiveness of Improvements on All Classes of Highways. In Effectiveness of Roadside Safety Improvements, Rept. FHWA-RD-75-23, Federal Highway Department, U.S. Department of Transportation, Nov. 1974, Vol. 1-A.
5. H.E. Ross. Impact Performance and a Selection Criterion for Texas Median Barriers. Texas A&M Univ., College Station, TTI Res. Rept. 140-8, April 1974.
6. Institute of Traffic Engineers. Transportation and Traffic Engineering Handbook. Prentice-Hall, Englewood Cliffs, NJ, 1976.
7. E.R. Post and P.T. McCoy. Feasibility Study of Retrofitting Concrete Median Barriers. Civil Engineering Department, Univ. of Nebraska--Lincoln, Res. Rept. TRP-03-006-80, May 1980.
8. E.R. Post, R.J. Ruby, P.T. McCoy, and D.O. Coolidge. Cost-Effectiveness of Driveway Slope Improvements. TRB, Transportation Research Record 685, 1978, pp. 14-19.

Publication of this paper sponsored by Committee on Safety Appurtenances and Committee on Utilities.

Abridgment

Loads on Bridge Railings

JAMES S. NOEL, T.J. HIRSCH, C.E. BUTH, AND A. ARNOLD

Recent and ongoing research studies have addressed the problem of improving the performance of bridge-railing systems and extending the range of vehicles that can be restrained. This paper summarizes the results of one of these studies. A series of full-scale crash tests was completed that used several representative vehicle geometries and weights and an instrumented concrete barrier. The measured resultant loads, locations, and distributions are tabulated and discussed. Because the wall is relatively rigid—at least in comparison with most bridge railings—it is an obvious conclusion that the reported force magnitudes represent an upper limit. They are expected to be considerably smaller for collisions with more-compliant barriers. An equal corollary is that the contact duration will be longer.

The American Association of State Highway and Transportation Officials (AASHTO) Standard Specifications for Highway Bridges (1) sets forth design requirements for bridge railings. These requirements include limits on certain geometrics and set forth design loads. The basic load is a 10-kip static force applied at any location along the longitudinal axis of the railing; the vertical distribution depends on the railing configuration. The specifications further require that elastic structural analysis and design procedures be employed.

These requirements are intended to produce bridge-railing designs that will function adequately for most traffic conditions that involve full-sized automobiles; the reserve load capacity of the railing, besides its elastic strength, offers some degree of protection for heavier vehicles such as school buses.

Characteristics of the vehicle population are changing. The advent of the smaller, subcompact automobile and its increasing popularity present new considerations to the designer of bridge railings. Also, recent catastrophic accidents that involved large vehicles have brought about an increased awareness of a need to provide better protection for these vehicles. Several recently completed and ongoing research studies have addressed the question of design requirements and performance standards for bridge railings. This paper presents a portion of the results from one of these studies.

An instrumented concrete wall designed specifically to measure the magnitude and location of vehicle impact forces was constructed. The relatively rigid wall, as shown in Figure 1, consisted of four 10-ft-long concrete panels each supported by four link-type load cells. Each of the massive panels (42 in high and 24 in thick) had an accelerometer to account for inertia factors. Surfaces that made contact with adjacent panels (and the supporting slab) were Teflon coated to minimize friction. A simple computer program was used to calculate force magnitudes and locations panel by panel from the electrical outputs. A static calibration of the system provided the correspondence factors required by the computer program. The results were successfully confirmed by using a dynamic calibration that involved a large mass and contact pad.

Eight actual full-scale impact tests were completed: two used subcompact 1800-lb sedans, two used compact 2250-lb sedans, two used full-sized 4500-lb sedans, one used a 66-passenger 20 000-lb school bus, and one used a two-axle 32 000-lb intercity bus. In most of the tests, the angle of impact was 15°; however, in two tests, it was more than 20°. Vehicle speeds in all tests were near 60 mph.

The results of these tests were measured and recorded on magnetic tape and on film. These data were analyzed to determine the resultant magnitudes, locations, and distributions of the contact forces. Once the time-changing magnitudes and locations of the resultant forces on the four instrumented wall segments during each collision are known, it is necessary to make judgments concerning the distributions of the contact (or bearing) stresses.

The first of these judgments concerned how to handle force spikes and other rapidly changing phenomena observed from the instrumented-wall outputs. These spikes are of little consequence to the required structural integrity of bridge railings. Therefore, maximum forces were obtained by averaging the data over 0.05-s intervals. Two such 0.05-s intervals were inevitably appropriate for each of these tests--one for the initial impact of front fender, bumper, and wheel with the rail and one for the second, or final, impact as the rear of the vehicle rotates into the rail. Each 0.05-s increment was chosen to give the largest average resultant force.

Figure 1. Instrumented wall.

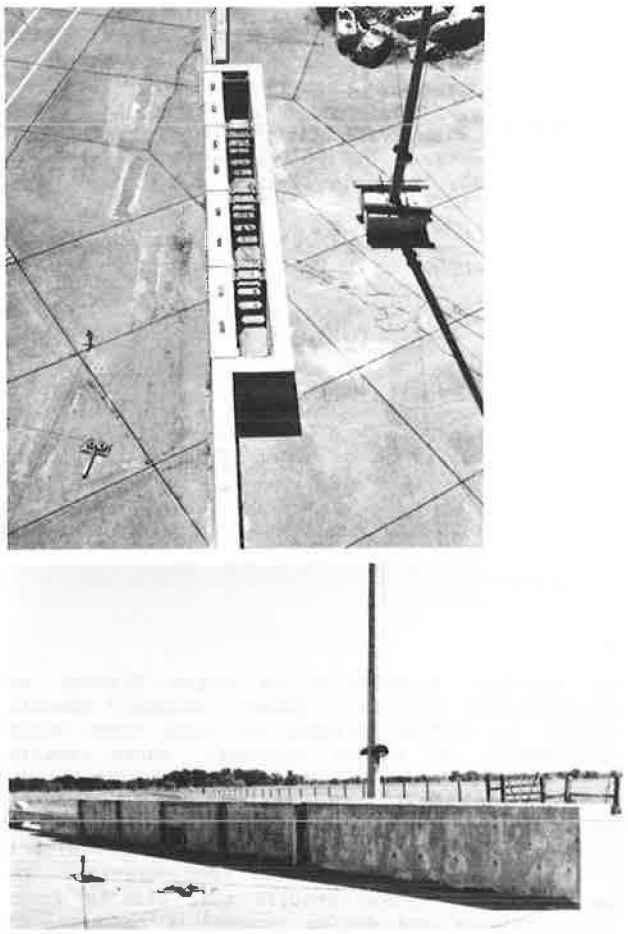

Figure 2. Measured data from test that used 4740-lb vehicle, 59.9 mph, and 24.0°.

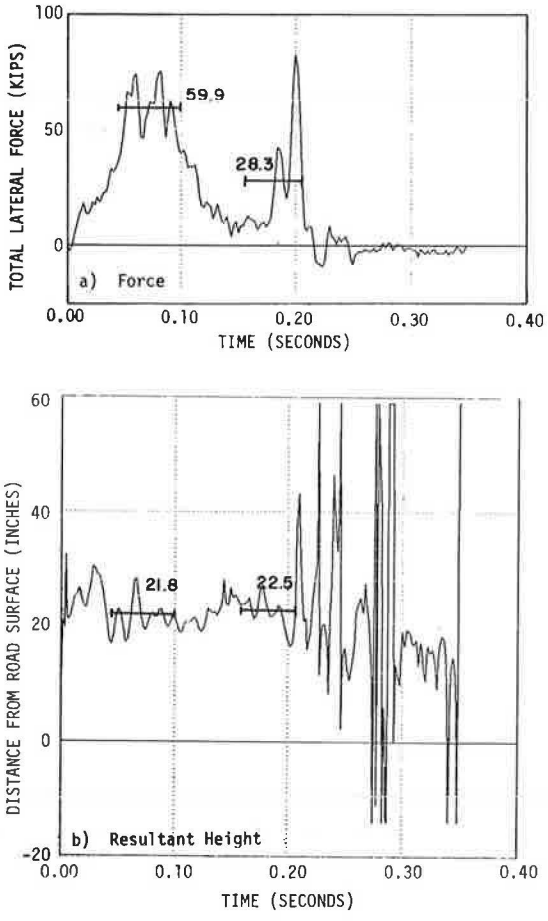

Figure 3. Measured data from test that used 20 030-lb vehicle, 57.6 mph, and 15.0°.

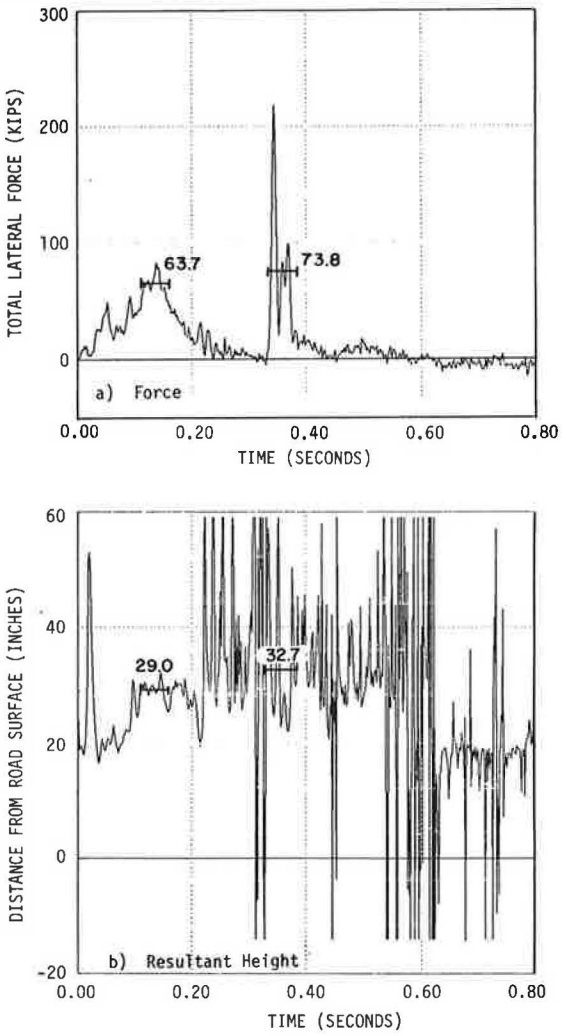

Figure 4. Measured data from test that used 32 020-lb vehicle, 60.0 mph, and 15.0°.

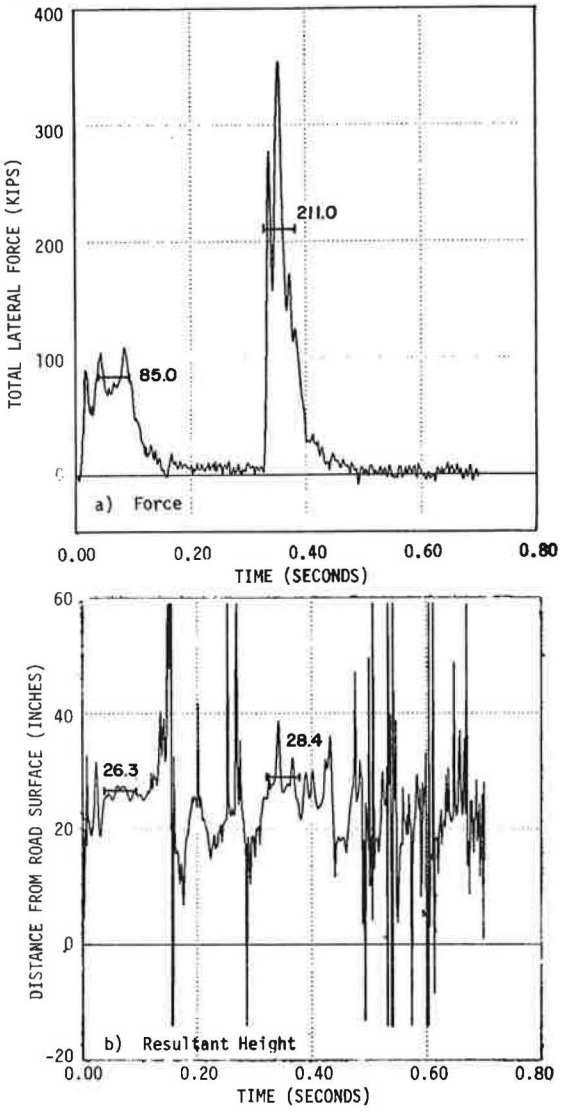

Figure 5. Distribution of contact pressures.

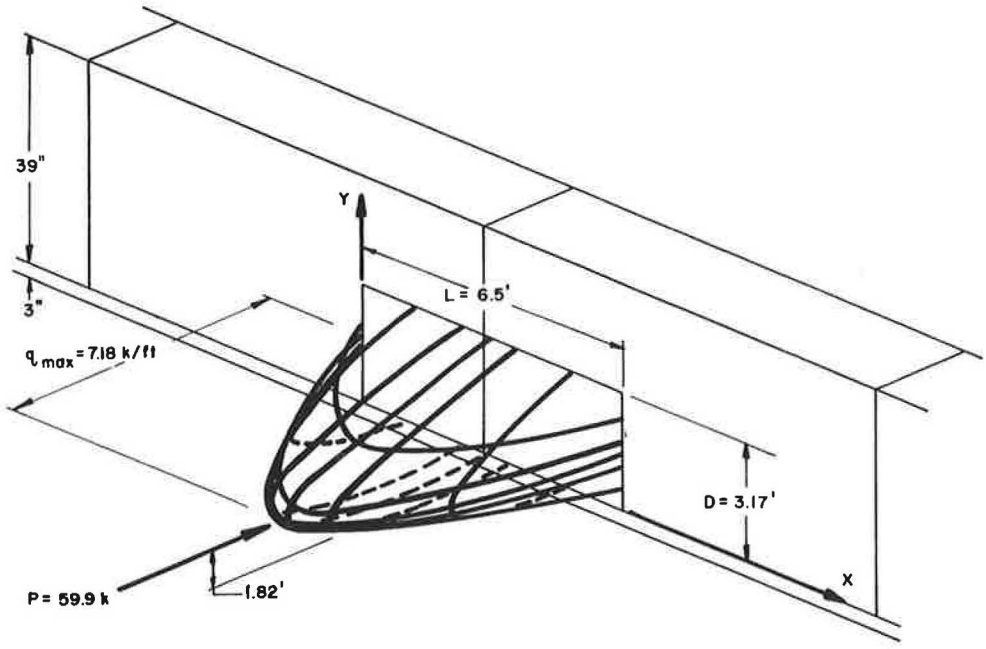

Figure 6. Longitudinal distribution for initial impact (top) and final impact (bottom) of 4740-lb vehicle at 59.9 mph and 24.0°.

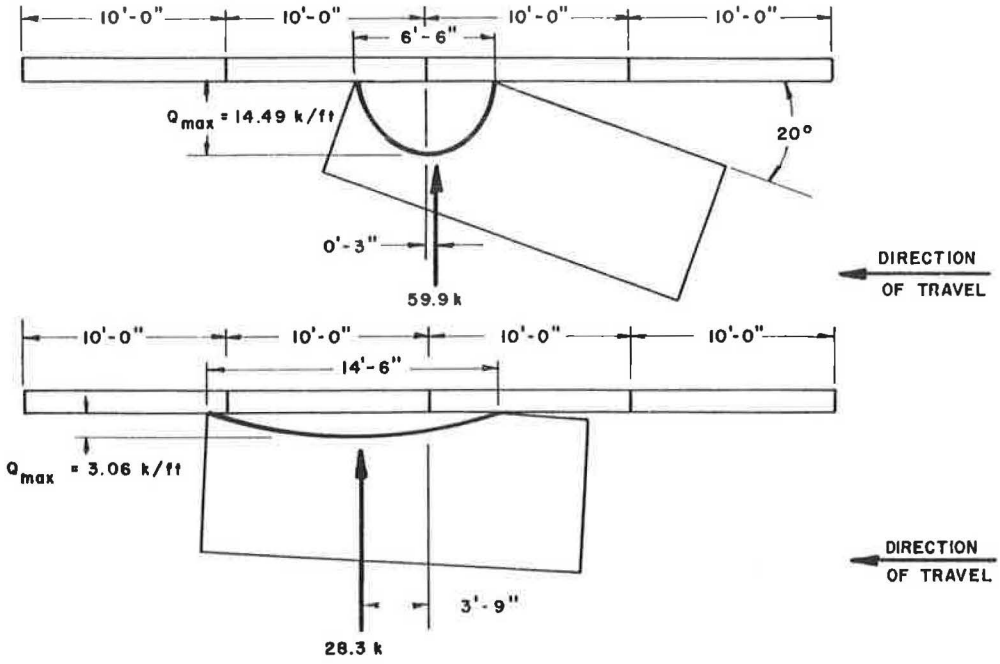

Table 1. Distribution of forces calculated from the instrumented-wall tests.

Test Condition				Resultant				Maximum Force (kips/ft²)	
Weight (lb)	Speed (mph)	Angle (°)	Impact Phase	Height (in)	Magnitude (kips)	Contact Height (ft)	Contact Length (ft)	Per Unit Area	Per Unit Length
2 050	59.0	15.5	Initial	17.0	18.4	2.33	5.0	3.89	5.76
			Final	18.7	8.4	2.58	7.6	1.11	1.82
2 090	58.5	21.0	Initial	19.0	21.1	2.67	6.0	3.25	5.52
			Final	20.7	13.1	3.00	8.0	1.35	2.58
2 800	58.3	15.0	Initial	18.1	18.5	2.50	5.0	3.85	5.81
			Final	15.3	13.9	2.08	10.8	1.82	2.01
2 830	56.0	18.5	Initial	19.3	22.0	2.92	4.8	3.65	7.61
			Final	21.3	22.5	3.00	10.2	1.52	3.48
4 680	52.9	15.0	Initial	21.4	52.5	3.08	7.3	5.73	11.24
			Final	24.0	28.3	3.25	10.7	2.01	4.16
4 740	59.9	24.0	Initial	21.8	59.9	3.17	6.5	7.18	14.49
			Final	22.5	28.3	3.25	14.5	1.48	3.06
20 030	57.6	15.0	Initial	29.0	63.7	2.17	12.3	5.88	8.12
			Final	32.7	73.8	1.58	25.5	4.51	4.54
32 020	60.0	15.0	Initial	26.3	85.0	2.58	6.3	12.90	21.20
			Final	28.4	211.0	2.25	15.0	15.40	22.10

Three examples of these resultant forces averaged over two 0.05-s intervals are shown in Figures 2a, 3a, and 4a for the impacts of the 4500-lb sedan, the school bus, and the intercity bus, respectively. Figures 2b, 3b, and 4b show the resultant heights during the same time intervals.

Definition of the manner in which the resultant forces are assumed to be distributed over the contact area also required engineering judgments. It was considered obvious that bearing pressure was present at all points of contact between the vehicle and the wall. It was equally obvious that the largest pressures by far were where the elements of the vehicle frame, especially the wheels, made contact with the wall. To include all these considerations in determining the pressure distribution seemed unduly complex. So, to simplify, it was decided to distribute the pressure as one-half a sine wave in both the horizontal and vertical directions. This consideration yielded the following equation:

$$R = \int_0^D \int_0^L q_{max} \sin(\pi x/L) \sin(\pi y/D)\, dy dx \quad (1)$$

where q_{max} is the maximum bearing intensity in kips per square foot, R is the resultant force in kips, and the coordinates x and y and the dimensions L and D (all in feet) of the rectangular contact area are shown in Figure 5. [To calculate the magnitude of the maximum pressure between the vehicle and the wall, the following equation was used: q_{max} = (59.9 kips) (π^2/4DL) = 7.16 kips/ft².] The length of the contact area was measured from the plan-view movie frame that fell nearest the center of each 0.05-s time interval (for both the initial and the final impacts).

An example of how these two frames looked (in this instance for the 4500-lb vehicle that impacted at 24°) and how the longitudinal distributions of contact pressure were deduced from them is indicated by Figure 6 (top and bottom). The depth dimension was deduced by subtracting the 3-in sill height (see Figure 5) from the height of the resultant to find D/2 or, when the resultant lay above (39/2) + 3 = 22.5 in (the mid height of the wall panels), by subtracting the resultant height from 42 in to find D/2. After integration and inversion to solve for the maximum intensity in terms of the measured resultant, one finds that $q_{max} = R\ (\pi^2/4DL)$. The double-sine distribution for the initial impact of the 4740-lb vehicle at 59.9 mph and 24° is shown in Figure 5.

A summary of results from all tests is given in Table 1. Data for both the initial and the final phases of the impact are given for each test. The column headed Height gives the distance from the pavement surface to the resultant impact force, whereas the column headed Contact Height gives the vertical dimension over which the force was distributed. Similarly, the contact length is the distance along the railing over which the force was distributed. These values were used to derive the data in the last two columns, which contain peak values (for the half-sine-wave distribution) of force per unit area and per unit length.

It should be noted that the force measurements were obtained from a nondeflecting barrier and represent the upper bound of forces that would be expected on service railings. Tests conducted on service railings that had typical deflection capabilities result in forces significantly lower than those shown in Table 1.

REFERENCE

1. Standard Specifications for Highway Bridges, 11th ed. AASHTO, Washington, DC, 1973.

Publication of this paper sponsored by Committee on Safety Appurtenances.

Strength of Fillet Welds in Aluminum Lighting Poles

JAMES S. NOEL, C.E. BUTH, AND T.J. HIRSCH

Tests were performed to ascertain the inherent strength of aluminum fillet welds such as those used to make lighting support poles for highways. It was found that two sources of excess strength beyond that recognized by current design specifications were often available. One was that the strength of a fillet weld when loaded so that the resultant forces are perpendicular to its length is 35-45 percent greater than when it is loaded parallel to its length. The other, applicable only to members that are hollow and round or near-round (as are virtually all the aluminum highway lighting support poles), was that the shape factor for such cross sections was 1.31 rather than 1.12, the shape factor often used for most metal structural shapes. Examples of a near-round member include many-sided polygons and ellipses in which the major and minor axes are nearly the same length. Because the shape factor represents excess strength beyond first yield, this finding represents a [(1.31/1.12) - 1] 100 percent = 17 percent increase in load-carrying capacity. A method is suggested for amending the applicable specifications to reflect these greater strengths.

Weld sizes used by manufacturers of spun-aluminum lighting poles were established primarily on the basis of tests conducted by the individual companies. Although experience has shown that these weld sizes are satisfactory, both state and federal highway engineers have questioned whether they can be justified by using only the requirements of the American Association of State Highway and Transportation Officials (AASHTO) (1).

The AASHTO specifications refer to the Aluminum Association's Specifications for Aluminum Bridge and Other Highway Structures (2), which calls for an allowable shear stress of 30 MPa in fillet welds of filler alloy 4043 with parent alloy 6063. This allowable stress was established on the basis of longitudinal shear stress tests of fillet welds and a bridge safety factor of 2.64.

The geometry at the base of most aluminum highway support poles is similar to that shown in Figure 1. The relatively thin-walled circular pole is connected into a cast-aluminum base flange by a circumferential fillet weld or welds as shown. Bending of the pole by the forces of nature causes the fillet welds to be stressed perpendicular to their lengthwise (circumferential) direction. Part of the purpose of this study was to determine whether an allowable stress greater than 30 MPa should be used because of the difference in strength between transverse and longitudinal loading of fillet welds.

The effect that the circular shape of the weld has on the bending strength of the joint was also included among the objectives. The published allowable stresses for bending of round and elliptical tubes take into account the greater strength of these shapes compared with that of other shapes. But these same effects are not recognized by the allowable stresses prescribed for circumferential welds.

The Tapered Aluminum Pole Group of the National Electrical Manufacturers Association elected to support a program designed to quantify the significance of these effects and, if possible, to suggest how the results could be incorporated into the existing specifications for such structures.

STRENGTH OF TRANSVERSE VERSUS LONGITUDINAL FILLET WELDS

Comparison of the results of the tests of weld splices in flat-bar specimens confirmed what has long been known by structural engineers, namely, that the load-carrying capacity of a fillet weld transverse to the direction of a tensile traction is considerably greater than that of a fillet weld parallel to the traction. Spraragen and Claussen (3) report that tests of fillet welds in the 1920s and 1930s had already determined that transverse fillets would carry up to 40 percent more load than would parallel fillets. Usually this difference in strength is ignored by design specifications, which are predicated on the weakest possible configuration for the weld and load. Associated commentaries and textbooks usually explain that the excess strength is disregarded, primarily to simplify calculations (4).

A simple strength-of-materials approach to demonstrating the excess strength, as opposed to a theory-of-elasticity approach, is quite convincing.

Figure 1. Typical pole base section.

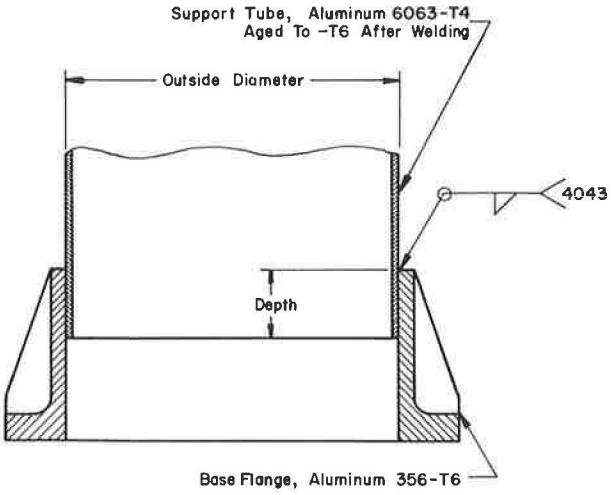

Consider a free body of a transverse weld on a double-lap shear specimen (Figure 2). For equilibrium in the horizontal direction, we have a tensile force P of the same magnitude on the horizontal face. In order to maintain complete equilibrium of the weld, a shear force P on the vertical face and a tensile force P on the horizontal face must be included. This results in a homogeneous state of plane stress everywhere in the weld such as that shown on a small cubical element in Figure 3a or, with Mohr's circle, that in Figure 3b. From the latter, one promptly sees that the maximum shear stress is $\tau_{max} = P/sL$ or $\tau_{max} = 0.707 (P/A_{throat})$, where s is the weld leg size and L is the weld length. In other words, the maximum shear in welds loaded transversely is only 71 percent as great as the maximum shear stress in a longitudinal fillet weld subjected to the same force. So it follows that the transverse shear strength should be 1.41 times as great as the longitudinal shear strength.

Much more complete explanations of this phenomenon can be found; one of the more elaborate is that offered by Kato and others (5,6). Their analysis used the von Mises criterion for yield, assumed the direct stress on the tensile face of the transverse weld to be uniformly distributed, and neglected the geometrical changes that occur during loading. Their conclusions were that a unit length of transverse weld could carry 1.46 times the load that a symmetrically loaded unit length of longitudinal weld could. These conclusions were subsequently confirmed by using a dense mesh finite-element computer program (1). One advantage of finite-element approaches for such calculations is that elastic solutions can be compared with elastoplastic solutions, a comparison that, in this instance, revealed little difference in the relative capacities of transverse and parallel fillet welds irrespective of the assumed material behavior.

The analyses have been very carefully corroborated by tests, especially for steel (3,7,8). However, there appears to be a paucity of comparable data for aluminum. This explains the motivation for performing the tests reported here.

Data summaries of flat-bar tensile test samples that have transverse and longitudinal splice welds are given in Table 1. The statistical summary is given below:

Statistic (MPa)	Type of Weld: Transverse	Type of Weld: Longitudinal
Avg, all specimens	177	132.0
SD	14	11.1
Lowest value	150	112.0
Mean minus 3 SD	135	98.6

The double-lapped, butt-joint test specimens were fabricated by using 4043 weld wire on 6063-T4 aluminum plate that was then precipitation heat treated (artificially aged) to the T6 temper after welding. All welds were terminated by using saw cuts to assure as little variation as possible in the effective lengths. The entries in the column headed Nominal Weld Stress at Failure were calculated by dividing the failure load by the weld length and the throat depth. The table indicates that a few of the welds had unequal leg lengths (sizes). The throat depth for a fillet weld that has unequal leg lengths is defined in Figure 4.

A comparison of the magnitudes of the average weld failure stresses in the two test configurations clearly and expectedly showed that the transverse weld was 177 MPa/132 MPa = 1.34 times as strong as the longitudinal weld. This result led directly to the decision to recommend that Table 7.1.3.2 [Allowable Shear Stresses in Fillet Welds for Bridge Type Structures in the Alumination Association's Specifications for Aluminum Bridge and Other Highway Structures (2)] be amended by adding a tabulation of allowable stresses for fillet welds loaded transversely in which the allowables are increased by a factor of 1.36. Thus, the allowable stress of 30 MPa (4.4 ksi) specified for 4043 fillets on 6063-T6 aluminum would be increased to 41 MPa (6.0 ksi). The justification is equally as applicable for 4043 welds on other aluminum alloys (see Figure 5).

BENDING LOADS VERSUS AXIAL LOADS

Tubes Welded to Flat Base Plate and Loaded in Axial Tension

The 12 specimens tested in this series were tubes 12.7 cm in diameter and approximately 2.1 m long welded to a flat base plate. An increasing axial tensile load was applied until failure occurred. The loading system consisted of a frame that had a hydraulic ram connected to the specimens by using a collect system. The failure mode was simultaneous failure around the circumferential weld and approximately on the plane defined by the throat of the weld based on the inscribed right triangle indicated in Figure 4.

The stresses in the welds at failure were calculated by using the following formula, which results in the conventional computation of stress on the throat of the weld:

$$f_t = P/\pi\psi(d + \psi) \quad (1)$$

where

f_t = tensile transverse shear stress (MPa),
P = applied load (N),
ψ = throat depth (mm), and
d = outside diameter of tube (mm).

Failure stresses calculated by using Equation 1 are presented in Table 2.

Tubes Welded to Flat Base Plate and Loaded in Bending

Each of the 12 specimens for this type of test consisted of a tube 12.7 cm in diameter and approximately 3 m long that had a 4.77-mm wall and was attached to a flat aluminum base plate by a single circumferential fillet weld. The specimens were loaded as cantilever beams. An increasing load was applied a measured distance from the weld until failure occurred. The loading rate was such that the time to failure was approximately 3 min. Failure mode was rupture of the weld in the region of highest tensile stress.

Stresses in the welds at failure were computed by using the following formula, which is based on

Figure 2. Free body of a simple transverse fillet weld.

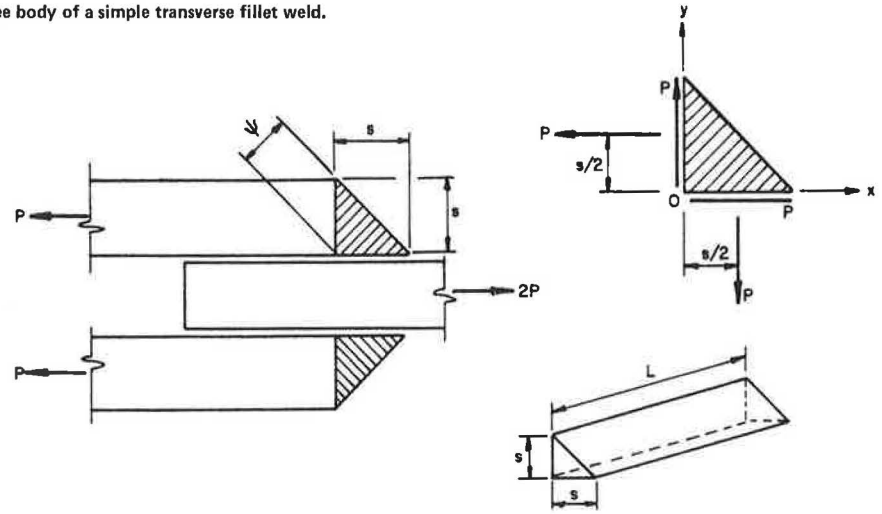

Figure 3. Simplified stress state hypothesized for fillet weld loaded as shown in Figure 2.

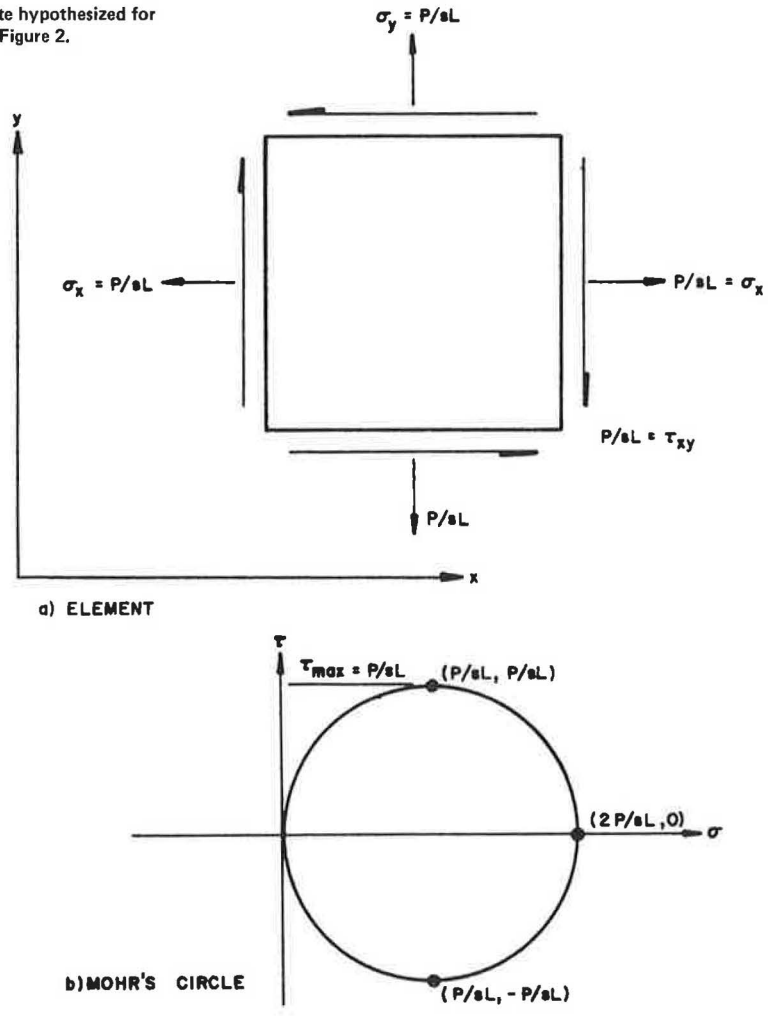

Table 1. Flat-bar specimens with transverse and longitudinal welds.

Average Weld Size (cm)	Weld Length (cm)	Failure Load (kN)	Nominal Weld Stress at Failure (MPa)
Specimen with Transverse Weld			
0.635 x 0.635	5.08	38.8	170
0.635 x 0.635	5.08	38.3	168
0.635 x 0.635	5.08	37.8	165
0.635 x 0.635	5.08	34.1	150
0.635 x 0.635	5.08	38.3	168
0.635 x 0.635	5.08	45.5	199
0.635 x 0.635	5.08	40.6	178
0.635 x 0.635	5.08	46.2	203
0.635 x 0.635	5.08	44.0	193
0.635 x 0.635	5.08	44.9	174
0.635 x 0.635	5.08	41.4	181
0.635 x 0.635	5.08	39.6	174
0.635 x 0.635	5.08	41.2	181
0.635 x 0.635	5.08	40.5	177
	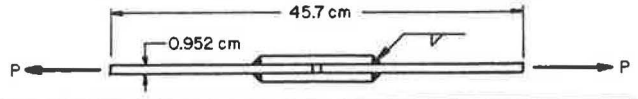		
Specimen with Longitudinal Weld			
0.762 x 0.635	14.5	78.7	112
0.635 x 0.635	14.7	85.0	128
0.635 x 0.762	14.6	102.0	143
0.635 x 0.711	14.4	96.1	141
0.762 x 0.635	14.5	95.4	135
0.762 x 0.635	14.2	97.7	141
0.635 x 0.635	14.7	89.6	136
0.635 x 0.635	15.0	80.9	120
	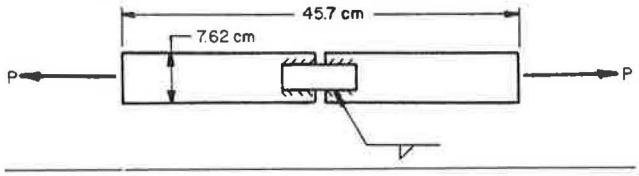		

elastic theory and results in the stress on the throat of the weld:

$$\sigma = M_b c/I \quad (2)$$

where

M_b = applied bending moment (N*mm),
c = (d + 2ψ)/2,
d = inside diameter of weld (mm), and
I = (π/64) [(d + 2ψ)⁴ - d⁴].

A comparison of the maximum stresses measured in the bending tests (summarized in Table 3) with those measured in the tension tests indicates a ratio of 164 MPa ÷ 101 MPa = 1.62. This increase is credited to the excess strength over and beyond the moment attained when the extreme fiber first yields.

Tubes Welded to a Sleeve and Loaded in Axial Tension

In this group of nine tests, the specimens consisted of two tubes 20.3 cm in diameter and approximately 1.4 m long with 4.77-mm walls. The tubes were connected at the ends by a sleeve and two circumferential welds so that tension applied to the system would cause a transverse load on the welds. Each tube was inserted 1.27 cm into the sleeve. The specimens were connected by means of a collect system to an expanding frame that applied an increasing tensile load until failure occurred. Failure occurred simultaneously around the circumferential weld. The welds consistently failed on a plane that approximated the throat of the weld based on the inscribed right triangle.

Figure 4. Method used to compute throat depth based on leg lengths of fillet weld.

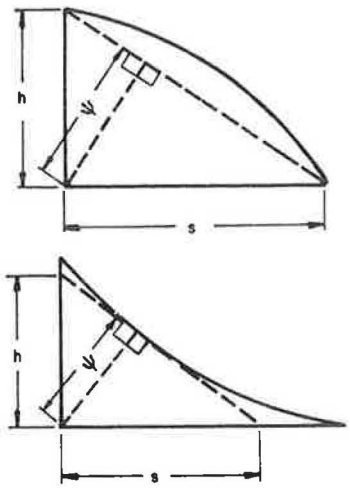

THROAT DEPTH = $s \cos \tan^{-1} \frac{s}{h} = \psi$

The stresses in the welds at failure were calculated by using the same method as that for the welds between tube and base plate. Table 2 presents these values also. The statistical summary from Table 2 is shown below:

Statistic (MPa)	Type of Weld To Flat Plate	To Sleeve
Avg, all specimens	102.0	113.0
SD	22.0	10.2
Lowest value	70.0	99.0
Mean minus 3 SD	35.5	82.5

Tubes Welded to a Sleeve and Loaded in Bending

The specimens for this test were two tubes 20.3 cm in diameter and approximately 1.4 m long with 4.77-mm walls. They were connected at the ends by a sleeve and two circumferential welds. The specimens were supported simply and had a span length of 2.6 m; they were loaded to failure by using two equal concentrated loads spaced 23 cm on either side of the midspan. This loading condition produced bending moment in the absence of beam shear on the weld joints. The applied load was incremented until failure occurred. The loading rate was such that the time to failure was 5 min. The welds failed consistently on the throat plane based on the inscribed right triangle. The failure mode was rupture of the weld in the region of highest tensile stress.

Weld failure stresses for these specimens were computed by using the elastic bending equation (used also for the tubes welded to a flat plate) and are presented in Table 3.

Again, the ratio of the average maximum bending stress to the average maximum axial stress is 137 MPa/113 MPa = 1.21. Although it is not 1.31, it should be noted that the maximum axial stress of 113 MPa is well above the ultimate stress expected to be nominal for this weld in simple tension. An inflated denominator would cause the ratio to appear too small.

Figure 5. Table 7.1.3.2 from Specifications for Aluminum Bridge and Other Highway Structures (2) showing changes suggested by test results.

TABLE 7.1.3.2
ALLOWABLE SHEAR STRESSES IN FILLET WELDS FOR BRIDGE TYPE STRUCTURES* -ksi

Filler Alloy ‡		1100	4043	4043 Transverse	5356 5554	5556
Parent Alloy						
	3003	2.8	4.4	6.0	–	–
Alclad	3004	–	4.4	6.0	6.5	7†
	5052	–	4.4	6.0	6.5	–
	5083	–	–	–	–	7.5
	5154	–	–	–	6.5	7.5
	5456	–	–	–	–	7.5
	6005, 6061, 6351	–	4.4	6.0	6.5	7.5
	6063	–	4.4	6.0	6†	6†

† Values controlled by the shear strength of the parent metal.

‡ Minimum expected shear strengths of filler alloys are:

Alloy	
1100	7.5 ksi
4043	11.5
5356	17
5554	17
5556	20

* When the welds join circular and near circular cross-sections which are to be loaded in bending these allowables may be multiplied by 1.17.

Note: 1 ksi = 6.89 MPa.

Table 2. Tubes welded to flat base plate and to a sleeve and loaded in axial tension.

Average Weld Size (cm)	Failure Load (kN)	Nominal Weld Stress at Failure (MPa)
Tube Welded to Flat Base Plate		
0.709 x 0.640	2.35	119
0.663 x 0.643	2.56	134
0.691 x 0.681	2.52	125
0.782 x 0.686	2.44	114
0.785 x 0.749	2.22	99
0.688 x 0.663	2.37	120
0.744 x 0.627	1.55	78
0.818 x 0.782	2.06	88
0.813 x 0.777	2.65	113
0.927 x 0.792	1.90	75
0.798 x 0.757	1.61	70
0.945 x 0.879	2.24	83

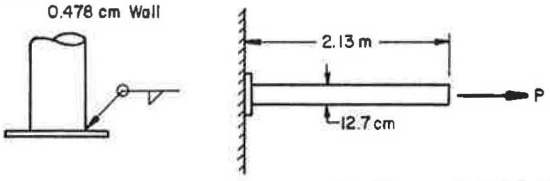

Tube Welded to Sleeve		
0.874 x 0.739	38.8	105
0.823 x 0.749	38.4	105
0.729 x 0.632	38.5	123
0.805 x 0.754	38.4	106
0.871 x 0.556	30.4	99
0.632 x 0.589	36.6	130
0.693 x 0.533	32.9	119
0.780 x 0.765	40.1	112
0.818 x 0.653	39.8	119

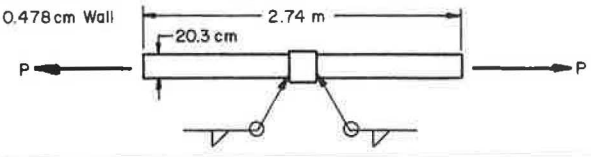

The calculated shape factor for typical lighting-pole dimensions is about 1.31. This can vary from 1.27 and more for very thin-walled circular shapes to 1.70 for solid circular shapes.

Shape factors for wide-flange shapes vary from about 1.10 to 1.18; the most frequent value is about 1.12 (8).

If one then compares the plastic moment of circular sections with the plastic moment of wide-flange sections, that for the circular section would be expected to be about 1.31/1.12 = 1.17 times greater than that for the typical wide flange.

TYPICAL LIGHTING-POLE BASES

Nine specimens configured as similar as possible to actual luminaire supports were then tested to assure the practicality of liberalizing the design allowables as suggested by theoretical considerations and laboratory tests. The cylindrical tube structures were 7.6 m long, had an outside diameter of 25.4 cm, and were 6.5 mm thick. This tube was inserted 1.27 cm into a cast-aluminum (356-T6) socket base and connected by means of a fillet weld all around the top of the base. These cantilevered beams were then subjected to a transverse end load. The transverse loads were increased at a rate that caused the average time to failure to be about 4 min. In all cases, failure was a result of a rupture of the weld in the region of maximum tensile stress. Failure occurred near the plane formed by the throat of the weld based on the inscribed right triangle.

The transverse shear stresses in the welds at failure were computed by using the following equation:

$$f_b = [M_B(d + 2\psi)/2] / [(\pi/8)(d^3\psi + 3d^2\psi^2 + 4d\psi^3 + \psi^4)] \quad (3)$$

where f_b is the transverse shear stress on the throat of the weld in megapascals and d is the outside diameter of the tube in millimeters.

It should be noted that stresses computed in this

Table 3. Tubes welded to flat base plate, to a sleeve, and into a support socket and loaded in bending.

Average Weld Size (cm)	Failure Load (kN)	Failure Moment (kN·m)	Elastic Failure Stress (MPa)
Tubes Welded to Flat Base Plate			
0.663 x 0.599	4.18	11.8	201
0.663 x 0.650	4.00	11.5	189
0.841 x 0.826	4.46	12.5	160
0.815 x 0.805	4.46	12.5	165
0.704 x 0.693	4.09	11.5	177
0.693 x 0.650	3.86	10.8	174
0.704 x 0.683	4.09	11.5	179
0.785 x 0.767	4.09	11.5	159
0.879 x 0.874	4.57	12.9	156
0.838 x 0.798	3.77	10.6	139
0.973 x 0.798	4.27	12.0	145
0.886 x 0.810	3.61	10.2	128
Tube Welded to Sleeve			
0.843 x 0.792	43.6	23.3	121
0.846 x 0.681	49.4	26.3	150
0.693 x 0.686	44.3	23.6	146
0.734 x 0.729	46.9	25.0	146
0.810 x 0.620	48.3	25.8	170
0.925 x 0.894	46.6	24.9	116
0.752 x 0.645	39.0	20.8	128
0.719 x 0.559	32.4	17.3	119
Tube Welded into Support Socket			
0.787 x 0.597	6.11	44.6	182
0.762 x 0.561	6.70	48.7	209
0.978 x 0.770	8.35	60.6	193
0.813 x 0.693	7.32	53.2	195
0.747 x 0.660	7.07	51.3	201
0.935 x 0.724	7.25	52.7	178
0.930 x 0.914	7.21	52.3	154
0.869 x 0.726	7.09	51.5	179
0.919 x 0.757	7.78	56.5	187

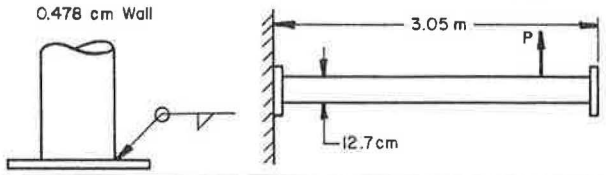

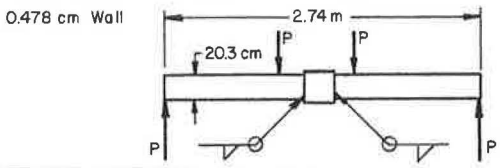

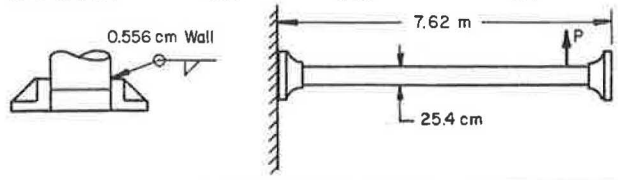

manner are based on elastic theory and a section modulus based on the weld throat, without regard to the direction of the applied load relative to the orientation of the weld. These stresses are given in Table 3. They vary from 152 to 207 MPa; the average is 186 MPa. Such luminaire bases thus demonstrate a factor of safety against their ultimate strength of 186 MPa/(1.36 x 1.31 x 30 MPa) ∿ 3.4, which is well above the prescribed 2.64 [we recall that the specifications (2) allowed a shear stress of 30 MPa].

The statistical summary from Table 3 is given below:

	Type of Weld		
Statistic (MPa)	To Flat Plate	To Sleeve	Into Support Socket
Avg, all specimens	164.0	137.0	186
SD	21.1	19.0	160
Lowest value	128.0	11.6	154
Mean minus 3 SD	101.0	80.1	139

CONCLUSIONS AND RECOMMENDATIONS

The data and theory presented here are in agreement with research reported in the literature and support the following conclusions:

1. The transverse shear strength of fillet welds is greater than the longitudinal shear strength. Commentaries and textbooks usually explain that the excess strength is disregarded, primarily to simplify design calculations. Tests reported here indicate that aluminum transverse welds are 34 percent stronger than longitudinal welds. A simple strength-of-materials calculation indicates that transverse fillet welds may have as much as 36 percent more strength than longitudinal fillet welds, whereas a more-sophisticated solution based on the theory of elasticity by Kato and Morita (5) suggests an even greater increase in strength, namely, 46 percent.

It is recommended that an allowable shear strength of 1.36 x 30 MPa = 41 MPa for aluminum fillet welds made of 4043 weld on 6063 parent metal aged to T6 temper after welding be permitted in typical lighting poles.

2. Round and oval tubular members and other beams of ductile materials exhibit bending strengths in excess of those predicted by elastic analysis procedures. This is due to the fact that, at ultimate loads, plasticity theory better describes the behavior of such members. Plasticity theory predicts that typical aluminum lighting-pole sections would exhibit strengths about 31 percent in excess of those predicted by elasticity theory. For wide-flange shapes and similar shapes, the excess strength is about 12 percent. This indicates that rounded and oval members are about 17 percent (1.31 ÷ 1.12 = 1.17) stronger in bending than are wide-flange shapes and similar shapes. This additional strength is recognized by the aluminum specifications (2) for the members themselves but not for the welds.

It is recommended that this 17 percent increase in the allowable stress in these types of aluminum beams be extended to the weld metal in circumferential joints in such members.

3. The two factors recommended above are additive. In other words, in a situation in which a circular-shaped fillet weld is subjected to a transverse shear as a result of bending moment, the allowable stress based on the throat area of the weld would be 30 MPa x 1.36 x 1.17 = 48 MPa.

4. The AASHTO Specifications for Structural Supports for Highway Signs, Luminaires and Traffic Signals (1) permit allowable stresses to be increased by 40 percent when stresses are produced by wind or seismic loading. Since the controlling design load for lighting poles is due to the wind, this 40 percent is especially significant and should be used. When this is done, the allowable stress would be 30 MPa x 1.36 x 1.17 x 1.40 = 68 MPa.

5. Table 7.1.3.2 of Allowable Shear Stresses in Fillet Welds for Bridge Type Structures in the Aluminum Association's Specifications for Aluminum

Bridge and Other Highway Structures (2) should be amended by adding a tabulation of allowable stresses for fillet welds loaded transversely in which the allowables are increased by a factor of 1.36. Thus, the allowable stress of 30 MPa specified for 4043 fillets on 6063-T6 parent metal shown would be increased to 41 MPa (footnoted to allow a further increase by a factor of 1.17 to 48 MPa if the fillet is joining round or near-round members subject to bending). The allowable of 41 MPa (6.0 ksi) is consistent with the factor of safety of 2.64. When it is intended that another factor of safety be used [for example, 2.34 in the Aluminum Association Specifications for Aluminum Structures (9)], this allowable could be modified accordingly if care is taken to assure that the shear strength of the parent metal is not exceeded.

REFERENCES

1. Standard Specifications for Structural Supports for Highway Signs, Luminaires and Traffic Signals. AASHTO, Washington, DC, 1975.
2. Specifications for Aluminum Bridge and Other Highway Structures. Aluminum Association, New York, April 1969.
3. W. Spraragen and G.E. Claussen. Static Tests of Fillet and Plug Welds: Review of Literature from 1932 to January 1, 1940. Welding Journal, April 1942.
4. J.C. McCormac. Structural Steel Design. 2d ed., Intext Educational Publishers, New York, 1971.
5. B. Kato and K. Morita. Strength of Transverse Fillet Welded Joints. Welding Journal, Welding Research Supplement, Feb. 1974, pp. 59s-64s.
6. B. Kato and T. Naka. Deformation and Strength of End Fillet Welds. Journal of the Faculty of Engineering, Univ. of Tokyo, Vol. 28, No. 3, 1966.
7. F.K. Lightenberg. International Test Series: Final Report. International Institute of Welding, New York, 1968.
8. L.S. Beedle. Plastic Design of Steel Frames. Wiley, New York, 1958.
9. Specifications for Aluminum Structures. Aluminum Association, New York, April 1976.

Publication of this paper sponsored by Committee on Safety Appurtenances.

Crash Tests of Light-Post Thrie-Beam Traffic Barriers

JAMES E. BRYDEN AND KENNETH C. HAHN

Thrie-beam corrugated steel rail (a W-beam that has a third corrugation) was tested as a single-rail upgrading for discontinuous bridge-rail panels and on S3x5.7 posts as a guiderail and double-faced median barrier. Tests were performed to determine rail deflection characteristics, structural adequacy, vehicle decelerations, and vehicle damage. Ten-gage Thrie beam was used for all tests. As a bridge-rail upgrading, the Thrie beam is suitable for 60-mph, 25° impacts by 4500-lb vehicles. As a guiderail or median barrier on S3X5.7 posts, it appears suitable as a longitudinal barrier, based on tests with 2250-lb and 3500-lb vehicles. Proposed design deflections for Thrie-beam guiderails and median barriers are close to those for box-beam guiderails and median barriers. Further testing of these guiderail and median-barrier designs would yield better definition of impact and redirection characteristics and would better indicate what actions could be taken to reduce the impact between the vehicle's wheel and the posts.

New York's most frequently used longitudinal traffic barrier systems consist of steel rail elements--cable, W-beam, or box beam--mounted on S3x5.7 steel posts. These light-post barriers depend primarily on rail tension or beam bending to redirect impacting vehicles because the posts yield on impact to prevent snagging of vehicles. Traffic accident studies confirm that their performance has generally been very good (1,2).

A new rail element called a Thrie beam was developed several years ago. It is a W-beam that has a third corrugation added. Tests reported by Southwest Research Institute (3) claim good performance for this rail element in strong-post designs, and other tests (4) indicate that tubular Thrie-beam bridge rail performs well as a bridge-rail upgrading system. However, before the work reported here was done, the Thrie beam had not been tested on S3x5.7 posts.

Despite the generally good performance of New York's light-post barriers, the Thrie-beam rail element seems to offer distinct advantages over current designs. The standard height of W-beam rail on S3x5.7 posts in New York State is now 33 in to the rail top. Less height increases the chances that large cars may penetrate the barrier (1). However, at the 33-in mounting height, small cars may tend to lodge beneath the rail.

To protect vehicles from snagging on rigid elements behind the 6-in vertical face of the box beam when there is a transition to a bridge parapet, a second rail element must be introduced before the transition. This second rail requires special hardware and must be terminated safely upstream well behind the main rail. Downstream, the box beam must be terminated flush with the concrete face to eliminate snag points. Very often the approach guiderail is a W-beam element that requires a complicated transition to box beam upstream of the bridge before the transition to the bridge parapet or rail.

Finally, a box-beam median barrier is troublesome to maintain. To replace any damaged posts, rail sections either 18 or 36 ft long that weigh 400 or 800 lb must be removed by using heavy mechanized equipment. Proper alignment of post paddles and rail slots and reassembly of the internal tube splices are difficult. Also, an impacted box-beam median barrier may bend at the mounting slots. Straightening damaged rails is very difficult and reassembly is impossible unless the rail elements are perfectly straight.

Because it is 20 in deep, Thrie-beam performance is much less sensitive to mounting height, and its resistance to penetration is greater for both small and large cars. At bridge parapets, the need for a transition from W-beam to box beam is eliminated. Neither the W-beam nor the Thrie beam need be terminated at concrete anchors. Instead, a commercially available transition of W-beam to Thrie beam is bolted in place to maintain rail tension. Beam

depth reduces the snag potential at bridge-rail parapets.

A 10-gage Thrie-beam rail on S3x5.7 posts could result in a median barrier or guiderail that has sufficient bending resistance and tension to produce deflections similar to those of box-beam median barriers or guiderails. Mounting details are similar to those for the W-beam and simpler than those for the box beam. Maintenance problems would be eliminated if the Thrie beam could be substituted for the box beam. By using S3x5.7 posts, the cushioning effect of the light-post systems would be maintained.

The overall aim of this study was to develop Thrie-beam traffic barriers and upgraded bridge rails that would result in improved motorist safety and lower maintenance costs. The safety aim would be realized through impact performance superior to that of current barrier designs (greater resistance to penetration), smoother transitions to bridge rails and parapets, and stronger and more forgiving bridge rails. The economic aims would be realized by eliminating special transitions and hardware and by easing median-barrier maintenance procedures as compared with those for box beams.

METHODOLOGY AND DESCRIPTION OF SYSTEMS

This study consisted of eight full-scale crash tests to determine the performance of Thrie beam for bridge-rail upgrading, guiderails, and double-rail median barriers. Testing details were taken from Transportation Research Circular 191 (5), and two major variations were used. For the bridge-rail tests, the standard impact conditions of 60 mph and 25° with a 4500-lb vehicle were the target conditions. For the guiderail and median-barrier tests, however, a 3500-lb vehicle weight was used because New York's light-post rail systems were developed by using 3500-lb vehicles and standard design deflections are based on that weight. Tests were also performed with 2250-lb sedans to evaluate impact severity.

Bridge-Rail Upgrading

The first Thrie-beam application tested was an upgrading of discontinuous-panel bridge railings. Such railings, designed to meet the 1957 American Association of State Highway Officials (AASHO) specifications (6), were installed in New York State through the mid-1960s. A three-post railing panel 34 in high, which is common on New York bridges, was chosen for testing.

A concrete footing 3 ft wide and 3 ft deep was used to anchor the bridge rail for these tests. It protruded 6 in above grade to present a 6-in curb height, which is common to almost all New York bridges; the remainder was below ground. For the transition tests, a firmly anchored timber curb, also 6 in high, was added to simulate the granite curb normally used on bridge approaches.

Thrie beam that was 10-gage rather than 12-gage was used because the added stiffness would help distribute impact loads over more bridge-rail posts, which reduced the chance of pocketing at panel ends and helped in the transition from guiderail to bridge rail. The first design (Figures 1 and 2) was tested by impacting on the bridge and on the approach guiderail. It consisted of spliced sections of 10-gage Thrie beam mounted directly onto the bridge rail; the rail top was 33 in above the pavement. The rail was held in place at each bridge-rail post by four 3/4-in bolts--two in each corrugation valley--around the post and through the 5/8-in backup plates. The approach rail was W-beam 33 in high that transitioned to the Thrie beam 53 ft upstream of the bridge and was mounted directly onto S3x5.7 steel posts on 6-ft 3-in centers. Near the bridge, post spacing narrowed to 4 ft 2 in (three spaces) and 3 ft 1-1/2 in (six spaces). The connection between post and rail was a single 5/16-in bolt at each post, except for the unconnected backup posts. An expansion splice, which consisted of a piece of Thrie beam 6 ft 3 in long that had the splice bolt holes elongated to 2-1/2 in, was installed at the bridge's upstream end. The 5/8-in splice bolts and the 5/16-in mounting bolt used in the expansion splice were installed handtight to permit longitudinal rail movement when the bridge expanded and contracted. Such a splice was used in each of these upgrading tests to determine whether splice slippage would adversely affect impact performance.

The first test was to confirm the system's adequacy to redirect vehicles that impacted on the bridge at standard conditions (4500 lb, 60 mph, 25°). The second test, which had an impact 10 ft upstream of the bridge rail, was conducted to determine whether the transition from guiderail to bridge rail that used S3x5.7 posts was strong enough to prevent rail pocketing and vehicle snagging on the end of the bridge rail.

After unsatisfactory performance in the second test, the transition was redesigned for the third (Figures 2 and 3). Five W6x8.5 posts on 3-ft centers were added just upstream of the bridge, and an S3x5.7 post pattern similar to that used in the previous two tests was installed upstream of the W6x8.5 posts. The transition was further strengthened by doubling the rail element for one and one-half rail lengths. The double rail extended 3 ft onto the bridge and 16 ft back onto the guiderail. The second rail element was simply placed over the first, and the splice bolt holes were adjusted as necessary to provide bolt clearance. The Thrie-beam approach rail was not tested at the change from light to heavy posts. Unlike the box beam, the wide bearing area of the Thrie beam does not cut into the vehicle sheet metal and thus keeps the vehicle's wheels relatively far from the heavy posts.

Impacts that used small cars at 15° were not included in the bridge-rail tests. Earlier tests by others (3,4) had already confirmed that Thrie-beam railing systems resulted in satisfactory redirection of small cars. Thus, as long as the strength of the bridge-rail upgrading proved adequate, redirection of small vehicles would not be a problem.

Guiderail and Median-Barrier

Bridge-railing upgrading tests were followed by two tests of guiderails (Figures 4 and 5). Ten-gage Thrie-beam rail mounted 33 in high on S3x5.7 posts at 6-ft 3-in centers was impacted by intermediate and compact cars.

Three tests of a median barrier were performed (Figures 5 and 6). Back-to-back 10-gage Thrie beam was bolted directly to S3x5.7 posts by using one 5/16-in bolt per rail at each post. Because of a possible wheel-snag problem detected in the two guiderail tests, rail height was reduced to 30 in. A post spacing of 6 ft 3 in was tested by using both an intermediate and a compact car, and a post spacing of 12 ft 6 in was tested with an intermediate-weight vehicle.

Ten-gage Thrie beam was used for the guiderail and median-barrier designs because it permitted duplication of deflection properties of box-beam barriers without the use of close post spacings and it eliminated the need to change beam thickness at bridge-rail transitions. Also, a single rail thickness for guiderail and bridge rail simplifies main-

Figure 1. Bridge-rail upgrading (tests 22 and 23).

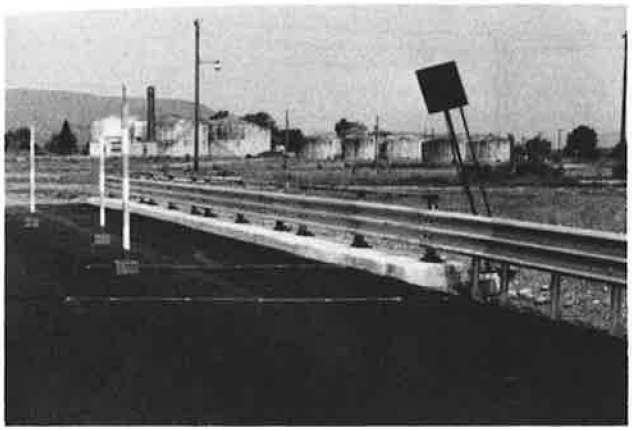

tenance inventory requirements and prevents the incorrect rail thickness from being used during repairs.

The guiderail and median barrier for these tests was installed on an asphalt pavement constructed over compacted gravel. This represents typical practice in New York State, where guiderail on new construction is installed on paved shoulders and medians. This condition may offer slightly greater post resistance than direct embedment in soil. However, New York's standard S3x5.7 posts include a soil plate 8x24 in, shown in past tests (7) to develop the full strength of the post even in weak soils. Thus, although the typical New York State post embedment tested may appear stiffer than direct soil embedment does, post reactions would probably be similar for both cases.

Figure 2. Details of bridge-rail upgrading (tests 22, 23, and 23A).

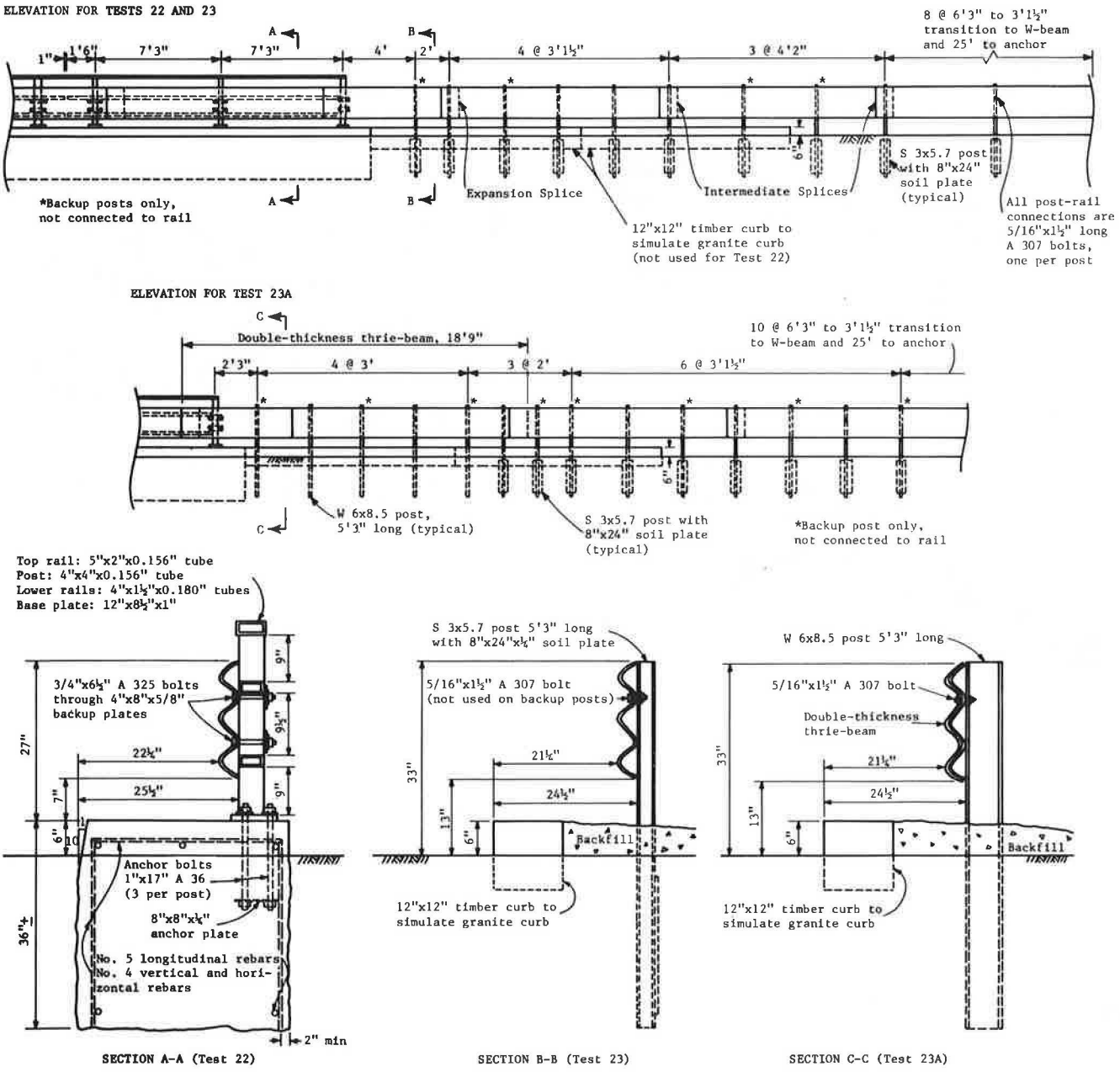

Figure 3. Bridge-rail upgrading (test 23A).

Figure 4. Guiderail with large car (test 24, top) and small car (test 25, bottom).

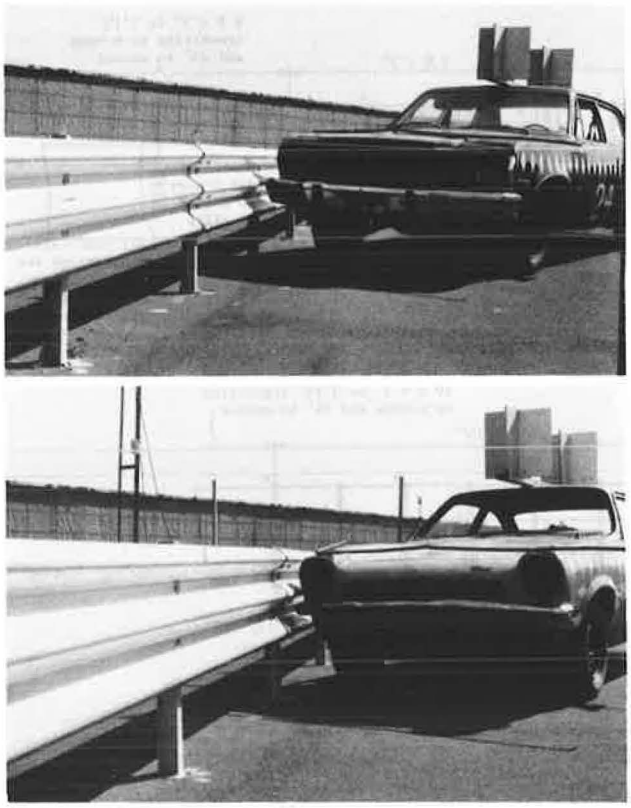

RESULTS

Bridge-Rail Upgrading Tests

Three full-scale crash tests of the Thrie-beam bridge-rail upgrading are summarized in Table 1. For the three tests of this upgrading, target impact conditions were 4500 lb, 60 mph, and 25°, although actual impact conditions varied somewhat.

For the first test (test 22), a 4500-lb sedan impacted the upgraded system at 25° and 53.3 mph 10 ft downstream from the first bridge-rail post. Impact occurred on the stone shield below the front bumper and on the right front wheel. No appreciable vaulting was apparent, because of the 6-in curb. The vehicle was in contact with the curb for 27 ft

Figure 5. Details of guiderail (tests 24 and 25, top) and median barrier (tests 26, 27, and 26A, bottom).

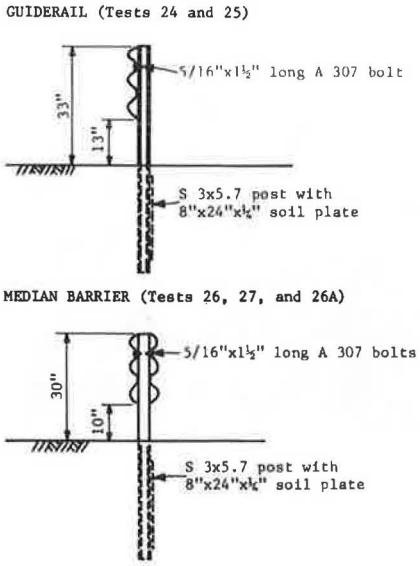

Figure 6. Median barrier that has 6-ft 3-in post spacing.

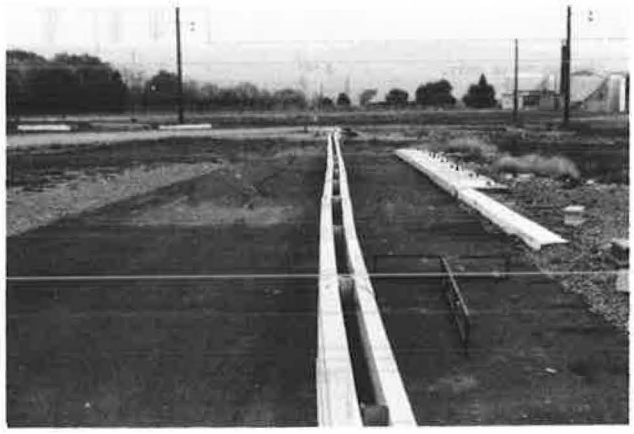

and with the rail assembly for 12 ft. Maximum dynamic rail deflection was 0.5 ft. On impact, the car rolled -2° (lett). The hood latch and right hood hinge broke, which allowed the hood to open and fall back over the windshield. As the car left the rail, it pitched +3° (down) and yawed a maximum of +17° (left) before straightening out along the exit trajectory. Redirection was fairly smooth and the car exited the system at 3°. After having left the barrier, the car traveled an additional 125 ft, turning to the right because of the severe damage to the right front suspension and sheet metal. The highest 50-ms decelerations were 9.8 g longitudinal and 2.8 g lateral. The vehicle suffered extensive front-end sheet-metal and suspension damage.

Rail damage was limited to one bent bridge-rail section and post and one bent Thrie-beam section. Permanent rail deflection was 0.2 ft, but no slippage occurred in the expansion splice at the end of the bridge. Slight bowing of the bridge-rail base plates resulted at posts on either side of impact, but neither the bridge-rail system nor the anchorage appeared close to failure. Based on this test, the Thrie-beam bridge-rail upgrading appears to have adequate strength to withstand impacts on the rail

Table 1. Results of bridge-rail upgrading tests.

Variable	Test 22	23	23A
Point of impact	10 ft onto bridge	10 ft before bridge	10 ft before bridge
Vehicle weight (lb)	4500[a]	4600[a]	4570[a]
Vehicle speed (mph)	53.3	51.7	60.9
Impact angle (°)	25	24	25
Exit angle (°)	3	22	11
Maximum roll (°)	-2	-7	+4
Maximum pitch (°)	+3	+6	-3
Maximum yaw (°)	+17	+19	-22
Contact distance[b] (ft)	27, 12	22, 18	21, 21
Contact time[c] (ms)	273	317	398
Deflection (ft)			
Dynamic	0.5	2.9	3.1
Permanent	0.2	1.8	1.2
Deceleration (*g*)			
50-ms avg			
Longitudinal	9.8	9.1	NA
Lateral	2.8	3.8	NA
Maximum peak			
Longitudinal	14.5	13.5	NA
Lateral	6.4	6.1	NA
Avg continuous			
Longitudinal	1.9	2.1	NA
Lateral	0.8	0.9	NA

[a] 1975 Plymouth used for test 22; 1970 Chrysler, for test 23; and 1967 Chrysler, for test 23A.
[b] First distance is on the curb; second, on the rail.
[c] Time is for the longer contact distance.

at standard strength-test conditions of 4500 lb, 60 mph, and 25°.

For the second test (test 23), a 4600-lb sedan impacted the approach rail at 24° and 51.7 mph 10 ft upstream of the first bridge-rail post. Impact was on the stone shield and right front wheel, and again no vaulting was seen when the 6-in curb was impacted. The car was in contact with the curb for 22 ft and with the rail for 18 ft. Maximum dynamic barrier deflection was 2.9 ft. On impact, the car began to redirect smoothly, but the Thrie-beam rail on the S3x5.7 posts deflected enough to result in pocketing at the leading end of the bridge rail. The subsequent sharp redirection and exit from the rail caused the car to roll -7° while it pitched +6°. During the exit along a 22° trajectory, the car yawed +19° as it crossed back across the pavement; it finally came to rest about 150 ft from the impact. The highest 50-ms decelerations were 9.1 g longitudinal and 3.8 g lateral. A sharp dropoff at the edge of the test pad caused the vehicle to roll over before coming to rest, but this was not directly attributable to the impact performance of the railing system.

Vehicle damage before the rollover was similar to that incurred in the previous test--bent front fenders, shifted bumper, dents on the right side, and suspension, wheel, and tire damage. Four guiderail posts were bent over on impact, and two others were deflected backward. Two Thrie-beam sections were damaged, as were three bridge-rail posts and one horizontal rail. Maximum permanent deflection of 1.8 ft was recorded on the approach guiderail, and the maximum permanent deflection on the bridge rail was 3 in at the first post. Again, no slippage occurred at the expansion splice. In addition, the base plate of the first bridge-rail post was bowed upward.

Because of the pocketing and steep redirection experienced in test 23, the approach guiderail system was stiffened for the next test as previously described. For test 23A, a 4570-lb vehicle impacted at 25° and 60.9 mph 10 ft upstream from the first bridge-rail post. The right front wheel impacted the 6-in curb with no apparent vaulting, and the right front fender impacted the rail. The car was in contact with the curb and rail for 21 ft; there was a maximum dynamic deflection of 3.1 ft. The vehicle was smoothly redirected at an exit angle of 11°. Maximum vehicle roll was +14°, and maximum pitch was -3°. The car was airborne about 8 in as it left the curb. There was no measurable vehicle yaw until well afer the vehicle left the rail, when the damaged right front suspension resulted in a yaw of -22°. The accelerometer system malfunctioned on impact, so no deceleration data were recorded. However, based on the barrier deflection observed, review of test films, and recorded impact speed, decelerations would probably have been similar to those recorded in the first two tests. The vehicle suffered damage to the front-end sheet metal and bumper, the right-side fenders and doors, the right-side tires and wheels, and the suspension. Also, hood-latch failure caused a cracked front windshield when the open hood fell back onto the glass. None of the guiderail posts were damaged, although five were pushed back. All three bridge-rail posts in the first panel were bent backward; there was a maximum permanent deflection of 6 in. At the first post, the base-plate weld was broken and the plate was bowed upward. The second base plate was bowed, but the weld remained intact. Both thicknesses of Thrie beam were damaged in two rail panels; the result was a total of four damaged pieces. Maximum permanent deflection of the Thrie-beam approach rail was 1.2 ft, and again no slippage occurred at the expansion splice.

Guiderail Tests

Two full-scale crash tests of the Thrie-beam guiderail are summarized in Table 2. For both tests, 10-gage Thrie-beam rail was mounted at a height of 33 in and post spacing of 6 ft 3 in was used.

In test 24, a 3600-lb sedan impacted at 56.0 mph and 26°. Before impact, the car snagged momentarily on the guidance-system release post; the result was a +5° vehicle pitch at impact. Initial vehicle-rail contact was on the right end of the front bumper and right front fender. As the rail deflected, the bottom twisted under slightly, and a maximum dynamic deflection of 3.6 ft was observed. The right front

Table 2. Results of guiderail tests.

Variable	Test 24	Test 25
Vehicle weight (lb)	3600[a]	2300[a]
Vehicle speed (mph)	56.0	60.9
Impact angle (°)	26	25
Exit angle (°)	11	6
Maximum roll (°)	-13	-3
Maximum pitch (°)	+5	+15
Maximum yaw (°)	-7	-90
Contact distance (ft)	30	50
Contact time (ms)	555	821
Deflection (ft)		
Dynamic	3.6	2.1
Permanent	1.3	0.8
Deceleration (g)		
50-ms avg		
Longitudinal	7.3	3.8
Lateral	9.4	5.2
Maximum peak		
Longitudinal	27.7	27.0
Lateral	29.1	23.7
Avg continuous		
Longitudinal	0.9	1.1
Lateral	0.1	0.6

[a]1974 Matador used for test 24; 1973 Vega, for test 25.

Table 3. Results of median-barrier tests.

Variable	Test 26	Test 27	Test 26A
Vehicle weight (lb)	3500[a]	2240[a]	3500[a]
Vehicle speed (mph)	60.9	68.9	63.3
Impact angle (°)	25	25	25
Exit angle (°)	11	13	11
Maximum roll (°)	+10	+16	+16
Maximum pitch (°)	+5	+8	+4
Maximum yaw (°)	-8	-22	-13
Contact distance (ft)	20	25	46
Contact time (ms)	394	332	542
Deflection (ft)			
Dynamic	2.2	1.2	3.9
Permanent	1.0	0.8	2.5
Deceleration (g)			
50-ms avg			
Longitudinal	11.2	9.8	2.8
Lateral	6.6	4.9	8.0
Maximum peak			
Longitudinal	23.7	31.8	12.8
Lateral	24.3	27.7	17.6
Avg continuous			
Longitudinal	3.6	1.9	0.7
Lateral	3.3	1.3	2.9

[a]1973 Matador used for test 26; 1973 Vega, for test 27; and 1972 Ford, for test 26A.

wheel contacted the exposed posts and bent them to the ground. The force of these impacts on the wheel was so great that the wheel was torn completely off the car. After about 30 ft of contact, the vehicle left the rail at an angle of 11°. Due to the missing right front wheel, the vehicle rolled a maximum -13°, yawed -7°, and pitched +5°. Vehicle containment and redirection appeared acceptable, in spite of the wheel contact with the exposed posts. A total of six posts were damaged--the first was pushed back by the rail but not hit by the car; the next four were deflected by the rail and then bent completely down by the right front wheel; and the last was deflected slightly by the rail and impacted by the right front wheel, at which point the wheel separated from the car. Decelerations were not very high if the wheel snag is taken into account. Maximum 50-ms averages were 7.3 g longitudinal and 9.4 g lateral.

Vehicle damage included a bent front bumper, crushed right front fender, flattened right rear tire, and dented right-side doors and right rear fender. The right front tire and wheel were torn completely off the car. Three sections of Thrie beam were dented and six S3x5.7 posts were bent over, the middle four completely to the ground. Permanent barrier deflection was 1.3 ft.

For test 25, a 2300-lb sedan impacted the barrier at 60.9 mph and 25°. Initial redirection was smooth; the maximum dynamic deflection was 2.1 ft. Again, the right front wheel impacted the exposed posts and was driven back into the wheel well. After about 15 ft of contact, the car rolled -3°, pitched +15°, and then spun out, but the right front corner remained in contact with the rail. After sliding along the rail about 35 ft further, the car exited at an angle of 6° but yawed -90°. Maximum 50-ms average decelerations were quite low for the high speed and angle impact--3.8 g longitudinal and 5.2 g lateral. Containment and redirection were generally quite acceptable, in spite of the impact of the wheel on the exposed posts. Vehicle damage included both front fenders crushed, the hood sprung and driven back to the windshield, the right side dented, and the right front wheel broken from its suspension and driven back under the chassis. Barrier damage was limited to two bent Thrie-beam sections and four damaged S3x5.7 posts. The first was deflected back, but the other three were bent nearly to the ground by the wheel impact. Permanent rail deflection was 0.8 ft.

Median-Barrier Tests

Results of three full-scale crash tests of Thrie-beam median barriers are summarized in Table 3. Because the two previous guiderail tests resulted in contact of the wheel with the exposed posts, the mounting height of the Thrie-beam rail was reduced to 30 in. Post spacing was 6 ft 3 in for the first two tests, but for the third it was increased to 12 ft 6 in to permit greater dynamic deflections. It was hoped that this would reduce deceleration and wheel-post impact problems but still hold dynamic deflections similar to those experienced with the box-beam barrier systems.

In test 26, a 3500-lb sedan impacted the rail at 60.9 mph and 25°; there was contact between the vehicle's right corner and the rail. Redirection was generally smooth and resulted in a maximum dynamic deflection of only 2.2 ft. Again, the exposed posts were impacted by the right front wheel, which was driven back against the wheel well and firewall. Maximum vehicle roll was +10° about 10 ft after initial barrier contact. This roll was caused partly by the damage to the right front wheel and partly by the barrier's tipping out slightly at the top. After 20 ft of contact, the vehicle exited at 11°, pitched +5°, and yawed -8°. Peak 50-ms decelerations were 11.2 g longitudinal and 6.6 g lateral. Vehicle damage included bent front bumper and headlight assembly, crushed right front fender, sprung hood and right front door, dented right-side doors and rear fender, mangled right suspension, and right front wheel and tire torn from the suspension and driven back against the inside fender and firewall. Six Thrie-beam sections were bent--three each on the front and back of the posts--and six S3x5.7 posts were bent at the ground line; their tops were deflected from 3 to 12 in. Permanent barrier deflection was 1.0 ft.

In test 27, the 2240-lb sedan impacted at 68.9 mph and 25°. Despite the severe impact, redirection

was relatively smooth; the maximum dynamic deflection was 1.2 ft. The right front wheel again impacted the exposed posts and was driven back against the inner fender and firewall. During 25 ft of contact with the barrier, the vehicle rolled a maximum of +5° as the barrier top tipped back, but no noticeable yaw or pitch was observed. As the vehicle exited along a 13° trajectory, roll and pitch became more severe (+16° roll and +8° pitch). However, 25 ft after the vehicle's departure, roll was back to 0°, pitch was +5°, and yaw was -22°. Peak 50-ms decelerations were 9.8 g longitudinal and 4.9 g lateral.

Vehicle damage included bent bumper, buckled hood, crushed right front fender, dented right-side sheet metal, sprung right-side door, and damaged right front suspension. Also, the right front tire was pulled partly off its wheel and wedged between the bent suspension and the inside fender wall. Barrier damage included four bent and buckled Thrie-beam sections--two each on the front and back of the posts--and five S3x5.7 posts bent back from 3 to 12 in measured at the top of the posts. Permanent barrier deflection was 0.8 ft.

In the final test of Thrie-beam median barrier (test 26A), post spacing was increased to 12 ft 6 in. The 3500-lb sedan impacted at 63.3 mph and 25°. Redirection was smooth; the maximum dynamic deflection was 3.9 ft. Because rail deflection was greater and post spacing was increased, the right front wheel was not damaged by the posts. However, the rail did tip out somewhat at the top, which was reflected in the vehicle trajectory. The vehicle exited at an 11° angle 46 ft after contact. Maximum roll was +16°, pitch was +14°, and yaw was -13°. Overall, decelerations were less severe than in the first two tests; peak 50-ms averages were 2.8 g longitudinal and 8.0 g lateral.

Vehicle damage was also less severe than in tests 26 and 27. The bumper, right-side fenders, and doors were dented and the right-side tires were flattened, but the wheels and suspension remained intact. Barrier damage was also lighter; four Thrie-beam sections were bent, all on the front of the system, and five posts were bent over from 4 to 18 in at the top of the post. Permanent deflection was 2.5 ft.

DISCUSSION OF RESULTS

The upgraded bridge rail developed during this research performed well and appears to offer a suitable alternative to other upgradings developed elsewhere (4). Its principal advantage is that it uses a single thickness of 10-gage Thrie-beam rail bolted directly to the existing bridge rail, which eliminates the need for the tubular Thrie beam. In the transition from light-post (S3x5.7) guiderail to the bridge rail, however, it was necessary to double the rail element and add heavy posts (W6x8.5) to prevent excessive deflection and pocketing at the first bridge-rail post. Vehicle decelerations experienced in these tests were not excessive and were comparable with those reported for other tests of very stiff bridge-railing systems. Vehicle redirection was good, except for test 23, which resulted in pocketing. That design was then modified and performed well in test 23A. Vehicle damage was moderate if the severity of the impacts is taken into account and compared favorably with other tests of upgraded bridge rails. Although impact speed in test 22 (on the bridge) was less than 60 mph, deflection and rail damage were moderate. Based on the results of that test, the upgraded railing system has strength adequate to withstand 60-mph 25° impacts from 4500-lb vehicles. This bridge-rail upgrading system thus appears suitable for implementation. Although no test was performed at the transition from light to heavy posts, the other two transition tests provide evidence that this part of the transition will perform satisfactorily. In tests 23 and 23A, the Thrie-beam rail effectively prevented wheel contact with the first bridge-rail post and with the W6x8.5 posts. The 20-in depth of the Thrie-beam rail thus should prevent wheel contact at the change from S3x5.7 to W6x8.5 posts. It must be remembered that the light posts separate from the rail on impact and bend over at the ground line and are thus exposed to wheel impact. The heavy posts, on the other hand, which are rigidly connected to the rail, are deflected back on impact and continue to be protected against wheel impact by the rail.

The guiderail and median-barrier designs also appear to offer acceptable performance; deflection characteristics are similar to those of the box-beam guiderail and median barrier now standard in New York State. Deflection characteristics for all four barriers are given in Table 4. First, standard design deflections for box-beam barriers are given. Based on a 60-mph 25° impact by a 3500-lb vehicle, design deflections for these barriers vary from 2 to 5 ft, depending on the rail element and post spacing selected. Next, actual test deflections for the Thrie-beam barriers are presented, which ranged from about 2 to 4 ft. Finally, proposed design deflections are provided for Thrie-beam guiderail and median barrier at two post spacings each. These design deflections were estimated from actual test results; corrections were added for impact speed, angle, and test-vehicle weights. The deflection for guiderail that has a post spacing of 12 ft 6 in is based on the effects of post spacing observed in the median-barrier tests and in earlier tests of W-beam light-post guiderail (8).

Tests of both guiderail and median barrier generally resulted in acceptable performance. The decelerations recorded in these tests seem reasonable for the severe test conditions. Although some values exceed the guideline recommendations of 10 g longitudinal and 5 g lateral, these impacts were at 25° rather than at 15°. Compared with previous tests of barrier systems (3,9-11) now classified as operational in the American Association of State Highway and Transportation Officials (AASHTO) barrier guide, some of the deceleration values are somewhat higher but are still within reasonable limits for 25° impacts. The two small-car tests, on the other hand, resulted in surprisingly moderate deceleration values, especially if the 25° impact angle and very high speeds (61 and 69 mph) are taken into account. Some vehicle roll was experienced during redirection, but none of the vehicles appeared close to rolling over. Exit angles were all acceptable, although some vehicles did yaw sharply toward the barrier after exit because of steering and suspension damage. Vehicle damage was moderate for all these tests, especially if the high impact speeds and 25° impact angles are considered. No damage to passenger compartments resulted, and damage was generally limited to the right front sheet-metal, grill, bumper, and right front suspension. Vehicle damage appears comparable with that resulting from other tests of Thrie beam and W-beam on heavy posts (3,9-11), which includes damage to the suspension. Because of the high speeds and impact angles for small-car tests, direct comparison with other tests is not possible. However, these results seem favorable if the high severity of these impacts is considered.

The only disappointing aspect of the test was the damage to the front wheel and suspension experienced

Table 4. Summary of barrier deflections.

Barrier Type	Post Spacing (ft)	Impact Conditions: Speed (mph)	Impact Conditions: Angle (°)	Impact Conditions: Vehicle Weight (lb)	Deflection (ft)
Existing box-beam barrier					
6x6x3/16-in guiderail	3	60	25	3500	4
6x6x3/16-in guiderail	6	60	25	3500	5
6x8x1/4-in median barrier	3	60	25	3500	2
6x8x1/4-in median barrier	6	60	25	3500	4
Tested Thrie-beam barrier					
Guiderail	6¼	56	26	3600	3.6
Median barrier	6¼	61	25	3500	2.2
Median barrier	12½	63	25	3500	3.9
Proposed Thrie-beam barrier					
Guiderail	6¼	60	25	3500	4
Guiderail	12½	60	25	3500	6
Median barrier	6¼	60	25	3500	2
Median barrier	12½	60	25	3500	3.5

Figure 7. Attitudes of several light-post barriers before and after impact.

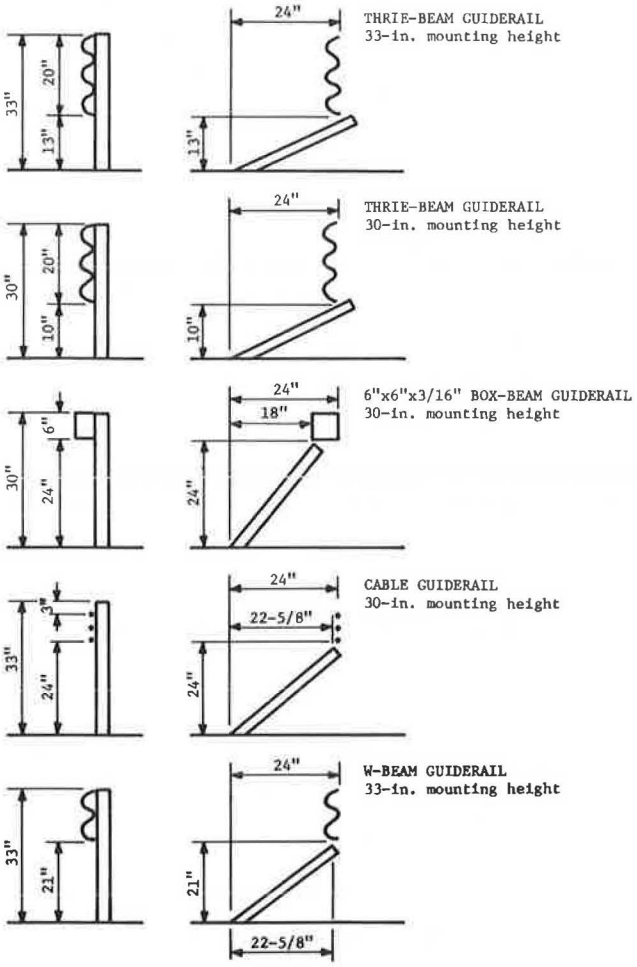

in four of the five guiderail and median-barrier tests. In spite of this damage, which resulted from contact between the wheel and the posts, vehicle decelerations were within acceptable ranges. Further, this suspension damage generally did not result in unacceptable vehicle trajectories. Such damage is not uncommon for impacts at high angles and high speeds and has been reported in tests of several barriers now in wide use (3,9-11). Several of these earlier tests also resulted in complete removal of the front wheel. Further, several tests used full-sized cars rather than the intermediate-sized cars used here.

Although this contact between wheel and posts did not appear to result in unacceptable performance, it is desirable to eliminate such damage if possible. Examination of the barriers after impact and close examination of the test films revealed two factors that contributed to the wheel-post impact problem. First, these barriers were all installed on an asphalt pavement; the posts were driven through several inches of asphalt. Combined with the 8x24-in soil-support plates, this resulted in posts that bent at the pavement surface on impact and did not push through the asphalt. This installation condition is typical in New York State, where guiderail and median barrier are frequently installed on asphalt shoulders or medians that are paved over compacted gravel subbases. This very stiff restraint may have increased the severity of the wheel-post impact somewhat. The second contributing factor is the relatively high stiffness of the barriers tested and the greater depth of the Thrie-beam section. As the rail deflected on impact, the rail mounting bolt was snapped, but the posts were bent back by the rail. However, the small amount of post exposed prevented contact of the post with the vehicle bumper or sheet metal. Instead, the main force on the post was imparted by the wheel, which resulted in the suspension damage experienced. For W-beam, cable, or box beam installed on light posts, the shallow rail depth would permit more vehicle sheet-metal contact on the post, which would partly bend it down before it was struck by the wheel. For W-beam and cable, greater deflections would also help eliminate this problem. The relation of several light-post barriers before and after impact is shown in Figure 7, and it can be seen that the Thrie beam is the most critical case for wheel-post impact.

The first effort to reduce contact between wheel and posts was to lower the rail height from 33 to 30 in. However, as seen in Figure 7, this cannot be expected to have much effect, because contact occurs after the rail and post have separated and the post has been bent laterally by the deflecting rail. The second effort, which was successful, was to increase post spacing from 6 ft 3 in to 12 ft 6 in as in the last test (test 26A). By increasing the spacing, greater deflection was permitted, which helped to move the wheel behind many of the posts and to permit the bumper and sheet metal to contact and bend the posts longitudinally. Increasing post spacing also results in fewer posts to contact. Depending on impact conditions, it is much more likely that the vehicle can be redirected without a severe wheel-post impact. Damage to the right front

suspension was successfully eliminated in test 26A, which used the wider post spacing.

Additional tests of the Thrie-beam light-post barriers are needed to provide performance data by using other post spacings and 12-gage rail sections. In addition, 60-mph 15° impacts by small cars will provide confirmation that this barrier system provides very good protection for small cars, although this is already indicated by the 60-mph 25° impacts reported here. Based on these tests, the 10-gage Thrie-beam barrier on S3x5.7 posts spaced at 12 ft 6 in and mounted at a height of 33 in appears suitable for both guiderail and median-barrier use on a trial basis. To reduce front-suspension damage, closer post spacings should be limited to transitions to more-rigid barriers. Limited field installations of this barrier system appear justified at this time, especially used as a bridge-rail upgrading. Because of the wheel-post impact problem, this barrier system does not provide a significant improvement in impact performance over existing barriers but it does provide three distinct advantages over existing systems. It performs well as a bridge-rail upgrading; it can be more readily transitioned to rigid barriers; and its greater depth provides improved vaulting-underride protection. As with any new barrier system, careful documentation of initial field installations is necessary to confirm the good performance indicated by these tests.

CONCLUSIONS

Based on eight crash tests of Thrie-beam bridge-rail upgrading, guiderail, and median barrier, the following findings can be stated:

1. A bridge-rail upgrading that consists of 10-gage Thrie beam bolted directly to discontinuous-panel bridge rail performed well during a full-scale test. This upgrading system is suitable for 60-mph 25° impacts by 4500-lb vehicles.
2. A 10-gage Thrie-beam transition from guiderail to bridge rail mounted on S3x5.7 posts was not stiff enough to prevent pocketing at the end of the bridge rail.
3. A redesigned transition to bridge rail that used a double layer of 10-gage Thrie beam mounted on W6x8.5 posts performed well and is suitable for 60-mph 25° impacts by 4500-lb vehicles.
4. Five tests of guiderail and median barrier that consisted of 10-gage Thrie beam mounted on S3x5.7 posts resulted in satisfactory vehicle containment, redirection, and deceleration.
5. Damage to the front wheel and suspension occurred in four of these five tests; it was caused by impact between wheels and posts. This damage was no more severe than that reported in many earlier tests of operational barriers, and the total vehicle damage in many cases was less.
6. Lowering the rail-mounting height from 33 to 30 in intensified the wheel-post contact problem because it reduced the chances that the post would be bent longitudinally by the bumper, sheet metal, and frame.
7. Increasing post spacing from 6 ft 3 in to 12 ft 6 in reduced conflict between wheels and posts by increasing barrier deflection and reducing the number of posts available for impact.
8. Guiderail and median barrier that consist of 10-gage Thrie beam mounted at 33 in on S3x5.7 steel posts appear to be suitable longitudinal barriers. They offer several distinct advantages compared with barriers now in use, which includes excellent properties as a bridge-rail upgrading system, simple transition to rigid barriers, and lower susceptibility to vaulting or underride problems compared with narrower rail elements.
9. Testing should continue to determine barrier characteristics at other post spacings and mounting heights and under less-severe impact conditions. Efforts should also continue to reduce conflict between wheel and posts, especially when the need for low dynamic deflections requires use of relatively close post spacings.
10. Design deflections are presented for this barrier system that are very close to those for box-beam guiderail and median-barrier systems.

ACKNOWLEDGMENT

The full-scale tests were supervised by Richard G. Phillips, assistant civil engineer, assisted by Peter D. Kelly, Robert P. Murray, and Alan W. Rowley, senior engineering technicians in the Appurtenances and Operations Section, Engineering Research and Development Bureau of the New York State Department of Transportation. Wilfred J. Deschamps of the Special Projects Section provided the electronics work required for this project. We acknowledge the assistance of the Structural Design and Review Bureau, especially Lawrence N. Johanson and William J. Winkler, in the design of the bridge-rail upgrading system. Thanks are also extended to William Hopkins of the Final Plan Review Bureau for assisting in the design of the guiderail and median-barrier systems. Region 1 maintenance personnel assisted with site-preparation work. Thrie-beam rail for these tests was provided by the Syro Steel Company. Readers interested in a more-extended and detailed discussion of these tests and their results, to be published early in 1981, may write the Publications Section, Engineering Research and Development Bureau, New York State Department of Transportation, State Campus, Albany, NY 12232, and request Research Report 85. This paper was prepared with the cooperation of the Federal Highway Administration, U.S. Department of Transportation.

REFERENCES

1. J. VanZweden and J.E. Bryden. In-Service Performance of Highway Barriers. Engineering Research and Development Bureau, New York State Department of Transportation, Albany, Res. Rept. 51, July 1977.
2. R.D. Carlson, J.R. Allison, and J.E. Bryden. Performance of Highway Safety Devices. Engineering Research and Development Bureau, New York State Department of Transportation, Albany, Res. Rept. 57, Dec. 1977.
3. M.E. Bronstad, J.D. Michie, J.G. Viner, and W.E. Beam. Crash Test Evaluation of Thrie-Beam Traffic Barriers. TRB, Transportation Research Record 488, 1974, pp. 34-44.
4. J.D. Michie and M.E. Bronstad. Upgrading Safety Performance in Retrofitting Traffic Railing Systems. Southwest Research Institute, San Antonio, TX, Rept. FHWA-RD-77-40, Sept. 1976.
5. Recommended Procedures for Vehicle Crash Testing of Highway Appurtenances. TRB, Transportation Research Circular 191, Feb. 1978.
6. AASHO Bridge Specifications. AASHO, Washington, DC, 1957.
7. M.D. Graham, W.C. Burnett, J.L. Gibson, and R.H. Freer. New Highway Barriers: The Practical Application of Theoretical Design. HRB, Highway Research Record 174, 1967, pp. 88-183.
8. J.L. Whitmore, R.G. Picciocca, and W.A. Snyder. Testing of Highway Barriers and Other Safety Accessories. Engineering Research and

Development Bureau, New York State Department of Transportation, Albany, Res. Rept. 38, Dec. 1976.
9. J.D. Michie, L.R. Calcote, and M.E. Bronstad. Guardrail Performance and Design. NCHRP, Rept. 115, 1971, 70 pp.
10. J.L. Beaton, E.F. Nordlin, and R.N. Field. Dynamic Tests of Corrugated Metal Beam Guardrail. HRB, Highway Research Record 174, 1967, pp. 42-87.
11. E.F. Nordlin, J.R. Stoker, and R.L. Stoughton. Dynamic Tests of Metal Beam Guardrail: Series XXVII. Transportation Laboratory, California Department of Transportation, Sacramento, Rept. CA-DOT-TL-6342-5-74-14, 1974.

Publication of this paper sponsored by Committee on Safety Appurtenances.

SERB: A New High-Performance Self-Restoring Traffic Barrier

M.E. BRONSTAD, C.E. KIMBALL, JR., AND C.F. McDEVITT

This paper describes the development and evaluation of a unique guardrail system. Features of this barrier include a simple gravity-dependent self-restoring stage for automobile impacts that bottoms at a second stage that is capable of redirecting large vehicles. Screening of preliminary designs was accomplished by computer simulation and cost analyses. The prototype barrier design was revised into a final configuration based on crash test results. The self-restoring barrier (SERB) guardrail has successfully redirected vehicles that range from a 950-kg (2100-lb) mini automobile to a 18 000-kg (40 000-lb) intercity bus at 95 km/h (60 mph) and a 15° angle. A unique feature of the new system is the self-restoring elastic 0.3-m (11-in) deflection of the rail, which provides forgiving redirection for most passenger car impacts without damage or permanent deformation of the system.

This paper describes the development and evaluation of a unique high-performance guardrail system. Features of this barrier include a simple gravity-dependent self-restoring stage for automobile impacts that bottoms at a second stage that is capable of redirecting large vehicles. The finalized design is a product of an in-depth investigation conducted by Southwest Research Institute for the Federal Highway Administration. Design criteria were developed first and conceptual designs were subsequently screened by computer simulation and cost analyses. The barrier system selected for crash test evaluation is considered the best of all design concepts investigated during the course of the project. A total of seven crash tests were conducted on prototype and finalized design installations. Included in the evaluations were mini, subcompact, and full-sized cars as well as school and intercity buses.

BACKGROUND

In the early 1970s, crash test evaluations in the United States began to use heavy vehicles to evaluate high-performance barriers. The collapsing ring bridge rail (1) and the concrete median barrier were subjected to impacts by intercity buses (2) and tractor trailers (3). The conditions of impact varied considerably, since there was no recognized standard impact condition for these heavy vehicles. Indeed, there were no standard heavy vehicles specified for crash testing.

The objective of this study was to design high-performance guardrail and median-barrier concepts. It was recognized that many agencies were replacing flexible metal barriers with concrete in urban areas due to frequent requirements for damage repair. A goal of this design study was to provide the agencies with a forgiving flexible barrier that would not require significant maintenance and at the same time would provide containment and redirection of infrequent impacts by heavy buses and trucks. A survey of selected states that were known to have significant heavy-vehicle traffic was conducted to determine deflection limits for the systems. Selection of design vehicles was also a consideration. The final product of the investigations was the set of design criteria for the high-performance self-restoring barrier (SERB) system given below:

1. Impact severity: Provide forgiving redirection for subcompact car for impacts up to 95 km/h (60 mph) and 15° angle,
2. Strength: Contain and redirect an 18 000-kg (40 000-lb) intercity bus impacting at 95 km/h and 15° angle,
3. Damage repair: Allow no significant damage during typical shallow-angle impacts with cars, and
4. Cost: Minimize installation cost.

SERB BARRIER

The SERB barrier is a staged system designed to be self-restoring for most impacts that occur at shallow angles. The tubular Thrie beam is mounted on alternate posts by using a double-hinged pivot bar and cable assembly (Figure 1a). When impacted by a vehicle, the beam deflects up and backward, providing 0.3 m (11 in) of stroke before bottoming on the posts (Figure 1d). As the beam is displaced, the vehicle follows the upward motion, which provides a banking effect that enhances smooth redirection. After bottoming, the SERB guardrail is a very strong barrier 1.0 m (38 in) high capable of redirecting heavy vehicles that impact at 95 km/h and a 15° angle.

FINDINGS

The first three crash tests were conducted on the prototype design shown in Figure 2 (all tests are summarized in Table 1). In this design, the tubular Thrie-beam rail is bolted directly to the single-hinged pivot bar. The rail 0.8 m (30 in) high became 0.9 m (35 in) high when it bottomed against the wood posts. Tests SRB-1 and SRB-2, which used passenger vehicles, were successful. Rollover of the school bus in test SRB-3 (Figure 3) led to the de-

Figure 1. Final SERB design.

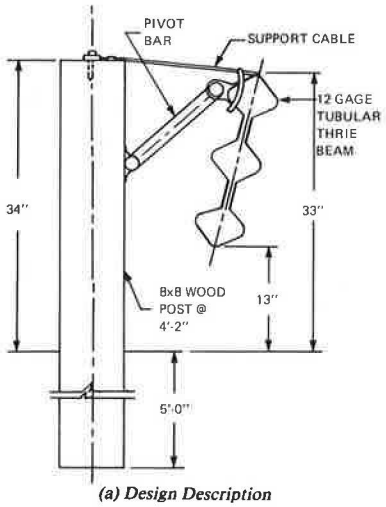

Note: 1 ft = 0.3 m; 1 in = 25 mm.

(a) Design Description

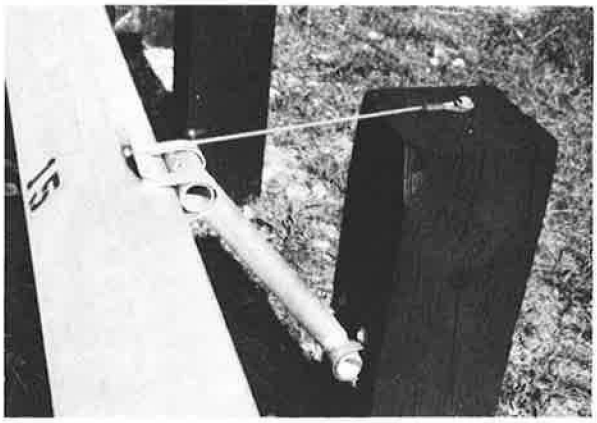

(b) Photograph

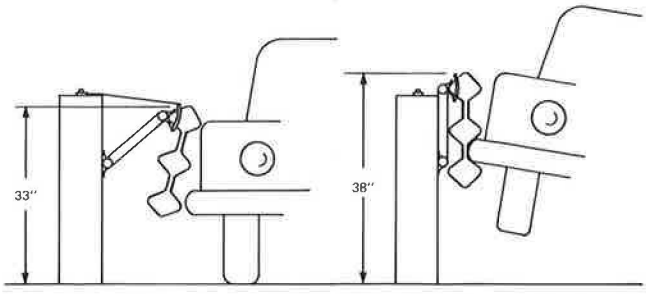

(c) At Impact *(d) At Bottom of Stroke*

sign modification described in Figure 1. Findings from the crash tests conducted on the finalized design are described in the following discussion.

Test SRB-4

The final barrier design installation was impacted with a 1974 Honda Civic that weighed 945 kg (2083 lb) at a speed of 88.0 km/h (54.7 mph) and a 17.1° angle. As shown in Figure 4, the vehicle was smoothly redirected and there was no barrier damage. Vehicle damage was limited to sheet-metal deformation (Figure 5).

Test SRB-5

A 1970 Chevrolet-Wayne school bus that weighed 9070 kg (20 000 lb) impacted the barrier at a speed of 97.4 km/h (60.5 mph) and a 13.8° angle. As shown in Figure 6, the bus was smoothly redirected and the maximum roll angle was 27°.

Damage to the installation included two beam sections, one post fractured below grade, one post split, most beam-pivot-bar attachment bolts sheared, and some support-cable lag bolts pulled out.

The bus damage was moderate during contact with the barrier; however, extensive damage occurred during recovery when the bus impacted another barrier installation. This damage prevented meaningful posttest photographs.

Figure 2. Prototype barrier installation.

Table 1. Summary of crash test evaluations of SERB guardrail.

Test	Barrier Design	Vehicle	Vehicle Weight[a] (lb)	Impact Speed (mph)	Impact Angle (°)	Vehicle Acceleration[b] (g)		Maximum Barrier Deflection		
						Lateral	Longitudinal	Dynamic (in)	Permanent Post (in)	Permanent Rail (in)
SRB-1	Original	1974 Chevrolet Vega	2 650	58.6	17.2	5.6	-2.0	12.0	0	0
SRB-2	Original	1973 Chevrolet Impala	4 700	60.6	24.6	9.2	-6.6	29.4	6.0	4.0
SRB-3	Original	1972 International chassis with Wayne school bus body	20 000	56.9	17.5	5.9	-3.0	31.0	19.0	12.8
SRB-4	Modified	1974 Honda Civic	2 083	54.7	17.1	6.4	2.3	10.8	0	0
SRB-5	Modified	1970 Chevrolet chassis with Wayne school bus body	20 000	60.5	13.8	9.4	-1.2	36.0	11.1	10.0
SRB-6	Transition	1974 Oldsmobile Delta 88	4 832	56.2	25.3	6.4	-5.4	10.5	7.8	7.8
SRB-7	Modified	1956 GMC Scenicruiser	40 000	57.0	15.8	4.7	-3.3	47.1	19.5	21.8

Note: 1 lb = 0.45 kg; 1 mph = 1.6 km/h; 1 in = 25 mm.

[a]Weight includes vehicle, two anthropomorphic dummies, and instrumentation. Buses are ballasted with loose sandbags in seats.

[b]50-ms average.

Figure 3. Test SRB-3.

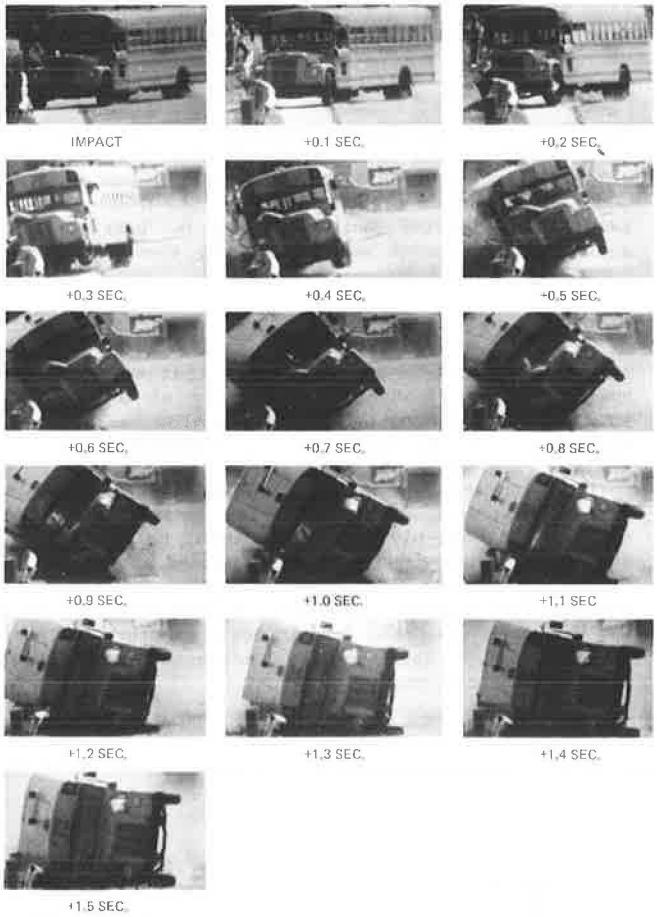

Figure 4. Test SRB-4.

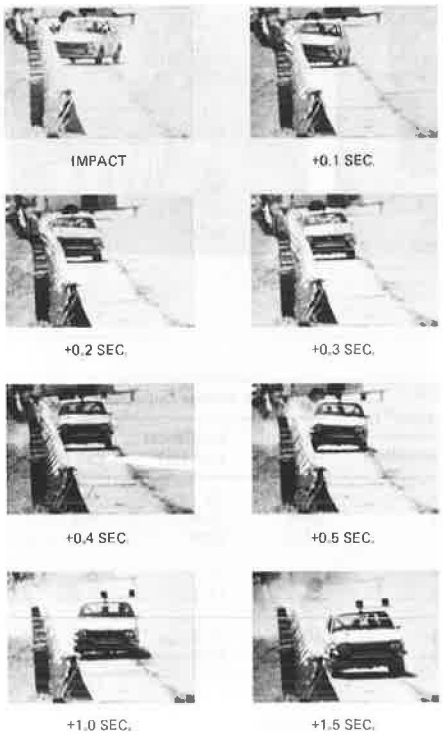

Figure 5. Vehicle and barrier condition after test SRB-4.

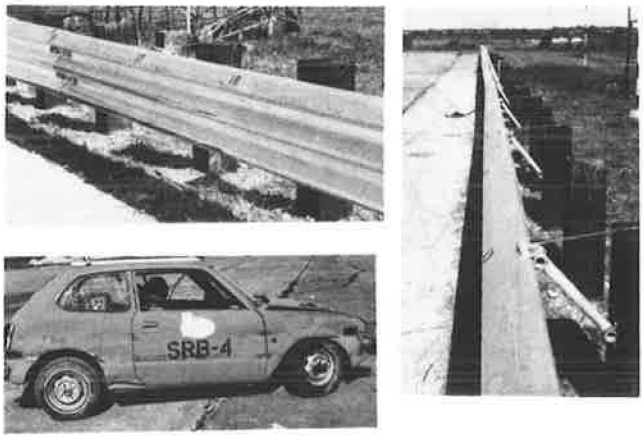

Figure 6. Test SRB-5.

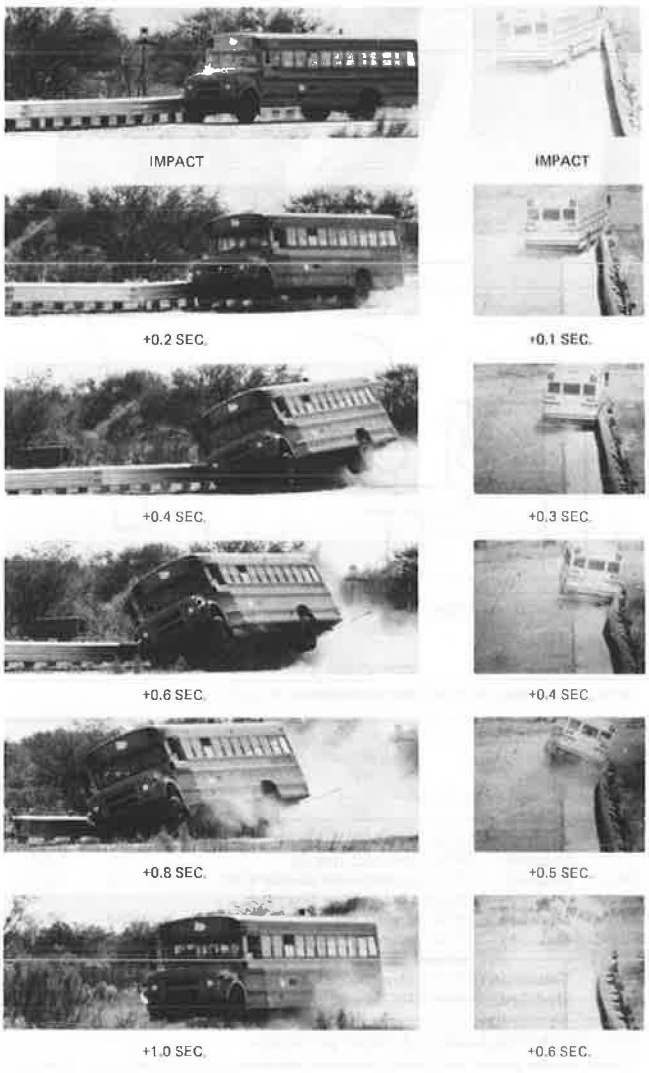

Figure 7. SERB end treatment.

Figure 8. Results of test SRB-6.

Figure 9. Test SRB-7.

Figure 10. Results of test SRB-7.

Figure 11. SERB median-barrier concept.

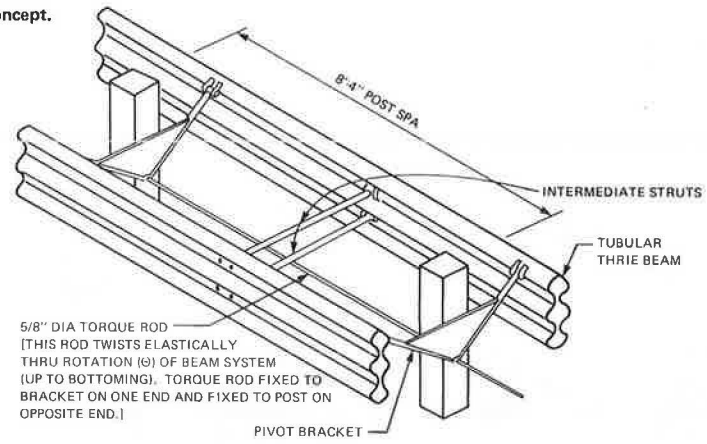

(a) Isometric View

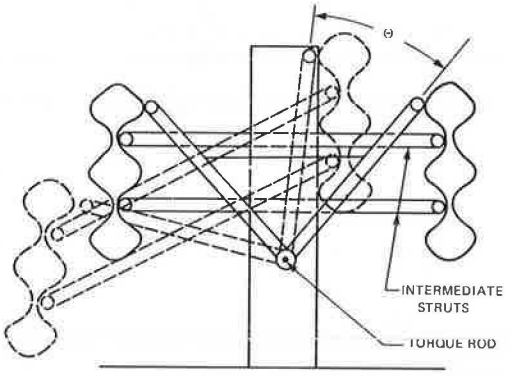

(b) Rotation of SERB Up to Bottoming

Note: 1 ft = 0.3 m; 1 in = 25 mm.

SERB End Treatment

The end of the SERB guardrail features a rigid steel support post set in concrete; four cables provide longitudinal anchorage (Figure 2). In order to shield the rigid support post, an end treatment was designed that uses standard W-beam guardrail terminals. A transition from a guardrail breakaway cable terminal (BCT) to the rigid end post was effected as shown in Figure 7. Other W-beam terminals or a crash cushion could also be used at the end.

Test SRB-6

The SERB end treatment was subjected to evaluation according to Transportation Research Circular (TRC) 191 (4) criteria for transition sections, i.e., a 2040-kg (4500-lb) car that impacts at 95 km/h and a 25° angle at the most vulnerable location.

A 1974 Oldsmobile that weighed 2192 kg (4832 lb) impacted the system 4.5 m (14.6 ft) upstream of the rigid end post with a speed of 90.5 km/h (56.2 mph) and a 25.3° angle. The vehicle was smoothly redirected (Figure 8b); maximum beam deflection was 200 mm (7.8 in).

For the test conditions, vehicle damage was typical for impacts with rigid barrier systems (Figure 8d). Barrier damage (Figure 8a and c) consisted of one Thrie-beam section, a transition section, and two posts.

Test SRB-7

A 1956 GMC Scenicruiser intercity bus that weighed 18 140 kg (39 908 lb) impacted the barrier at a speed of 91.8 km/h (57 mph) and a 15.8° angle. As shown in Figure 9, the bus was smoothly redirected and the maximum roll angle was 38°.

Damage to the installation was moderate; it included three rail sections and five broken posts, as shown in Figure 10. Maximum dynamic deflection of the railing system was 1.2 m (4 ft). Damage to the bus included the sheet metal, window, and baggage-door area (Figure 10). The bus was driven from the test site.

CONCLUSIONS AND RECOMMENDATIONS

A high-performance guardrail system was developed in this project primarily by using computer simulation and crash test evaluation. The original design criteria were met by the final design configuration. A late inclusion of a mini-sized car in the test matrix posed no problem in terms of achieving desirable barrier performance.

Barrier Design

The original design of this barrier was accomplished by using BARRIER VII (5) computer simulations. It is noteworthy that no changes were made to the beam, post, or post spacing of the guardrail system during its development. The 75-mm (3-in) change in railing height and revised hinge details demonstrably improved the performance of the final barrier for school buses, as shown by test SRB-4, but neither of these changes is pertinent when the capability of the simulation model is considered. Comparisons of experimental and simulation values demonstrated that the SERB guardrail performed much as predicted. Modeling of the wood posts in soil has always presented simulation difficulties, and this best explains the superiority of the car simulations (no post movement) as compared with those for the bus.

The predictable behavior of the SERB concept would allow other barriers to be readily designed for either higher or lower service conditions. By varying post size and/or spacing, for example, a more economical system could be achieved. Of course, the performance of this system would be changed with regard to barrier capacity for vehicle containment and/or maximum deflections.

Demonstrated Performance

Demonstrated performance of this unique barrier includes the following results:

1. No barrier damage or permanent deformation during an impact at 88 km/h (55 mph) and a 17° angle although maximum barrier deflection was 280 mm (11 in);
2. Vehicle acceleration values near compliance with TRC 191 for both Honda and Vega impacts (in this regard, the SERB guardrail is currently unique);
3. Containment and redirection of a wide range of test vehicles at a nominal 95 km/h and 15° angle [test vehicles included 945-kg minicar, 9070-kg school bus, and 18 140-kg intercity bus, all of which were driveable after having left the barrier (the SERB guardrail is unique among all known barriers for this performance range)];
4. Barrier damage for an impact at 95 km/h and a 25° angle with a 2040-kg car does not compromise the serviceability of the SERB guardrail, although repairs would be desirable;
5. For the most severe strength test (intercity bus), the goal of 1.2-m maximum dynamic deflection was met; and
6. An end treatment that included transition to an approved guardrail terminal was evaluated at the length-of-need zone.

Recommendation

The SERB guardrail system described is recommended for immediate installation when serious consideration of heavy-vehicle containment is warranted. Cost of the system is considered competitive. It is estimated to be $21-$27/linear ft ($17-$24 for materials, $2-$4 for labor).

For median-barrier applications, a more-efficient use of dual beams is suggested in Figure 11; however, tests have not been conducted on this configuration. Figure 12 shows a SERB application for sawtooth medians.

SERB Advantages

Advantages of the SERB guardrail systems when compared with other metal barrier systems include the following:

1. Damage repair from typical shallow-angle impacts is projected to be minimal;
2. Forgiving redirection is provided for all cars as well as containment of heavy vehicles under severe impact conditions;
3. The 1.2-m maximum deflection during the intercity bus test (a design goal) makes application of the SERB guardrail to current roadside clearances reasonable even when heavy-vehicle containment is a serious consideration.

Advantages of the SERB system when compared with concrete barriers include the following:

1. Stable redirection of all classes of cars with minimal rollover potential;
2. Demonstrated performance with heavy vehicles such as the school bus and the intercity bus;
3. Demonstrated well-behaved performance without

Figure 12. SERB median-barrier concept for sawtooth medians.

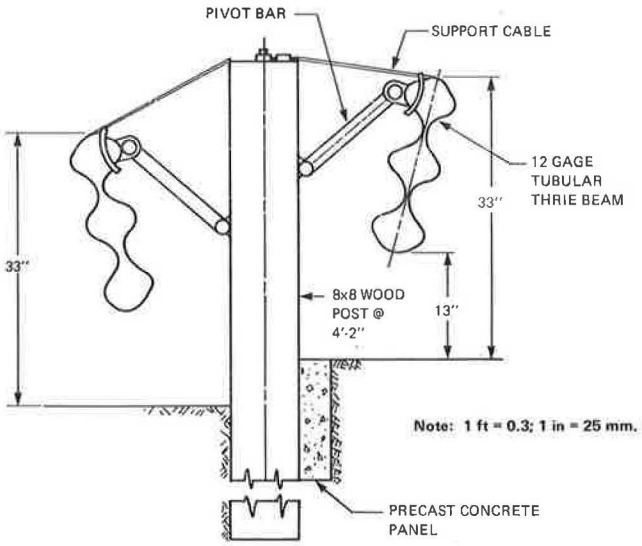

variables such as foundation support and rebar configurations, i.e., lightly reinforced to heavily reinforced concrete barriers and minimal to substantial foundation support; and

4. Definite advantage in performance for high angles of attack, i.e., those greater than 15°.

ACKNOWLEDGMENT

The work discussed in this paper was sponsored by the Federal Highway Administration Office of Research. The opinions, findings, and conclusions expressed in this paper are ours and not necessarily those of the sponsor or other agencies with which we are affiliated.

REFERENCES

1. C.E. Kimball and others. Development of a Collapsing Ring Bridge Railing System. Federal Highway Administration, U.S. Department of Transportation, Rept. FHWA-RD-76-39, Jan. 1976.
2. M.E. Bronstad and others. Concrete Median Barrier Research. Federal Highway Administration, U.S. Department of Transportation, Rept. FHWA-RD-77-4, March 1976.
3. E.R. Post and T.J. Hirsch. Truck Tests on Texas Concrete Median Barrier. Presented at the 52nd Annual Meeting, HRB, 1973.
4. Recommended Procedures for Vehicle Crash Testing of Highway Appurtenances. TRB, Transportation Research Circular 191, 1978.
5. G.H. Powell. BARRIER VII--A Computer Program for Evaluation of Automobile Barrier Systems. Federal Highway Administration, U.S. Department of Transportation, March 1973.

Publication of this paper sponsored by Committee on Safety Appurtenances.